COMPOUND URBAN FLOODING: THE EMERGING HAZARD FOR LARGE METROPOLITAN AREAS

by

Selina Jahan Sumi
A Dissertation
Submitted to the
Graduate Faculty
of
George Mason University
in Partial Fulfillment of
The Requirements for the Degree
of
Doctor of Philosophy
Civil, Environmental, and Infrastructure Engineering

Committee:

_____ Dr. Celso M. Ferreira, Dissertation Director

_____ Dr. Viviana Maggioni, Committee Member

_____ Dr. Mark H. Houck, Committee Member

_____ Dr. Paul Houser, Committee Member

_____ Dr. Sam Salem, Department Chair

_____ Dr. Kenneth S. Ball, Dean, Volgenau School of Engineering

Date: _____ Fall Semester 2020

George Mason University

Fairfax, VA

Compound Urban Flooding: The Emerging Hazard for Large Metropolitan Areas

A Dissertation submitted in partial fulfillment of the requirements for the degree of Doctor of Philosophy at George Mason University

by

Selina Jahan Sumi
Masters of Science
University of Louisiana at Lafayette, Louisiana, United States, 2015
Bachelor of Science
Bangladesh University of Engineering and Technology, Dhaka, Bangladesh, 2012

Director: Celso M. Ferreira, Associate Professor
Civil, Environmental, and Infrastructure Engineering

Fall Semester 2020
George Mason University
Fairfax, VA

DEDICATION

This is dedicated to my loving family.

ACKNOWLEDGEMENTS

I would like to express my deepest gratitude to my supervisor Dr. Celso M. Ferreira for his support, patience, encouragement, and his aspiring guidance throughout the period of my Ph.D. study. It was a great privilege to work under his supervision.

My sincere thanks go to my dissertation committee members Dr. Mark H. Houck, Dr. Viviana Maggioni, and Dr. Paul Hauser for their encouragement and insightful comments on my work.

I am very grateful to my friends who have always encouraged and supported me. My appreciation also extends to my fellow lab-mates in the Mason Flood Hazards Research Lab for their continuous help and support to execute this research work and for all the funs we have had together in last four years.

I would like to thank the Office of the Provost at George Mason University for providing funding for my research throughout the 4 years of my Ph.D. study. I am also grateful to them for offering me the Summer Presidential Fellowships during 2017, 2018, 2019, and 2020 which helped me to continue my research without any interruption in the summers.

Finally, I would like to thank my parents, brother, and sister for their prayers, support, and encouragement. I am very grateful to have a really big extended family with cousins, uncles, and aunts who have always motivated me to concentrate on achieving my goals. I would also like to thank my husband for supporting me in all the tough times and celebrating all the good times together.

TABLE OF CONTENTS

LIST OF TABLES

LIST OF FIGURES

LIST OF EQUATIONS

LIST OF ABBREVIATIONS

National Oceanic and Atmospheric Administration ..... NOAA
National Weather Service ..... NWS
Advanced Hydrologic Prediction Service ..... AHPS
Sea-Level Rise ..... SLR
U.S. Army Corps of Engineers ..... USACE
North American Vertical Datum of 1988 ..... NAVD88
United States Geological Survey ..... USGS
Digital Elevation Model ..... DEM
Curve Number ..... CN
One Dimensional 1D
Two Dimensional 2D
Soil Conservation Service ..... SCS
Natural Resources Conservation Service ..... NRCS

ABSTRACT

COMPOUND URBAN FLOODING: THE EMERGING HAZARD FOR LARGE METROPOLITAN AREAS

Selina Jahan Sumi, Ph.D.

George Mason University, 2020

Dissertation Director: Dr. Celso M. Ferreira

Flooding is one of the major natural disasters around the globe with wide-reaching impacts on the environment, economy, infrastructure, and human lives. In recent years, compound floods resulting from the co-occurrence of multiple flood drivers like riverine flow, storm surges, sea-level rise, and extreme rainfall have impacted several cities across the United States (US). Metropolitan areas, located in the coastal regions of the US, have become increasingly vulnerable to such flooding conditions due to their unique exposure to multiple flood hazards and population density, rapid urbanization, proximity to major rivers or lakes, and the probable risk of sea level rise. The goal of this study is to identify the major flood drivers impacting metropolitan areas in large tidal estuaries and to quantify their impacts on compound flooding. Washington, DC, and the surrounding communities in Maryland and Virginia is used as an example, because like many US coastal areas, it is often exposed to various flood hazards that overlap spatially and temporally, leading to the potential of compound flooding conditions. Results from

the historical data analysis (1931 to 2019) provided strong evidence that compound flooding in the region can be caused by a combination of storm surge or high coastal water levels, riverine flow, local wind, and urban runoff. These events had the highest duration and magnitude during the study period. Among the four *Major* flood events during this time, three were a result of compound flooding, and only one resulted from high riverine flow. Storm-surge driven coastal floods were more common in Washington, DC compared to river floods when the flood stages were either at *Moderate* or *Minor* stage. The local wind with speed above 5.5 m/s and urban runoff also plays a significant role impacting flood levels in the area. The variability in compound flooding extent and depth was also investigated using a 2D hydrodynamic model. Results suggested that locations around the study area can be locally divided into three zones based on the impact of flow and surges: highly riverine flow dominated upstream zone, transition zone with impact from both flow and surges, and coastal water level dominated lower zone. Flood depths during surge dominated events were significantly higher than flow dominated events, almost doubling in some locations towards downstream of the river. Small urban streams in the area were significantly impacted by flow, surge, and rainfall. Low gradient streams were more impacted by compound flooding compared to steep streams. Inundation results showed that cities like Washington, DC will face increased flooding in the long-term future because of sea level rise (SLR), particularly during surge dominated flood events. Finally, the comprehensive analysis of the compound flooding in the region has led to the development of a real-time flood forecast system for compound urban flooding. The spatial and temporal distribution of flooding was significantly

captured by the forecast system. This study has provided scientific insights into the physical characteristics and spatial variability of the compound flooding in metropolitan areas along the estuaries and implemented the outcomes of historical data analysis for flood inundation modeling and developing a real-time forecast system for urban areas.

INTRODUCTION

Flooding causes severe damage to the economy and human lives every year. Major freshwater flooding events in the US from 2004 to 2014 caused an average annual damage of $9 billion (National Academies of Sciences, 2019) and the second costliest hurricane, Sandy in 2012, resulted in between $78-$97 billion in damages (Kunz et al., 2013). The dynamic coastal-estuarine regions are at the interface of multiple natural hazards like storm surges, tidal and riverine flooding, wind, and high precipitation. Such hazards can interact with each other and result in compound floods with significantly higher peaks than usual flooding events (Mortlock et al., 2018). Moreover, rapid urbanization, proximity to major rivers or lakes, risk of sea-level rise, and precipitation variability due to climate change can put further pressure on vulnerable coastal environments (Pasquier et al., 2018). While a significant dependence is not always existent between the compound flood drivers, it is highly uncertain how the climate can influence this complex non-linear relation in the future. The lack of adequate information on these interactions remains an important obstacle for decision-making (Pasquier et al., 2018).

Major floods in 2017 and 2018 are mostly remembered as coastal flooding events, but in many cases, intense rainfall and high storm surges resulted in compound flooding with higher peaks (University of Maryland and Texas A&M University, 2018). Few

studies have estimated the sensitivity of coastal regions to compound flooding (Pasquier et al., 2018; Paprotny et al., 2018). There has been considerable shifts in the pattern and intensity of flood that favor co-occurrence of high surges with high rainfall (Wahl et al., 2015; Saleh et al., 2017; Zscheischler et al., 2018). A number of studies have investigated statistically the complex dependence structure between the variables of compound flood such as rainfall and storm surges (Zheng et al., 2013; Wahl et al., 2015; Paprotny et al., 2018; Wu et al., 2018), river flow and storm surges (Svensson and Jones, 2002; Svensson and Jones, 2004; Kew et al., 2013; Paprotny et al., 2018; Sadegh et al., 2018; Hendry et al., 2019), and river flow and water level (Moftakhari et al., 2017; Bevacqua et al., 2019; Saleh et al., 2017; Mashriqui et al., 2014), and design discharge and sea level rise (Ward et al., 2018).

In the last few decades, major urban flooding has impacted coastal cities around the world including New Orleans, Rio de Janeiro, Queensland, Yangon, and Mumbai (Jha et al., 2011). While urban flooding has been widely studied, comprehensive investigations on compound urban flood variability in metropolitan areas located near a tidal river is still not available. Coastal metropolitan cities like Chicago, Houston, Baltimore, New York City, and Washington, DC are subject to compound flooding due to high riverine flow, runoff from inland precipitation events, local wind, and surge-driven coastal inundation along the tidal rivers (National Academies of Sciences, 2019). Recent advances in computational hydraulic modeling has allowed researchers to explore the dependence between hydrological extremes through different modeling techniques (Pasquier et al., 2018). Simplified one-dimensional (1D) modeling tools (Oubennaceur et

al., 2018; Adams et al., 2018), advanced multi-dimensional (1D/2D/3D) models and coupled hydrological-hydraulic or hydrodynamic models are being applied for more detailed simulation of river-floodplain interactions (Patel et al., 2017; Finaud-Guyot et al., 2011; Mark et al., 2004).

Investigating the propagation of compound floods into the inland areas of coastal and estuarine zones is extremely challenging due to the complex dynamics between hydrological and coastal processes, and the variation in meteorological drivers (Saleh et al., 2017; Dimitriadis et al., 2016). Advanced hydrodynamic models are being used to study the complex characteristics of flooding in the urban areas with multiple flood drivers (Barthélémy et al., 2018). National Weather Service (NWS) provides forecast on Potomac River flow, water level, and flash-flood events in the region (Mcenery et al., 2005) through the Advanced Hydrologic Prediction Service (AHPS). AHPS also provides flood plain maps for some areas based on the flood levels in Washington, DC station. However, there is greater uncertainty on how the flood at this station will propagate into inland flooding (Couasnon et al., 2019), especially in a real-time forecast system.

This study aims to provide reliable scientific information on the complex interactions of storm surge, wind, riverine flooding, sea-level rise, and runoff from high precipitation leading to compound flooding. The goal is to identify major flood drivers impacting the Washington, DC metropolitan area, quantify their impacts on compound flooding, and investigate how the compound flooding propagates into inland flooding. We assessed the variability of flood depth and extent resulting from different flood drivers, identified the hotspots of compound urban flooding, analyzed the compound

flood characteristics in the streams, and finally investigated the impact of sea-level rise and compound flood on the study area. The outcomes from this analysis were implemented in a hydraulic modeling framework for real-time urban flood forecast in the area. Studying compound flood variability in Washington, DC can be considered as part of a larger effort to explore the compound flooding along major rivers and large metropolitan cities. The science questions explored through this study are:

- *What are the major flood drivers that cause compound flooding in a river-estuarine transition zone? What is the impact of each flood drivers in generating the compound flood peaks in the tidal river?*
- *How does compound flooding in a tidal river impact the spatial and temporal variability of flooding in the urban areas? To what extent the compound flood drivers impact urban flooding?*
- *Can an integrated state of the art modeling framework accurately forecast compound flooding conditions in real-time?*

Chapter 1 addresses the first research question by identifying the major flood drivers impacting the metropolitan areas of Washington, DC located in a large tidal estuary. The contribution of each driver to the flood levels at DC station has been quantified through a number of steps. Flooding in Washington, DC has been classified into different types based on the flood drivers associated in the flooding events. This study implemented analysis of historical observations for different flood drivers and its interaction during the period of 1931-2019. To further analyze the impact of certain flood

drivers, a hydrodynamic model was implemented to simulate flood conditions in Washington, DC.

Chapter 2 comprises investigation of the spatial and temporal variability of the compound flooding in Washington, DC resulting from multiple flood drivers: riverine flow, coastal storm surges, and urban runoff. The impact of these flood drivers were estimated in different urban locations along the tidal Potomac River. Moreover, the propagation of flow and surge in the adjacent streams were investigated to identify the hotspots of compound urban flooding along the river and the streams. Finally, this study has investigated how sea-level rise can impact the flood prone areas in future. A 2D hydrodynamic model was implemented with a set of possible runoff, storm surges, and river discharges that can generate both extreme and non-extreme flood events.

Chapter 3 presents the development and implications of a real-time system with 2D hydrodynamic model along the tidal Potomac River to generate flood forecast for the rivers, streams, and inland urban areas. The system was tested for efficient and timely forecast for the region ahead of any severe flood event. Forecasted water levels and inland flood depths were validated by using information from different official and publicly available resources. The real-time system archives forecasted depths for a number of locations adjacent to the rivers and streams that are mostly impacted by compound flooding from coastal, riverine and runoff impacts.

1 COMPOUND URBAN FLOODING IN WASHINGTON, DC: A LOCAL APPROACH FOR STUDYING THE COMPOUND FLOOD CHARACTERISTICS IN LARGE METROPOLITAN AREAS ALONG TIDAL RIVERS

Abstract:

Flooding is one of the costliest natural hazards around the world and has significant social impacts in the United States (US). In recent years, the increasingly intense and more frequent floods in metropolitan areas, along large estuaries, have demonstrated the importance of understanding different flood drivers in river-estuarine transition zones. Predicting flood levels in real-time in tidal areas, where major rivers meet coastal and estuarine zones, is still challenging for operational forecasting. The goal of this study is to identify major flood drivers impacting the Washington DC area and to quantify their impacts on compound flooding. This study used the water levels at the Washington, DC station from the National Oceanic and Atmospheric Administration (NOAA) as a proxy to represent flooding in DC, and the surrounding communities in Maryland and Virginia. The region is often exposed to various flood hazards (high flow from major rivers, inland precipitation, and surge-driven coastal inundation) that overlap spatially and temporally, leading to the potential of *compound* flooding conditions. Results from the historical data analysis (1931 to 2019) provided strong evidence that *compound* flooding in this region can be caused by a combination of storm surge or high coastal water levels, riverine flow, local wind, and urban runoff. The co-occurrence of

multiple flood drivers resulted in *compound* flooding conditions that had the highest duration and magnitude during this period. Among the four *Major* flood events during this time, three were a result of *compound* flooding driven by a combination of riverine flow and coastal water levels and only one was a result of a riverine flow driven flood. However, storm-surge driven floods were more common in Washington, DC compared to riverine flow driven floods during this period for *Moderate* and *Minor* flood events. *Moderate* and *Major* flood stages were mainly the result of *compound* floods. Moreover, the local Southward and Northward winds with speed >5.5 m/s can significantly increase or decrease the water levels at Washington, DC, potentially playing a significant role impacting flood levels in the area. Finally, urban runoff also plays an important role impacting flood levels but only in certain conditions when impacts from wind and upstream flow or coastal water levels are negligible. While this study focused on the Washington, DC metropolitan region, it highlights the need to refine current forecast and design flood models in large estuaries by considering the potential complex interactions between different compound flood drivers that can be applicable to many large metropolitan areas located in tidal estuaries across the globe.

1.1 Introduction

Catastrophic flooding events challenge the global economy every year with widespread environmental, economic, and social consequences. Multiple compound flood events have impacted the US in recent years and the damages caused by the combined effects of storm surges and extreme rainfall during coastal storms have highlighted the importance of compound flooding studies (Van Oldenborgh et al., 2017).

Moreover, compound flood risk is comparatively higher for the Atlantic and Gulf coasts compared to the Pacific Coast, and such events have increased significantly over the past century at major coastal cities (Wahl et al., 2015; Aerts et al., 2013). For example, Hurricane Harvey, in 2017, demonstrated the destructive effects of compound flooding when precipitation and coastal flooding conditions occur at the same time or in quick succession (Saleh et al., 2017; Zscheischler et al., 2018). Hurricane Sandy, in 2012, caused widespread inland flooding in the New York City with the highest recorded storm surge in almost 300 years coinciding with high tide, high wind speeds, and waves (Zscheischler et al., 2018). Major floods in 2017 and 2018 (Hurricanes Florence, Harvey, Maria, and Irma) are mostly remembered as coastal flooding events, but in many cases, intense rainfall during the storms was the main cause of flooding (University of Maryland and Texas A&M University, 2018). Coastal cities, like Washington DC, will face flooding and subsequent environmental changes in future due to the sea level rise (Ayyub et al., 2012).

Studies from regional to global scale have developed conceptual models for quantifying the risk of compound flooding events in the present and under future climate (Huong and Pathirana, 2013; Bevacqua et al., 2017; Paprotny et al., 2018; Ward et al., 2018). Potential global hotspots under risk of compound flooding and its likelihood in Europe have been investigated by Paprotny et al. (2018) and Ridder et al. (2018). In the coastal areas of Netherlands, compound flooding occurs when storm surges prevent river discharge from flowing towards the open sea and, at the same time, high intensity precipitation inundates the urban areas (Van Den Hurk et al., 2015). A continental scale

study has considered the impacts of storm surges and river discharge based on its timing, joint statistical dependence, and return period (Couasnon et al., 2019) and found that this dependence is a result of the interactions between the synoptic weather systems and topography. Moftakhari et al. (2017) used a bivariate relation between riverine and coastal flooding conditions when either one of the factors was at its extreme state demonstrating how the dependence between these factors strongly influences the joint probability of flooding.

Existing methods examined statistically the complex dependence structure between proxy variables of different flood hazard types such as rainfall and storm surges (Zheng et al., 2013; Wahl et al., 2015; Paprotny et al., 2018; Wu et al., 2018), river flow and storm surges (Svensson and Jones, 2002; Svensson and Jones, 2004; Kew et al., 2013; Paprotny et al., 2018; Sadegh et al., 2018; Hendry et al., 2019), and river flow and water level (Moftakhari et al., 2017). Multiple studies have also analyzed the compound impact of tide and surge (e.g., Ikeuchi et al., 2017), design discharge and design sea level (Ward et al., 2018), and high sea-level and precipitation (Bevacqua et al., 2019). The statistical dependence between extreme rainfall events and storm surges has been demonstrated earlier (Van Den Hurk et al., 2015) and challenges remain to quantify its strength (Zheng et al., 2013). Fewer studies have investigated the sensitivity of coastal regions to compound flooding (Pasquier et al., 2018; Paprotny et al., 2018). No direct correlation between the compound flood drivers have been established so far, although numerous statistical methods have been suggested to quantify such compound events (Hao et al., 2018). Santiago-Collazo et al. (2019) reviewed the most recent studies on

extreme flood using compound inundation models and emphasized the need for the analysis of the complete interaction between storm surge, riverine flow, and rainfall induced runoff.

The goal of this study is to identify major flood drivers impacting the Washington, DC metropolitan areas in tidal estuary of the Potomac River and to quantify their impacts on compound flooding. This study focused on Washington, DC and the surrounding communities because the region is impacted by various flood hazards that lead to compound flooding conditions and can serve as an example to many major metropolitan areas around the globe situated in large estuaries. Furthermore, the impacts of climate change-driven sea level rise will likely increase flood risk in the area (National Capital Planning Commission, 2008). The main flood drivers identified for this study are: riverine flow, coastal water levels (storm surge), urban runoff, and local winds. The approaches implemented in this study were mainly based on the analysis of historical observations of different flood drivers and its interactions. However, to further analyze the impact of wind speed and direction, the Delft3D Flexible Mesh model (Deltares, 2019) was implemented to simulate flood conditions in Washington, DC. Furthermore, the methodology developed in this study can be applied to similar metropolitan areas located in the tidal regions across the globe which are affected by multiple flood drivers.

1.2 Methodology

1.2.1 Study Area

The Washington, DC Metropolitan Area is home to the capital of the US, several strategic Defense Bases, Federal offices, and headquarters of multiple international organizations. This area is currently highly urbanized and experienced significant flood-induced losses throughout time, which demonstrate its vulnerability to flood hazards. For example, the Great Flood of 1889 inundated the areas along Rock Creek near Washington, DC (Johnson, 1889). Extreme flooding was observed at Alexandria and Washington, DC due to the Chesapeake-Potomac Hurricane of 1933 (Roth and Cobb, 2001). Several low lying areas around the region including Haines Point, Navy Yard, and the Naval Air Station were inundated by the Great Potomac Flood of 1936 (National Weather Service, 2020a). High flood water reached the Jefferson Memorial during the Flood of 1942 (National Weather Service, 2020b). Little Falls and Rock Creek were flooded significantly during Hurricane Agnes in 1972 (National Weather Service, 2020b).

The region (Figure 1) is located within the Chesapeake Bay Watershed along the upper tidal Potomac River, the Anacostia River and several urban and sub-urban watersheds such as the Rock Creek Park, Four Mile Run, Difficult Run and many others. The drainage area of the Anacostia River is 315 km^2 and the Rock Creek is 160 km^2, which are very small compared to the Potomac River drainage area of 30,000 km^2 (Huanxin et al., 1997). The tidal Potomac River has a total distance of approximately 183km. This river flows downstream from Washington, DC and connects with the Chesapeake Bay at Lewisetta, VA. The Chesapeake Bay, the largest bay in the US, with

the length of 320 km, is a partially mixed estuary (Cho et al., 2012). The tides in the Potomac River originates from the Atlantic Ocean and propagates into the river through the Chesapeake Bay (Wang et al., 2015). The tidal Potomac River, from Indian Head, MD to Chain Bridge, VA, is about 50 km long and includes the Anacostia River, Tidal Basin, Washington Channel, Roosevelt Island Channel, Broad Creek, Dogue Creek, Piscataway Creek, Pohick Bay, Gunston Cove, and tidal inlets of Accotink Bay (Schaffranek, 1987). The tidal range near the entrance of the Potomac river from Chesapeake Bay is about 0.3 m and near Washington, DC is 0.8 m (The Great Chesapeake Bay Swim, 2019).

Washington DC station is particularly an interesting site to study compound flood. Lewisetta geographically and hydraulically defines the boundary between the Chesapeake Bay and the Potomac River. The tidal and surge propagation from Lewisetta (mouth of the Potomac River in the Chesapeake Bay) to the upstream is well studied (Mashriqui et al., 2014; Feng et al., 2017; Khalid and Ferreira, 2020). Moreover, Mashriqui et al.(2014) studied the effect of freshwater and coastal water events on Wisconsin Avenue (WA) and the DC station and found that the DC station has significantly greater tidal influence compared to the WA even though they are located in close proximity. Furthermore, wind and surge propagation from the Chesapeake Bay have optimal conditions to propagate water towards DC (Mashriqui et al., 2014). The study by Feng et al. (2017) showed that the annual peak at DC is temporally associated with the annual maximum upstream freshwater flow input or downstream water level or sometimes both. Moreover, Feng and Brubaker (2016) has concluded that using the DC

data as a proxy for the annual peaks at their Washington, DC inland site was a reasonable approach as it covers all the possible upstream and downstream events that cause the annual peak in the study site (Feng and Brubaker, 2016).

1.2.2 Data Processing

This study considered instantaneous, hourly and daily mean data of streamflow, water levels, and wind magnitude and direction at 10 meter height from 1931 to 2019. Historical streamflow data for flood analysis was collected from the United States Geological Survey (USGS, 2020), and the wind and water level data were collected from the National Oceanic and Atmospheric Administration's Tides and Currents database (NOAA, 2020a). Rainfall data was collected from the National Centers for Environmental Information (NOAA, 2020b). In order to evaluate the effects of riverine-driven flooding in the region, we defined the Little Falls Gage Station (USGS gage: 01646500) flows at the Potomac River as a proxy for riverine flows. Flooding from the Anacostia River was only observed when the Potomac River was also flooded (National Capital Planning Commission, 2008). A report by (National Capital Planning Commission, 2008) has concluded that the Anacostia river flow is high during the events when Potomac River flow is also high. We have found similar results from our analysis as well. For example, the Northwest and Northeast Anacostia rivers had the maximum streamflow of 509 m^3/s and 340 m^3/s on Jun 22, 1972, the same date when the Potomac River flow was high due to flooding from hurricane Agnes. Appendix E (Figure E1) shows different events during which both Potomac and Anacostia River flow were high. Therefore, the Anacostia River flooding had no independent impact as a flood driver in

Washington, DC. However, we used the Anacostia River flow as an upstream boundary (USGS gage: 01651000 and 01649500) for the Delft3D FM model to simulate the water level in the full model domain.

In order to evaluate the impacts of storms surges or coastal effects, we relied on a downstream boundary condition at Lewisetta, VA (NOAA station: 8635750) that would represent the influence of the coastal water levels from the Chesapeake Bay towards flooding in Washington, DC. Sewells Point (NOAA station: 8638610) water level data was also used as a proxy to complement the missing data at Lewisetta for the years of 1931-1979. Sewells Point station is about 134 km downstream to Lewisetta (See details in Figure D2 of Appendix D). Studies also suggest that local winds can have an effect on water levels in the Potomac River (Mashriqui et al., 2014; Wang et al., 2015). Therefore, we relied on the Washington, DC station (NOAA station: 8594900) as a proxy for wind-driven flooding in DC and collected water level (period: 1931-2019) and wind (period: 2008-2019) data from this station. Moreover, the streamflow at Rock Creek (USGS gage: 01648000) and rainfall at the Washington Reagan National Airport (COOP: 448906) were used to represent urban runoff driven flood conditions.

There is only one station for wind data in Washington, DC, but it provides a reasonable proxy for the impact of wind on water levels. We analyzed the impact of wind collected from the DC station to the water level of the same station. Therefore, this minimizes the variability of wind impact on water level. Similarly, the rainfall is highly variable in the region. Moreover, the Potomac River watershed covers a significantly large area. While Little Falls flow includes the rainfall impact in the large upstream

watershed, there is still rainfall over the urban areas which contribute to inland flooding separately. In order to account for urban flooding, we selected one station at Rock Creek as a proxy to represent local rainfall generated urban flooding because the only rainfall station in the region, located at Reagan Airport, no longer provides observed data. The stream flows in Rock Creek and the other adjacent streams are presented in Figure B6 (Appendix B).

In this analysis, the station names were presented in short forms like Little Falls = LF, Washington, DC = DC, Lewisetta = LWT, Anacostia = ANA, Sewells Point = SWP, and Urban Runoff or Rock Creek = RC. The study area with the locations of the stations upstream and downstream of Washington, DC is shown in Figure 1.

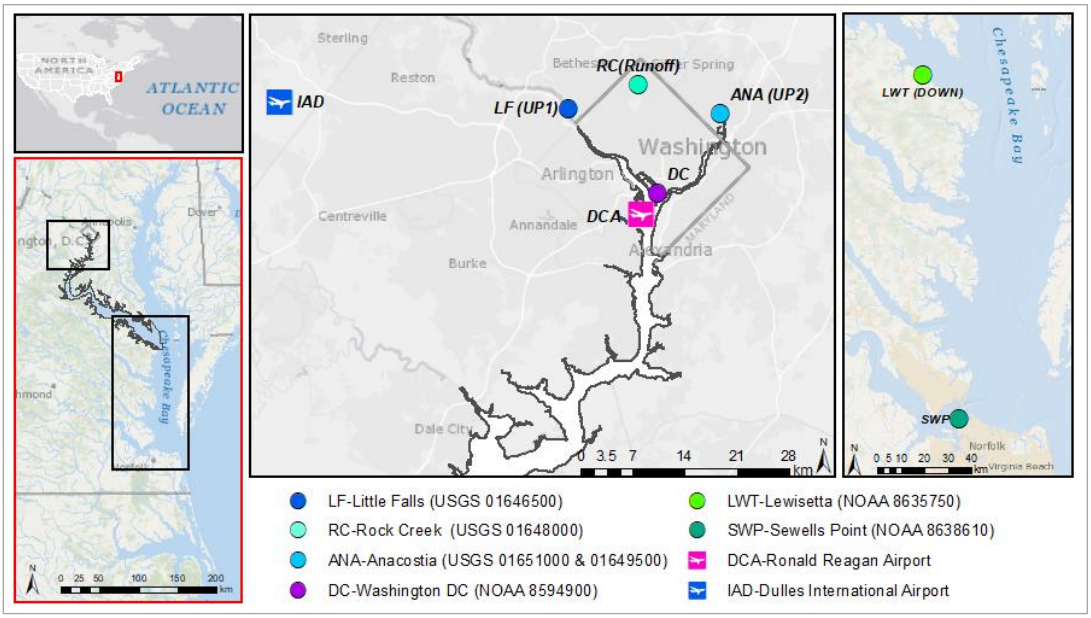

Figure 1 Study area with the locations for available data (UP1 = upstream boundary at Potomac River, UP2 = upstream boundary at Anacostia River, Runoff = urban Runoff boundary, and DOWN = downstream boundary at Lewisetta)

The data analysis was divided into three periods: a) 1991-2019 b) 1980-1990 and c) 1931-1979. Data for the most recent period (1991-2019) was available with the smallest recording interval time (15 minutes from the USGS and hourly from NOAA). On the other hand, from 1980 to 1990, the USGS data (LF flow) is only available on a daily average temporal scale and it was converted into daily maximum data. The converted dataset was validated against the LF flow from 1991-2018 with an agreement of $R^2 = 0.97$. See Appendix D (Figure D1, D2, D3, and D4) for further details. R^2 describe the degree of collinearity between datasets. The correlation coefficient, which ranges from −1 to 1, is an index of the degree of linear relationship between two observed and simulated. If correlation co-efficient (r) = 0, no linear relationship exists. If r = 1 or −1, a perfect positive or negative linear relationship exists. Similarly, R^2 describes the proportion of the variance in measured data explained by the model. R^2 ranges from 0 to 1, with higher values indicating less error variance. Typically R^2 values greater than 0.5 are considered acceptable, indicating that the simulated data can significantly represent the observed values (Moriasi et al., 2007).

In order to make the daily maximum water level at LWT consistent with the LF daily scale, the daily water levels were calculated for 1980-1990 from the hourly data. From hourly data of Lewisetta water level, we selected the maximum value from each day between 00 hours to 23 hours. A flowchart is presented to summarize the processing of the data in Appendix D (Figure D4). The dataset from 1931-1979 also only had daily maximums, except that SWP data was used as a proxy to missing LWT data. The proxy dataset was used after calibrating, validating (period 1991-2019), and adjusting for

5 hours of time difference to correspond with the LWT observation, presenting a R^2 value of ~0.7 (Appendix D). While the datasets from 1931-1979 were analyzed to understand the impact of flood drivers, these results are not presented in the figures. The data analysis mainly focused on the most recent 1980-2019 dataset as all the LWT, LF, and RC stations had available data.

The National Weather Service (NWS) provides different flood stage values such as *Action*, *Minor*, *Moderate*, and *Major* at different stations across the nation (National Weather Service, 2020c), which were used to identify and classify flood levels at the DC station, as a proxy of flood levels in the DC region (Table 1). The levels displayed are station or point measurements by NWS. These station measurements also represent the same flood types in the surrounding area. If the stage at any station is equal to or above *Action* stage, it is identified to be at flood stage. A flood day was defined as a day in which daily maximum water levels at DC equaled or exceeded the NWS *Action* stage. On the other hand, flood event duration consisted of a number of days during which the DC station was flooded continuously above action stage, and therefore, the duration was variable.

In this paper, water level exceeding the action stage is considered as flooding if no specified flood stage is mentioned. The areas impacted by compound flooding in the region, by definition are close to the tidal-riverine environment and are well represented with a proxy station such as the Washington, DC station. Water level in DC has been used by NWS (see Appendix E) as well to identify the flood inundation in the city. We used a similar approach where the flooding in DC area can be estimated by the water

level at DC station. In practice, a flood warning is issued when *Moderate* or *Major* flooding is expected during an event (NOAA, 2020c). In order to use a consistent unit system, the vertical datum was converted from NWS stages to NAVD88 stages, and the units from feet to meter for this study. Finally, a rating curve data from the USGS was used to convert LF and RC streamflow data into water levels (Equation D3, Appendix D) to compare with the NWS flood stages.

Table 1 National Weather Service flood stage categories (NOAA, 2020c)

Stations (Datum:NAVD88)	***Action***	***Minor***	***Moderate***	***Major***
LF (stage m)	1.52	3.05	3.66	4.27
Estimated (flow m^3/s)	~ 610	3790	5100	6450
DC (stage m)	0.7	0.85	1.19	1.7
LWT (stage m)	0.51	0.66	0.82	0.97

1.2.3 Flood Types in Washington, DC

The four flood drivers analyzed for this study are: riverine flow, coastal water level (storm surge), urban runoff, and local winds. In order to estimate the flooding potential of different flood drivers at the DC station, each flooding event in the historical period was classified as *river* flood, *coastal* flood, *compound* flood and *other* flood (to potentially include urban and wind-driven flooding). The basic assumptions for our analysis were:

i. *River* flood: DC flooded only due to high riverine flow from LF (LF>1.52m stage) and LWT was below *Action* stage;

ii. *Coastal* flood: DC flooded only due to high coastal water level from LWT (LWT> 0.51m stage) and LF was below *Action* stage;

iii. *Compound* flood: LWT, LF and DC were all flooded (LF > 1.52 m, LWT > 0.51 m stage) during the same event. The term 'single-peak *compound* flood' or here after '*compound* flood' was used when the flooding event had only one peak resulting from both riverine flow and coastal water level for the duration of the event.

iv. Multi-peak *compound* flood: a '*compound* flood' event that had more than one significant flood peaks at the DC station during the same event, both from riverine flow and coastal water level over multiple days.

v. *Other* flood: DC was flooded (DC > 0.7 m stage) but neither LF nor LWT flooded (LF < 1.52 m, LWT < 0.51 m stage).

The sources of such flooding can be either runoff or wind. The runoff is actually a proxy of the rainfall-generated local urban runoff and represented by the streamflow in Rock Creek. Runoffs generated from nearby streams (smaller watershed) are termed as urban runoff in this study. Such runoff may not be always the contributing factors for flooding in DC. However, in some cases, when there is a high intensity rainfall within short period of time, the resulting runoff can be a dominant flood driver. Moreover, wind speed in certain directions can also contribute to flooding in DC by increasing the water level. For example, during the *other* flood in 2012, the DC peak was at the Minor stage but neither LF nor LWT could reach the Action stage. Such events are usually generated from wind or local runoff.

Examples of these four types of flooding (*river*, *coastal*, *compound*, and *other*) events are showed in Figure 2. During Hurricane Isabel in 2003, a *Major* coastal water level from LWT generated the first flood peak in DC. After few hours, DC started to reach flood stage again due to a high riverine flow that hit the station and generated two other peaks in the next two days. This event had three types of peaks: one *Major* flood peak from coastal water level, one *Minor* flood peak from riverine flow, and then a *Moderate* flood peak from both riverine flow and coastal water level. During the *other* flood in 2012, the DC peak was at the *Minor* stage but neither LF nor LWT could reach the *Action* stage. In some days, LF or LWT were above action stage but DC did not have any flooding. Such events were classified as *no floods*. Although our study did not focus on this category, such events helped to demonstrate the impact of flood drivers in reducing the peak at DC.

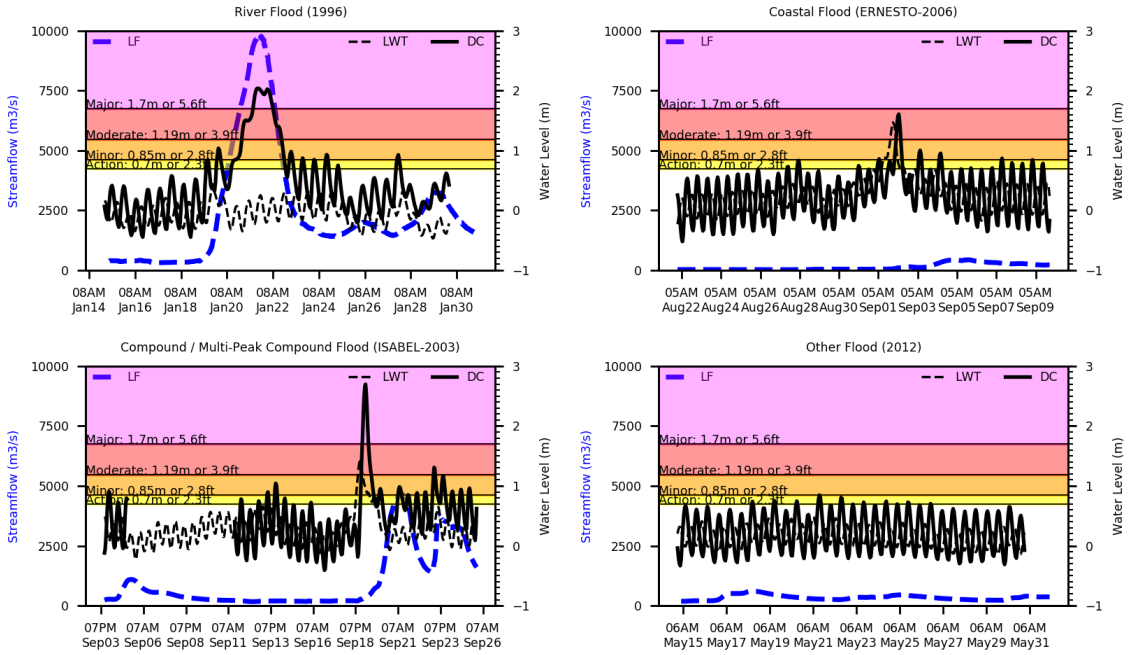

Figure 2 Different types of flooding in the study area (blue dotted line is flow at Little Falls, black dotted line is water level at Lewisetta and black firm line is water level at Washington, DC. Time is in UTC)

Flooding events from different hurricanes were also classified based on these four types. Due to the unavailability of continuous hourly data, the hurricanes were analyzed for the period of 1991-2019. In the years 1994 and 2004, the stations had a large amount of missing data (Jan-Sep) and no significant flooding occurred during the last three months (*Action* flood of 0.82 m in 1994 and *Minor* flood of 1.04 m in 2004). Therefore, those years were excluded from the daily flood analysis.

1.2.4 Impact of the Flood Drivers

The contribution of each flood drivers at the DC station was evaluated considering multiple factors. Time lag between the DC peak and Lewisetta or Little Falls peak was estimated by plotting a large number of events. The duration of an event in DC was also estimated to define how long flood waters can stay in the area when a flooding

occurs either from a single driver or multiple drivers. Time lag was an important parameter in classifying the peak water level in DC. The time lags were measured for 336 storms during 1931-2019 by calculating and analyzing the time of peak for the flow and water levels at different stations. It was observed that the peak at DC occurs 6-8 hours after the peaks at Lewisetta. However, the flow at Little Falls and water level at DC start to increase almost at the same time and decrease also at the same time, therefore time lag is zero for these two stations. A detailed method on time lag is added to the Appendix B (Figure B3 and Table B1). The flood components at different stations are presented in Figure 3, where Δt is the time difference between the peaks at upstream riverine flow (LF) or downstream water levels (LWT or SWP) and the peaks at DC, Δd is the total duration of an event in any station, and the ΔF values show the magnitude of the water level above the action stage. The main focus in this study was the Δd and ΔF for DC, meaning the magnitude and duration of flood at DC. The value of Δt between LF and DC is approximately 0 hours while between LWT and DC is 6-8 hours. The subscripts represent the station names (Little Falls - ΔF_{lf}, Washington, DC- ΔF_{dc}, Lewisetta -ΔF_{lwt}, and Sewells Point - ΔF_{swp}). Water level peak at DC were presented as total water level (F_{DC} or ΔF_{dc} + action stage) where, F_{DC} = impact from LF + LWT+ other flood drivers.

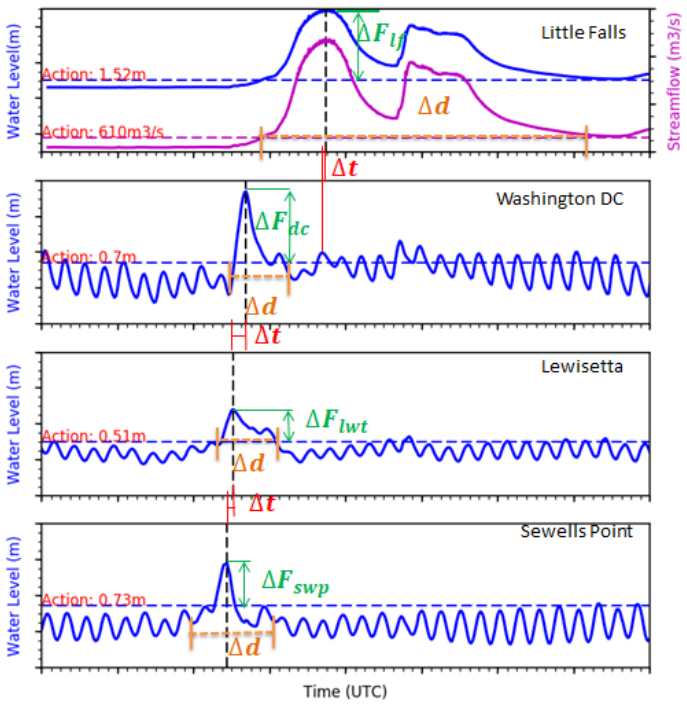

Figure 3 Flood components at different stations (purple line shows streamflow and blue line shows water level)

A bivariate probability distribution was generated using the riverine flow and coastal water levels data to identify the range of flow and water level that are more likely to coincide and cause flooding in DC. The two variables, flow in Little Falls and surge in Lewisetta are considered independent due to the low correlation (0.16) and lower R^2 (0.01) values between them (presented in Appendix C). Annual maximum flow at Little Falls and annual maximum water level at Lewisetta were used to generate a bivariate probability distribution. Annual maximum flow at a range between 0-10000m^3/s with an interval of 1000m^3/s and water level range of 0-2m with an interval of 0.2m was used to generate the probability distribution. Chi-square goodness-of-fit test was used to determine how well the data fits into normal distribution and the test decision h = 0

proved the data to have normal distribution at the 5% significance level. Correlation matrix may not provide a complete understanding of the interactions between the drivers (Moftakhari et al., 2017), it can still provide an understanding of the dependence between the drivers. However, a high correlation (0.91) between coastal water level and DC flood level was observed. Based on previous numerical studies (Mashriqui et al., 2014; Feng and Brubaker, 2016; Feng et al., 2017; Khalid and Ferreira, 2020) and our high correlation results, we have demonstrated that Lewisetta or coastal water level has significantly higher impact on DC flood level (dependent variable) than any other drivers. The independent variables or the flood drivers were weakly correlated (<0.35) and the R^2 values are less than 0.1(Appendix C). A multivariate regression analysis (Table 2) was performed for estimating the relative contribution of the flood drivers (riverine flow, costal water level, urban runoff, and local wind speed and direction) to flooding at the DC station. We selected 336 storms from 1931-2019 and generated scatter plots for estimating the R^2 values and also the correlation matrix. The time period for the regression analysis was 2008-2019 due to the availability of continuous wind data.

Table 2 Regression Outputs

Regression Statistics	
No. of Observations	336
R Square	0.75
Intercept	0.19
Flood Drivers	*Coefficients*
LF	0.13
LWT	0.91

The equation for estimating the contribution of each flood river is:

Equation 1

$$LF * RF + LWT * CF + RC * UF + SPD * WF + Intercept = F_{DC}$$

Equation 2

$$LF * 0.13 + LWT * 0.91 + RC * 0.05 + SPD * (\pm 0.02) + 0.19 = F_{DC}$$

where, RF = River factor, CF = Coastal factor, UF = Urban factor, WF = Wind Factor. The units of the drivers are meter for LWT, LF, and RC because flow is converted to water level using the rating curve equation for respective stations. Wind speed (SPD) unit is m/s. RF, CF, and UF has not unit. Unit of the Intercept is meter. Wind factor, WF is in seconds, so that (m/s)*s = m.

1.2.5 Numerical Modeling of Wind Impacts at the Washington, DC Station

Due to the short data record and complex changes in magnitude and direction of the wind in the region, it was difficult to isolate the impacts of wind forcing from the other flood drivers. Note that major wind-driven circulation in the Chesapeake Bay is already taken into account on the coastal water levels from LWT. However, the effects of local winds impacting water levels between LWT and the DC station are not captured when using the water levels in LWT as a proxy for coastal effects. Therefore, in order to expand the wind conditions observed in the shorter historical period and isolate its impact, a set of numerical model simulations were performed. The Potomac and Anacostia Rivers were modeled as unstructured numerical grids using Delft3D Flexible Mesh Suite (Deltares, 2019). The study area was divided into three reaches along the Potomac and the Anacostia River: Upper Potomac, Lower Potomac, and Lower Anacostia. Rock Creek was added as a tributary to the model. Therefore, the model had

four boundaries: Little Falls, Lewisetta, Anacostia, and Rock Creek. A Manning's roughness coefficient of 0.015 was used for all the grids with a uniform viscosity value of $10 m^2/s$ after calibrating the model. Detailed calibration on Manning's n and horizontal diffusivity and viscosity are provided in Appendix A. The hydrodynamic model simulates water level only within the rivers. However, as mentioned earlier, information of this simulated water level can be translated to the inland inundation. Two observation stations were added to monitor the water level outputs. One was near Dahlgren, VA and the other one was at the Washington, DC gage location.

The model was set-up with the upstream and downstream boundary conditions using streamflow and water level data respectively similar to the proposed study area. The highest maximum observed wind speed at Washington, DC station during the historical period (2008-2019) was approximately 15 m/s. However, maximum wind speed in the International Airport at Dulles and Reagan National Airport (location shown in (Figure 1) during 2000-2010 was approximately 30 m/s (Lombardo and Ayyub, 2015). Therefore, we used a maximum wind speed of 30 m/s for the model simulations. In this study, 30m/s speed is considered as the maximum range for model simulations to provide a high end margin. The airport stations mentioned in the study are close to the DC station. Also, we are not considering impact of wind directly to the urban environment; rather we only consider the impact of local winds on the DC water level, which is later translated to flood inundation in the urban area. This is a hypothetical evaluation to investigate the potential impacts of different local wind magnitudes and direction to the local flood levels. To provide further details, inland flood inundation

based on DC flood stages is presented in Figure E3 of Appendix E. Northward wind in the Potomac River can push the water downstream and Southward wind can push the water upstream (Wang and Elliott, 1978). Wang et al.(2015) also identified wind as a potential factor for Potomac River along with fresh water flows and tides. The most frequent wind speed in the station was 1-6 m/s, while the threshold for significant impact was 5.5 m/s. Therefore, the wind impact on flood levels at the DC station was investigated by forcing the model with 2, 4, 5, 10, 15 and 30 m/s wind in both North and South directions for *other* events only. In the next step, all the four types of flood (*river*, *coastal*, *compound*, and *other*) and *no flood* events were forced with 30 m/s wind speed to six directions for calculating the probable maximum change of DC peaks due to local wind effects. These simulations helped to estimate the dependency between the water level and wind speed at different speeds and directions.

1.3 Results and Discussions

1.3.1 Quantification of Flooding in Washington, DC

1.3.1.1 Identifying Flood Days for Each Flood Types

The Washington, DC *Major* floods in DC were not as common as the *Moderate* floods (Figure 4). It was evident that *Moderate* flooding can occur before and after *Major* flood days indicating the potential for higher peaks and longer flood duration. For example, a *Major* flood impacted the area in Nov 5th, 1985 while the previous day had a *Moderate* flooding. In the 62 days of *Moderate* flooding during 1980-2019, March had the maximum *Moderate* flood days. The highest number of moderate flood days was

observed in 2018 (14 days) and the second highest was in 2011 (9 days). As expected, the *Action* and *Minor* floods were more frequent but with lower impacts.

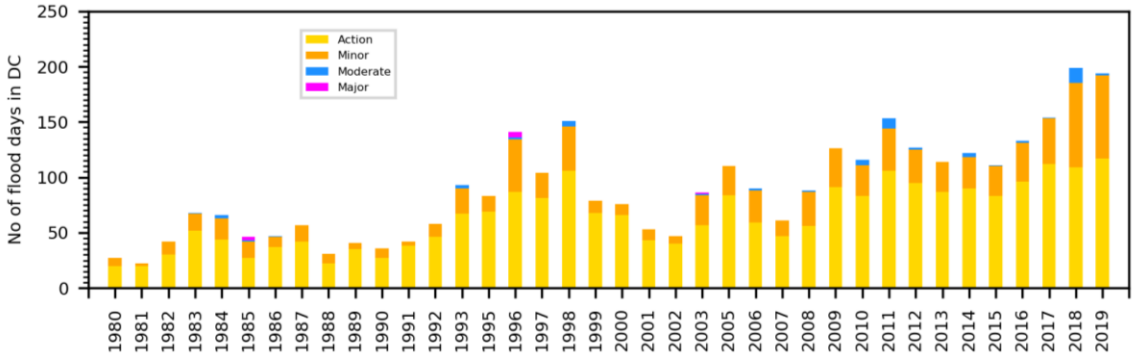

Figure 4 Number of flood days in Washington, DC for each flood stage category

The classification of the flood days per flood driver (*river*, *coastal*, *compound*, and *other*) is shown in Figure 5. This analysis demonstrates an increasing linear trend in the number of *coastal* flood days from 1980 to 2019, which can be correlated to the long-term trend of increasing water levels in the Chesapeake Bay. For example, the SLR rate for Lewisetta is 0.0054 m/year with 95% confidence interval of +/- 0.00061 m/year (NOAA, 2020a). On the other hand, *river* flood days did not have any specific detectable increase over the years. The *river* flood days were higher during two of the *Major* flood years (1996 and 2003) and also in 1998 and 2018.

A detailed analysis to identify the cause of *other* floods suggested that the urban runoff, wind speed, and direction provided significant contributions for the *other* flooding events. Few events were the product of urban runoff or higher streamflow from adjacent small streams. However, further analysis suggested that these events can cause

widespread urban flooding while not causing considerable impact in the DC river station. Dependence between surge and rainfall was studied by Paprotny et al. (2018) in areas close to the ocean and such dependence was evident along the coastlines of the United States (Wahl et al., 2015). Besides, precipitation and extreme winds can co-occur in some coastal areas (Zscheischler et al., 2018), which was evident during the runoff induced flood of June 2015. However, in local scale, high dependence was not present between surge and urban runoff in DC because of the spatial difference resulting from the 160km distance from the bay. Rainfall induced runoff was observed in Rock Creek 1-2 days before the surges from hurricanes Fran 1996 and Isabel 2003 because it was raining in DC region as well. However, the correlation of these variables was very low (0.01). Moreover, the combination of wind speed > 5.5 m/s and extreme rainfall induced urban runoff before and after coastal storms can contribute to flooding in DC.

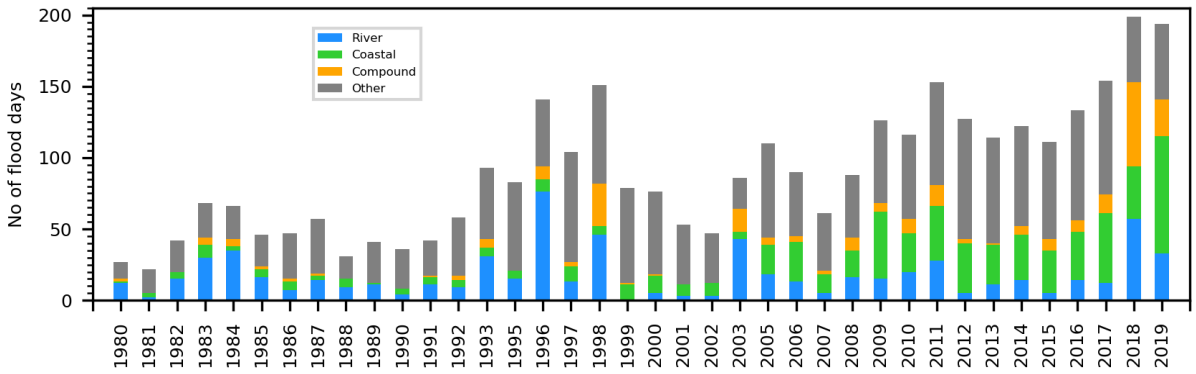

Figure 5 Classification of the DC flood days

1.3.1.2 Maximum Flood Potentials

Flood events were ranked based on magnitude and duration as presented in Figure 6. *Major* flooding in DC resulted mostly from *compound* flooding events. However, the river flow also had the potential to cause *Major* flooding in the National Capital Region in one event. Among the four *Major* events, three were *compound* flooding and the other one was a *river* flood. These four events caused widespread damage and are known as 1985 Election Day flood, The Winter flood of January 1996, Hurricane Fran 1996, and Hurricane Isabel 2003. The blue bar above *Major* flood line in Figure 6 shows the *river* flood of 1996. The flood of Jan 1996 originated about two weeks before the event from snow melted increased river flow due to high temperature and rainfall (US National Weather Service Baltimore/Washington, 2020). This was a fully freshwater or *river* flood from upstream riverine flow and was equally damaging as the tidal flood of 1985. The Tidal Basin and Old Town Alexandria also experienced severe flooding during this event. There were 34 *Moderate* flood events with 23 *compound* floods, 9 *coastal* floods and 2 *river* floods during 1980-2019. Total number of *other* flood events was 213 while the total number of *river*, *coastal*, and *compound* floods was 251. Among the eight *Major* floods from 1931-1979 (not shown in figure), three were *river* floods (Great Potomac Flood of 1936, Record Flood of 1942, and Hurricane Agnes in 1972). The other five events were *compound* events, including the Chesapeake-Potomac Hurricane of 1933 and Hurricane Hazel of 1954. Maximum duration during this time period was 11 days for *compound* flood, 10 days for *river* flood and 5 days for *coastal* flood.

The ascending order of flood duration shows that flood durations during *compound* events were significantly higher than *river* or *coastal* floods in DC. The highest five durations (13-22 days) were observed during *compound* and multi-peak *compound* flood events. A *river* flood in 2003 had the maximum duration of 12 days while for *coastal* event the maximum duration was 11.5 days in October 2013. The timing of the peak for each flood driver (Kew et al., 2013; Klerk et al., 2015; Wahl et al., 2015; Moftakhari et al., 2017; Wu et al., 2018; Couasnon et al., 2019) or distance between the sources of those flood drivers (Zheng et al., 2013) can play important role in measuring the *compound* flood potential. The dependence between the flood drivers can be strongest when occurred simultaneously (Svensson and Jones, 2004). However, considering only the day of maximum peak can often underestimate the other peaks of the same event coming from multiple flood drivers in the consecutive days. The total duration of flood provided the scope to estimate the highest maximum flood potential at DC by allowing sufficient lag time for all the flood drivers to have their impacts on DC. This analysis showed that considering only the riverine flow or coastal water level independently would have underestimated the *compound* flood peaks and flood duration at DC during Hurricane Isabel, because the event was a combination of three different peaks from coastal and riverine water. Kumbier et al. (2018) suggested that ignoring the riverine flow in coastal areas can underestimate the flood extent by 30% and flood depth by 1.5m. A summary of the *Major* floods from 1931-2019 is presented in Table 3.

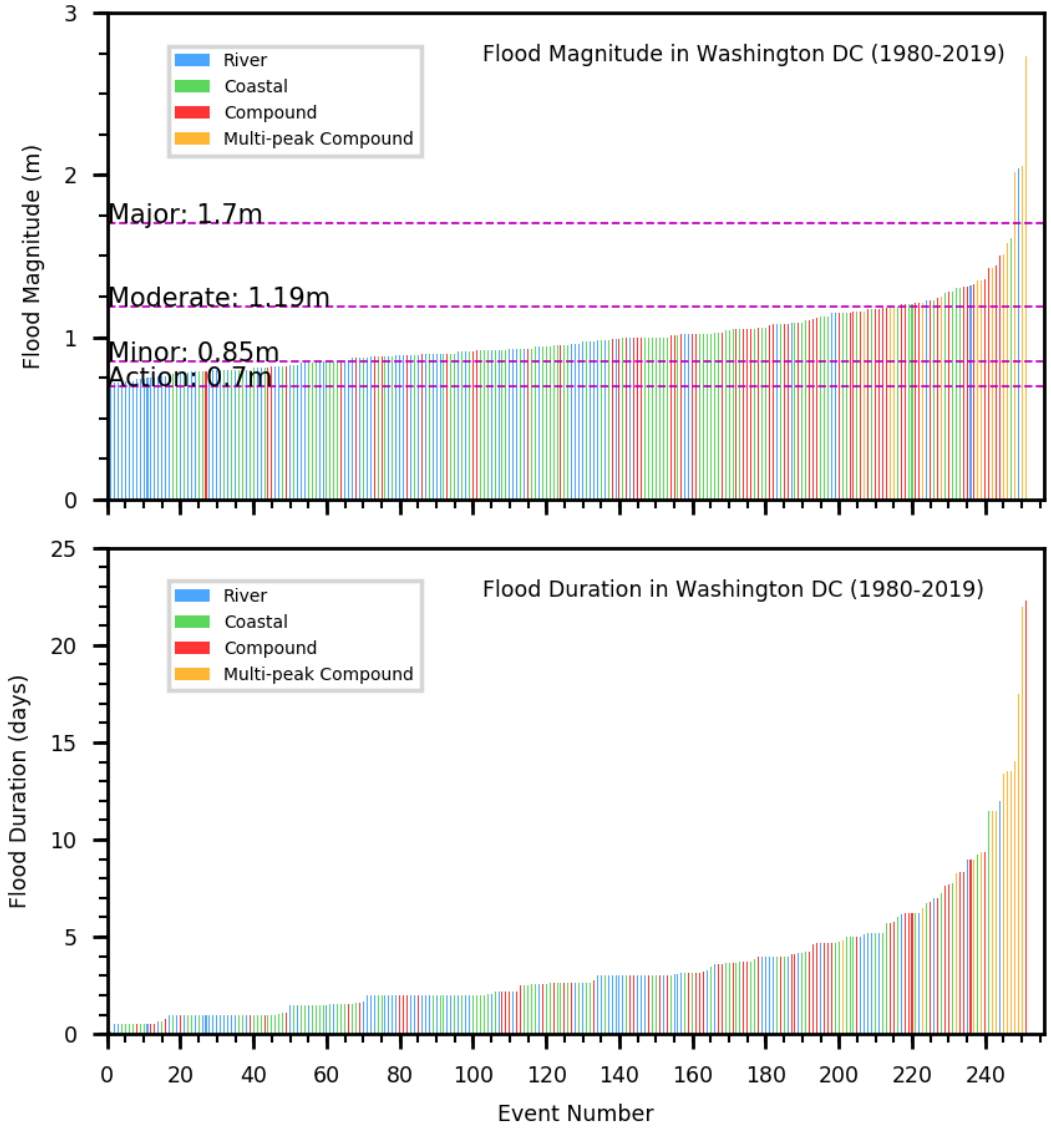

Figure 6 Flood magnitude and duration over the years (1980-2019)

Table 3 Major floods during 1931-2019

Major Flood Events in DC	DC WL (m)	Type
Chesapeake-Potomac Hurricane 1933	2.60	Multi-peak Compound
Great Potomac Flood of 1936	2.79	River
Flood of 1937	2.22	Multi-peak Compound
Record Flood of 1942	2.95	River
Hazel 1954	1.93	Compound
Hurricane Agnes 1972	2.22	River
Flood of 1974	1.84	Compound
Flood of 1979	1.76	Compound
1985 Election Day floods	2.02	Multi-peak Compound
The Winter Flood of January 1996	2.04	River
Hurricane Fran 1996	2.06	Multi-peak Compound
Hurricane Isabel 2003	2.73	Multi-peak Compound

1.3.1.3 Flood Type Attributed to Flood Stages

The relative number of different flood types for each flood stage is shown in Figure 7. Most of the *Action* stages at DC were attributed to the *other* flood types resulting either from local winds or urban runoff. Based on the detailed analysis, urban runoff and wind were the flood drivers that caused flooding in DC when neither LF nor LWT had any flood level. Therefore, these two drivers were attributed to the *other* flooding category in the area. The plot is shown in the Figure E2 in Appendix E. The floods when LWT<*Action* stage and LF<*Action stage* are flooding in DC that cannot not be explained by these two drivers. During those events, either runoff was high or wind direction was upward from Bay towards DC. Such *Action* stages were also generated by *river* and *coastal* floods but those were much less in number compared to the ones generated by wind and runoff. While *Minor* stages were mainly the result of *coastal* floods, some *river* and *compound* floods and very few *other* floods also brought *Minor* flood stages in DC. *Moderate* and *Major* flood stages were mainly the result of

compound floods. Although *coastal* floods could reach *Moderate* flood stage in the region, these did not show any potential for generating a *Major* flood stage. However, *river* flood alone did show the potential for such *Major* flood stage during this period.

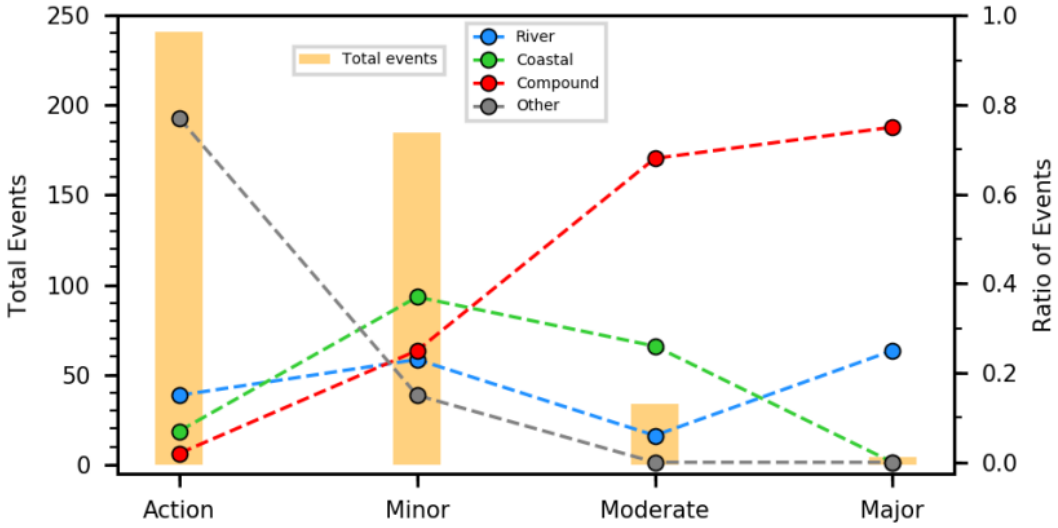

Figure 7 Relative number of different flood types in DC

1.3.1.4 Relevance of Each Flood Components

In order to understand the relevance of the flood drivers, different flood types and their magnitudes at LF, LWT and, DC are shown in Figure 8. The circles in this plot are not single events; rather they represent all the significant peaks of any event. For example, Isabel 2003 was a multi-peak *compound* flood; one peak was from coastal water level (LWT) and other peaks were from riverine flow (LF) and a combination of both. This event had three circles, indicating the relation between first peak at DC with LWT peak, the second peak at DC with LF peak and the third peak at DC with another LF and LWT peak. When LF and LWT were at *Action* stage, they generated an *Action* stage

flood at DC. It was also evident that, most of the time, floods from LF did not reach DC if LF was in *Action* stage and LWT was below the threshold value of 0.35m. The threshold range of 0.35 m-0.49 m water level at LWT had the potential to cause flooding in DC, although it was below *Action* stage (0.51 m) in LWT itself. Similarly, a threshold for the stage at upstream (LF) was estimated as 1.4 m, which can cause flooding in DC although LF is below *Action* stage (1.52 m). Therefore, several combinations of the threshold values and flood stages for the flood drivers can be attributed to the flooding in DC. Sadegh et al. (2018) and Ward et al. (2018) used an advanced statistical technique, copula based methods, for estimating the co-occurrence of flood drivers by using annual design discharge and water level.

An *Action* stage water level at LWT can generate a *Moderate* flood at DC when high winds speed pushes water upstream. No such impact was observed on *river* flood at DC. Therefore, the wind impact was higher on tide dominated floods compared to flow dominated floods. Winds with speed >5.5 m/s can push water from the Potomac towards the Chesapeake Bay and reduce the water level in DC (Mashriqui et al., 2014b). For example, in the presence of a high Northward wind, *Major* flood stage at LWT created *Minor* floods at DC. The green circles in the light green shaded area above the *Major* flood line show such events. *Other* floods can be attributed to urban runoff or wind speed or in some cases threshold values of costal water level and riverine flow. Thus, by analyzing the relevance of the flood drivers, we could distinguish the situations favorable for *Action*, *Minor*, *Moderate,* or *Major* floods in DC. Some of the major coastal flooding (in LWT) is shown as minor (in DC), because the water level was major in LWT but it

caused a minor flood in DC. This indicates that probably there was another flood driver reducing the impact of LWT water levels at DC by decreasing its peak. In later discussion in the manuscript (Figure E2 in Appendix E), we hypothesize that this is due to the local wind effects. We further demonstrate that the local wind can impact the water levels at the DC station by generating minor floods even though LWT water level is high enough to cause a major flooding. Similarly, wind direction and speed can change a water level below *Action* stage and increase to an *Action* or higher stage flood. Furthermore, we provided historical evidence from storms in the paper (Figure 13) in which these exact effects are observed.

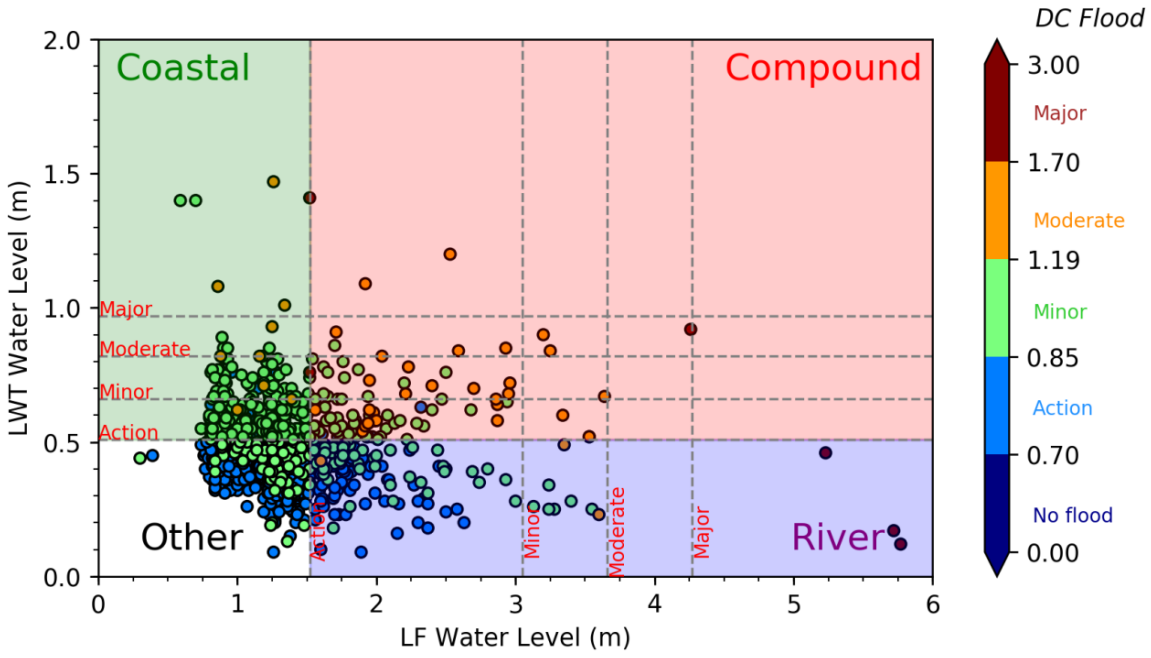

Figure 8 Relevance of each component to flooding in DC. Brown circles in the purple shaded area show the Major river flood peaks that resulted in Major peaks in DC. Brown circles in the pink region indicate Major compound flood peaks. In this region, an orange circle is a Moderate flood at DC resulting from both LF and LWT flood stages. The circles in the white region are the Other flood peaks.

1.3.1.5 Flooding during Hurricanes

The Chesapeake Bay is often impacted by major flooding from the Atlantic hurricanes. A Category 2 hurricane, like hurricane Isabel in 2003, has the potential to cause severe damage to the region (Shen and Gong, 2009). Hurricanes of categories 4 and 5 have almost doubled in both number and proportion in the period of 1970-2004 for all the ocean basins (Webster et al., 2005). Therefore, the hurricanes discussed in the previous sections, along with some additional events in this region, are also attributed to the different flood types. Among the 29 hurricanes considered in this study (Figure 9), one resulted in a *river* flood at DC (Arthur in 1996), seventeen hurricanes caused *coastal* floods and six caused *compound* floods. During hurricanes Irene, in 2011, and Floyd, in 1999, the LWT station was above *Major* and *Moderate* flood stages (1.41 m and 0.83 m respectively) but the water level at DC was below flood stage causing a *no flood* condition. Again, during the river flood of 1996, riverine flow (LF) was at *Major* flood stage but coastal water level (LWT) was below *Action* stage. During the river flood, no wind impact was present to reduce the water level at DC; therefore, a major flood in LF generated a major flood in DC. Hurricane Ernesto, in 2006, brought a *Moderate* flood to DC from *Major* coastal waters (LWT), while the riverine flow (LF) was below *Action* stage. The negative impact of wind reduced the impact of coastal water level in this case. A detailed plot for all the events with LF, LWT, RC, and wind are presented in the Appendix E, Figure E2 for better understanding. *Other* types of floods were observed during hurricanes Bob in 1991 and Andrea in 2013. During hurricanes, surge-driven coastal water levels can travel to DC and increase the water level resulting in a *coastal*

flood. A study by Mashriqui et al.(2014) showed that storm surge is a dominant factor for flooding in DC during hurricanes. However, a *river* flood during a hurricane can also occur due to high rainfall associated with the hurricanes, which was the case for hurricane Arthur in 1996. High precipitation increased the flow in the Potomac and Anacostia Rivers and adjacent small streams and caused flooding in DC. In some cases, both high riverine flow and coastal water level generated *compound* floods like hurricanes Fran 1996, Isabel 2003, Cindy 2005, Hanna 2008, Sandy 2012, and Bonnie 2016.

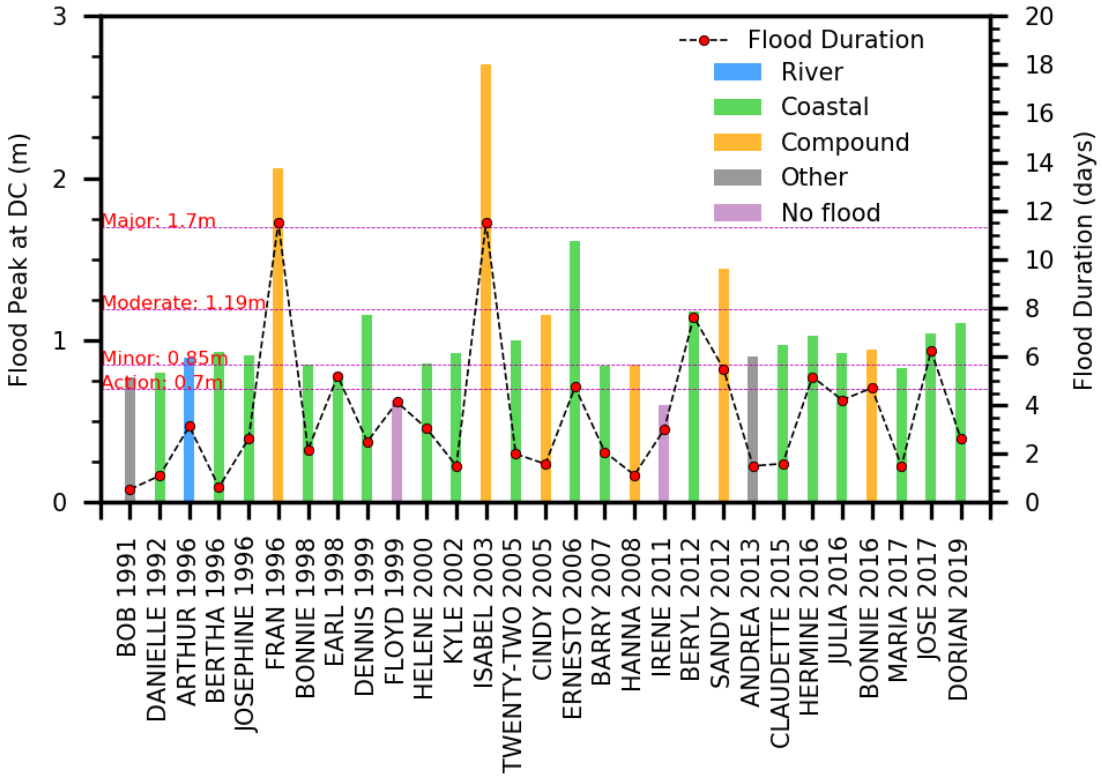

Figure 9 Flood types during hurricanes in the region from 1980-2019

1.3.2 Implication of the Flood Drivers

1.3.2.1 Impact of Each Flood Driver

For this study, we focused mostly on the physical interaction and the local impact of upstream flow, downstream water level, wind, and urban runoff in the DC station. The regression analysis was done considering the water level at DC to be the dependent variable and LWT water level, LF flow, wind, and urban runoff as independent variables (Appendix C). The flood drivers showed correlation less than 0.35, which corresponds to weak correlation (Taylor, 1990). LF flow is independent of the local urban runoff in RC because the rainfall in Rock Creek is not the same that increases flow at LF. Moreover, LF flow is the contribution from the large Potomac River watershed. Although DC is considered a coastal city, the location is about 160km far from the coastal station at LWT. Therefore, a rainfall in DC does not necessarily mean a rainfall in LWT or vice versa. Moreover, surge from LWT does not travel up to LF which is a totally flow dominated station neither the LF flow reaches down to LWT. However, a rainfall in LWT is certainly correlated to the surges in LWT. Similarly, LF flow is dependent on the rainfall in Potomac watershed, but not the urban runoff at RC. The DC station is located between a fully flow dominated station at LF and a fully coastal dominated station at LWT and therefore presents an interesting location to study the impact from both.

We use the term impact of flood drivers as the contribution of the drivers in terms of water level to DC flood peaks. Coefficients from the regression analysis were used to quantify the impact of each flood driver to the flooding in DC. The R^2 value was 0.75 and the intercept was 0.19 (Table 2). The intercept in the equation is an expression of the

difference between the elevation of downstream and the upstream stations. Adding the 0.19m depth makes the water level at upstream and downstream equivalent. For example, the action stage at Washington DC is 0.7m while the action stage at LWT is 0.51m which shows a difference of (0.7-0.51) = 0.19m. Coefficients from the regression analysis were named as: river factor = 0.13, coastal factor = 0.91, urban factor = 0.05, and wind factor = - 0.02 if wind at DC is going in downstream and 0.02 if the wind is coming to DC from Chesapeake Bay. For example, the impact of 30 m/s Southward wind can be calculated as: 30*wind factor = 30*0.02 = 0.6 m water level change in DC and an added intercept of 0.19 results in 0.6+0.19 = 0.79 m. The total water level at DC station (F_{DC}) was a combination of the relative contribution from all of these flood drivers (Equation 2). The results shown in Figure 10 are the expected change in the DC water level caused from a range of possible values of the flood drivers (from Equation 2) based on the historical data.

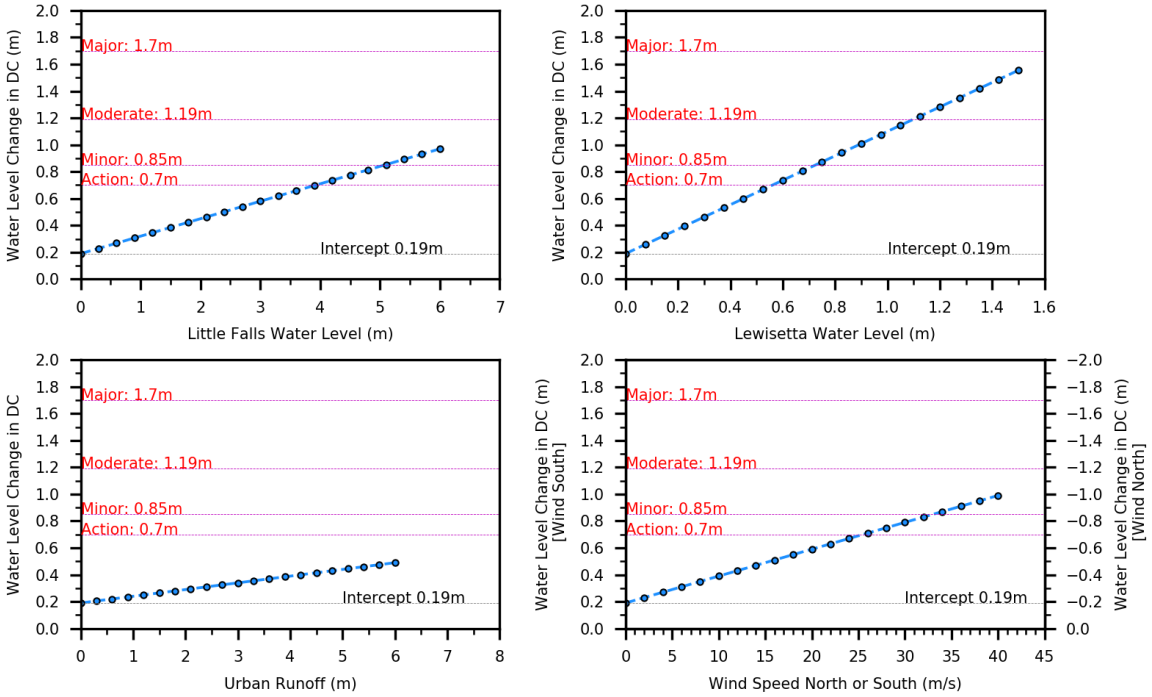

Figure 10 Impact of the individual flood drivers on the flood stage at DC station with added intercept value of 0.19

1.3.2.2 Impact of Sea-level Rise

The maximum observed coastal water level at LWT was ~1.48 m during the historical period. However, based on the historical rates of sea-level rise (SLR) by NOAA for the LWT and DC station, mean sea-level increase of 0.54 m and 0.34 m respectively are expected for the next 100 years (NOAA, 2020a). The projected values of SLR are usually used to estimate increased flood consequences in the future, although the actual change in SLR might be different than the estimated values. By adding the SLR value, LWT water level can be expected to reach ~2 m for the same historical conditions in 2120. As this is a simplistic approach that uses projected values from NOAA, the predicted future impacts might not be accurate, but provides an indication on how the

increase in sea-level will impact the flood levels in DC. In order to evaluate these changes, the water level changes in DC due to the coastal water level of 0-2 m is calculated and shown as a black dashed line in Figure 11. One set of scatter plots (orange circles) represent the water level peaks at LWT and DC during historical *coastal* floods and the other set (green circles) represent the same peaks with DC and LWT sea level rise added to the values. A coastal water level of 2 m can generate 2*0.91 + 0.19 = 2.01 m water level in DC as calculated from the regression line. However, the green circles show that the water level at DC can be 1.95 m. This is because the dashed line is considering only the water level, while the green circles have impacts from other flood drivers associated with the historical values.

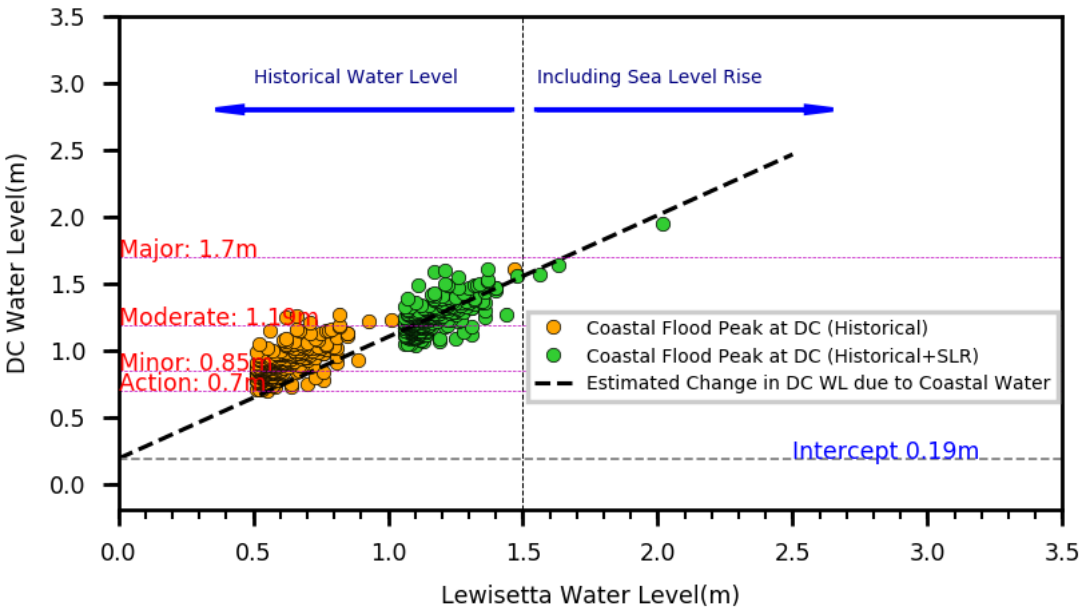

Figure 11 Potential sea level rise impact on LWT and DC water level

1.3.2.3 Probability of Flooding from Upstream and Downstream Boundary

In order to identify the likelihood of flooding in DC from different flood drivers, a bivariate probability distribution (Figure 12) was generated using the upstream riverine flow and downstream coastal water level. A multivariate probability in this study was disregarded because of the complex temporal variation of wind speed and direction. Moreover, urban runoff is rarely high enough (flash flood events) to make an impact on DC flooding alone. However, those events were not presented in Figure 6 because the urban runoff or wind only driven floods usually generate action stage floods and in some cases minor floods. There are more than 300 such events which will disrupt the visibility of the figure. So, all the flood events including other event numbers are shown in Figure 7. The bivariate distribution showed that the probability of riverine flow being in the range of 1000-2000m^3/s while water level in the range of 0.6-0.8 m is 0.02. The maximum probability was 0.09 when LF flow range was 3000-4000 m^3/s and LWT water level range was 0.8-1.0 m (Table 4). Furthermore, it was observed that *compound* events such as hurricane Sandy 2012, Sep 2011 flood, and Mar 2010 flood had the three highest probabilities (0.09, 0.06, and 0.05 respectively). The flood of Sep 2011 was a *Minor* flood and the other two events were *Moderate* floods. *River* flood events like Jan 1996 (flow 9000-1000 m^3/s and water level 0.4-0.6 m) had the lowest probability of $1.77x10^{-5}$. The water level DC_{Exp}, calculated from Equation 2, shows the peak at DC to be expected when riverine flow and coastal water level are the dominant flood drivers without any wind or runoff. DC_{Obs} *is the* observed flood peak at the DC station.

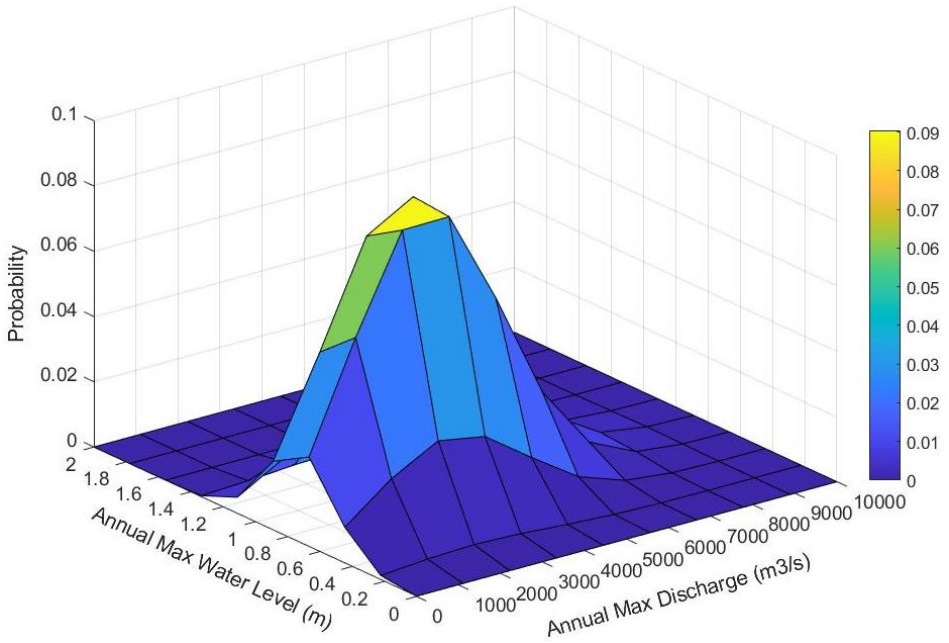

Figure 12 Bivariate probability between LF (Δx = 1000) and LWT (Δy = 0.2)

Table 4 Flood probabilities with different flood types and flood stage (table from image file)

Flood Events	LF (m^3/s)	LWT (m)	DC_{Obs} (m)	DC_{Exp} (m)	Probability	Flood Type	Flood Stage
Jan1996	9000-10000	0.4-0.6	2.04	1.38	$1.77x10^{-5}$	*River*	*Major*
Ernesto2006	0-1000	1.4-1.6	1.61	1.71	$1.02x10^{-4}$	*Coastal*	*Moderate*
Isabel2003	4000-5000	1.4-1.6	2.73	1.92	$9.16x10^{-4}$	*Compound*	*Major*
Fran1996	8000-9000	0.8-1.0	2.06	1.64	$1.60x10^{-3}$	*Compound*	*Major*
Jun2013	0-1000	0.4-0.6	0.85	0.84	$6.00x10^{-3}$	*Other*	*Minor*
Irene2011	0-1000	1.0-1.2	0.14	1.36	$9.60x10^{-3}$	*No Flood*	-
Mar2010	5000-6000	0.8-1.0	1.57	1.47	0.05	*Compound*	*Moderate*
Sep2011	3000-4000	0.6-1.0	1.16	1.17	0.06	*Compound*	*Minor*
Sandy2012	3000-4000	0.8-1.0	1.44	1.40	0.09	*Compound*	*Moderate*

1.3.3 Simulation of Wind Effects on the Flooding in DC

1.3.3.1 Wind Impact on DC Water Level

The goal for the model simulation was to understand how the local winds can impact the water levels in DC during different flood events. The importance of winds on the water levels in tidal rivers is extremely variable and depends on the direction,

consistency, and duration of the wind speed (Schaffranek, 1987). Historically, wind speed was usually higher during the months of June, July, August, and September. Seasonal wind analysis showed that *other* flood types were more frequent in the months of Jul, Aug, and Sep when Southward wind was dominant, therefore impacting the water levels upwards. On the other hand, during Hurricane Irene in 2011, significantly high wind speed (>5.5 m/s), aligned in a consistent Northward direction pushed the water downstream, and therefore, the water levels at DC went below flood stage (Figure 13) even when water level at LWT was above action stage. The reverse scenario, that is, when winds pushed the water high enough to cause flooding in DC, while LWT and LF were below flood stage, was evident in Nov 2019. Similar scenarios in several other events were investigated over the years. As expected, the wind impact was higher when aligned directly towards North (N) or South (S) rather than at an angle (NNE ESE, ENE, SE, NE, WSW, SW, SSE, SSW, NNW, WNW, and NW).

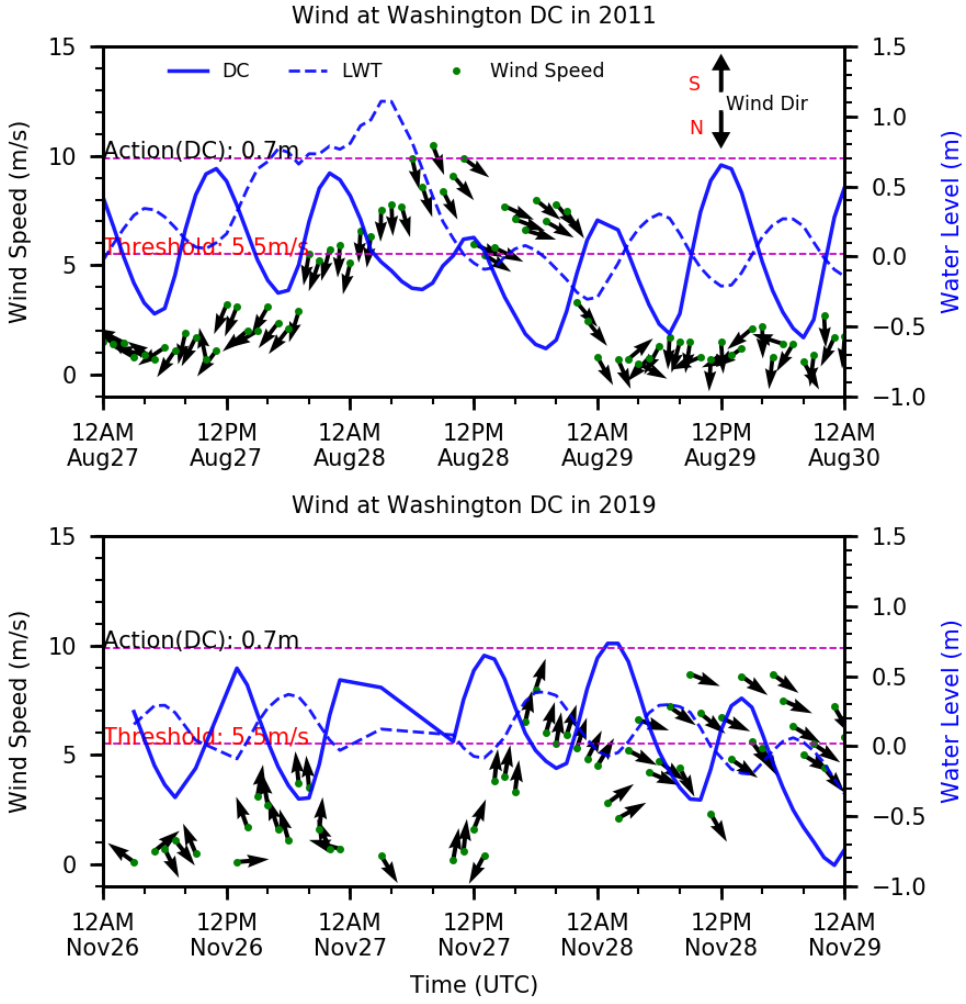

Figure 13 Northward and Southward wind impacts on DC flooding

1.3.3.2 Wind Impact on Other floods

In order to further explore the impact of local winds on the water levels in DC, simulation outputs are shown with different wind speed scenarios (Figure 14) in which wind was the only dominating factor for flooding (*other* flood events). It was evident that LWT and LF water level thresholds and Southward wind of 15 m/s can cause *Action* stage flooding when wind is blowing for the duration of at least 15 hours. A 30 m/s

Southward wind with the same boundary conditions can cause *Moderate* flood stage. If the 30 m/s wind is forced for a shorter period of time (5 hours), the flood stage can reach only up to a *Minor* level. However, during the available historical records, high wind speeds (30 m/s S) blowing for over 15 hours were not observed in this region. The wind speeds of 2, 4, 5, and 10 m/s alone were not sufficient to cause flooding in DC when LF and LWT were below *Action* stage.

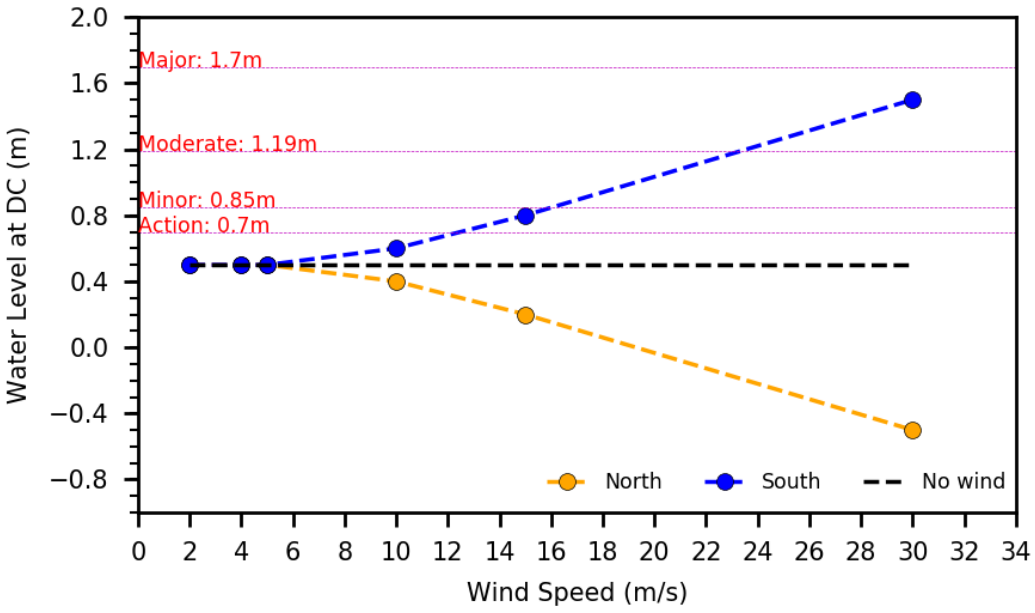

Figure 14 Impact of wind speeds on DC water level during *other* floods considering duration of over 15 hours.

1.3.3.3 Wind Impact on River, Coastal, and Compound Floods

Impacts of local winds effects at the DC water levels varied during *river*, *coastal*, and *compound* events due to the constant (30 m/s) and consistent N, S, NE, NW, SE, and SW wind forcing. Among all the events, as expected, the highest impact was observed

from N and S winds, which is presented through the blue bars in Figure 15. For example, Hurricane Isabel, in 2003, had an observed peak of 2.73 m at the DC station. The simulated water level without local wind forcing was 1.7m. A 30 m/s Northward wind forcing decreased the simulated peak to 1.23 m and a Southward wind increased the simulated water level to 2.6 m. The results suggest that the historical wind speed was probably in a Southward direction as the simulated water level is close the observed value with Southward wind forcing (Note: no local wind data available for validation). Moreover, the peaks of *coastal* events, like hurricane Ernesto, and the maximum peaks of *compound* events, generated from coastal water level, like hurricanes Isabel and Sandy, were impacted more by the Southward and Northward wind compared to riverine flow dominated peaks. The peak of Jan 1996 flood and the maximum peak of the *compound* flood during hurricane Fran in 1996 were less impacted in comparison to the above mentioned coastal peaks, as these peaks were dominated by riverine flow. During hurricane Irene in 2011, Northward wind played a significant role by reducing the water level up to 0.66 m compared to the 'no wind' scenario. The maximum impact, 1 m change in water level in both directions, was observed during *other* event in June 2013.

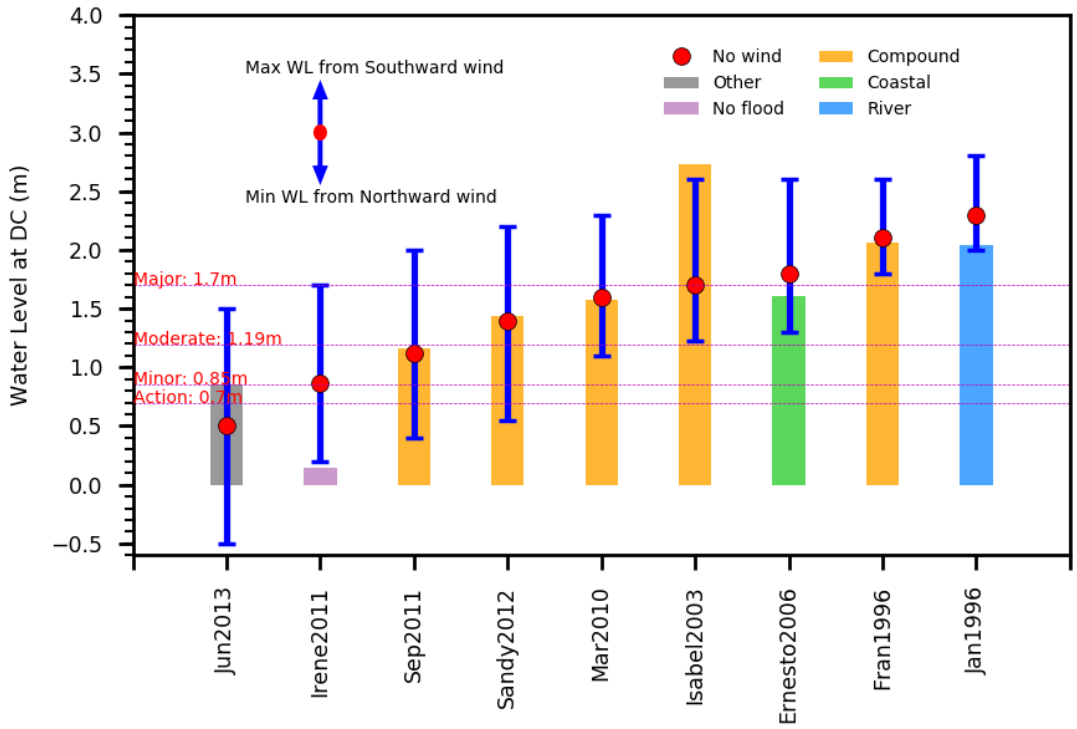

Figure 15 Changes in DC water level due to 30m/s wind during different types of flooding (colored bars represent observed water levels at DC)

1.4 Conclusions

Compound flooding occurs due to the coincidence of multiple flood drivers and can result in significantly higher peaks and longer duration than single flood driver induced events. The magnitude and duration of floods in DC can be attributed to the impacts from different flood drivers including riverine flow, coastal water level or storm surge, urban runoff and local wind. However, the interaction between these flood drivers is complex and required extensive data-driven analysis to estimate the contribution of each flood drivers on flood stages in DC. The flood events were classified as *river* flood, *coastal* flood, *compound* flood and *other* flood, based on the flood drivers associated with the flooding. Moreover, the flood days in DC were categorized as *Action*, *Minor*,

Moderate and *Major* flood days. During 1980-2019, four *Major* floods were observed in the DC station, three of which were *compound* floods (Nov 1985, hurricane Fran 1996 and hurricane Isabel 2003) and the other one was a *river* flood (Jan 1996). The *other* floods were mostly the result of low water level and high wind speed leading to *Action* or *Minor* flooding. In few cases rainfall induced urban runoff events were responsible for floods in DC. Although *Minor* flood stages in DC were mainly generated by *coastal* floods, few *river* and *compound* floods could also generate such flood stage. However, *Moderate* and *Major* flood stages were mainly the result of *compound* floods.

The maximum *compound* flood peak in DC was 2.73 m during hurricane Isabel in 2003 and the maximum duration of *compound* floods were around 12-19 days. The highest five durations were observed during *compound* and multi-peak *compound* flood events. Moreover, LF had the maximum peak of approximately 10,000 m^3/s during the *river* flood of Jan1996 while LWT had the highest peak of 1.48 m during hurricane Ernesto in 2006. Results suggested that the coastal water level at LWT alone had the highest potential to create flood conditions in DC, although it did not reach the *Major* flood stage during these events. In order to estimate the impact of individual flood drivers, coefficients from the multivariate regression of the flood drivers were used as factors along with an intercept of 0.19. The impact factors for the flood drivers were: 0.13 for LF, 0.91 for LWT, 0.05 for RC, and 0.02 for wind speed. For example, a wind speed of 30 m/s can have a maximum impact of 30*0.02+0.19 = 0.79 m on water level at Washington, DC. Moreover, the interaction between storm surges and riverine flow along the Tidal Potomac River presented a complex scenario with the coincidence of high wind

speed towards North or South directions. Coastal water level dominated peaks for any events were impacted more by the wind compared to river dominated peaks at DC. Sea-level rise can also have significant impact on the flood peak at DC by increased water levels in the Chesapeake Bay.

The study has some limitations due to the need to interpolate datasets when some historical values were missing. Use of the interpolated data might impact the results. Moreover, we have used water level values from a proxy station as proxy which is 134km far from actual station. The differences in the tidal amplitude might introduce some uncertainty even after adjusting the data with regression analysis. The impact of wind was studied for shorter period (Jun, 2008 to Dec, 2019) compared to the other flood drivers. Wind data and urban runoff from one local station may have introduced bias due to the fact that wind and runoff are spatially variable. Furthermore, we have considered only one station for studying the compound flood characteristics which has the scope the generate uncertainty in the results. The flood drivers for the compound flooding in DC were considered independent based on the low correlation (<0.35) and R^2 (<0.1) values. The weak correlation might have some impact which was ignored in this study. The advanced statistical technique like copula methods may be implemented in future for local flood studies like this to provide further understanding about the flood characteristics.

This study has identified the major flood drivers impacting the Washington DC metropolitan area. The results demonstrate the importance to refine the current flood forecast and design models in large estuaries by considering the potential complex

interactions between the *compound* flood drivers: riverine flow, coastal water level, local wind and urban runoff. Furthermore, it demonstrates the potential impacts of climate change-driven sea-level rise to the compound flooding in this metropolitan area. The approach implemented in this study was mainly based on the analysis of historical observations of different flood drivers and its interaction in DC. However, this methodology can be applied to similar metropolitan areas located in tidal regions, in order to identify flood drivers and estimate the contributions of those drivers towards urban flooding. The water level in DC, once estimated from the multivariate equation, can be translated into spatially variable inland water depth based on the flood inundation area provided by the NWS. This can also be a helpful tool to provide inland flood depth information during any flood event.

2 SPATIO-TEMPORAL VARIABILITY OF FLOODS RESULTING FROM MULTIPLE DRIVING MECHANISMS: AN ASSESSMENT ON THE URBANIZED WASHINGTON, DC METROPOLITAN REGION

Abstract:

Coastal and estuarine cities are vulnerable to compound flooding from multiple flood drivers, including high riverine flow, runoff from intense rainfall, and coastal storm surges. Spatial and temporal variability of the flooding extent and depth are driven by the complex interaction between these flood drivers, which often result in extremely high flooding over a longer period of time. While compound flooding hotspots can be identified and analyzed at the continental and regional scales, local-scale complexities play a major role in the interaction between the flood drivers. In this study, we investigated the spatio-temporal variability in inundation extent and depth due to compound flooding conditions in the Washington, DC metropolitan area using a two-dimensional (2D) hydrodynamic model. Results suggest that locations around the study area can be locally divided into three zones based on the impact of riverine flow and surges: highly riverine flow dominated zone, the transition zone with impact from both flow and surges, and coastal surge dominated zone. Flood depths during surge dominated events were significantly higher than flow dominated events, almost doubling in some locations towards downstream of the river. Coastal flood duration was longer compared to the riverine or compound floods adjacent to the river. However, riverine flow and

surge was less relevant for the inundation in the urban areas compared to the rainfall induced runoff. While riverine flow and surge had a minor impact on the overall urban flooding of the National Capital Region, these drivers significantly impacted the regions along the main rivers and the small streams with its impacts propagating up to 8km upstream. This length or distance of influence depends on the slope of the streams, i.e., the distance was lower for steep streams and higher for low gradient streams. Results also showed that the region will face increased flooding in the long term future because of sea level rise (SLR), particularly during the surge dominated events. This study provided scientific insight into the spatially and temporally variable interaction of the compound flood drivers and the consequences of such flooding in the metropolitan areas like Washington, DC, located along the river-estuarine transition zones.

2.1 Introduction

Flooding is one of the most frequent natural disasters resulting in devastating impacts on the environment, societies, and economies around the world (Bhandari et al., 2017; Ammar et al., 2020). The average annual cost of flood damages by coastal surges and inland flooding during 1980-2017 was approximately $4 billion in the US (NOAA, 2018; Afshari et al., 2018). Compound flooding events, due to the simultaneous occurrence of multiple flood drivers (e.g. coastal storms, riverine flow, and urban runoff), can have significantly higher impacts than flooding from a single driver (Bevacqua et al., 2019; Hu et al., 2019). The co-occurrence of multiple events can lead to extreme impacts even when the single drivers are not at their extreme state (IPCC, 2012; Bevacqua et al., 2017; Zscheischler et al., 2018; Visser-Quinn et al., 2019;). For example, severe flooding

was caused by the joint occurrence of rainfall and coastal flooding during Hurricane Irene in 2011 (Liu and Smith, 2016) and by coastal surges and riverine flow during Hurricane Harvey in 2017 (Zscheischler et al., 2018) .

Compound flooding in estuaries is driven by hydrological, oceanographic, and meteorological phenomena (Couasnon et al., 2019; Saleh et al., 2017; Bevacqua et al., 2019). Coastal communities experiencing frequent hurricanes and tropical storms are usually subject to flooding from heavy inland rainfall and coastal storm surges (Resio and Westerink, 2008; Ray et al., 2011). Few studies have investigated the likelihood of compound flood events at the continental scale considering multiple variables (Huong and Pathirana, 2013; Bevacqua et al., 2017; Paprotny et al., 2018; Ward et al., 2018). Studies (Santiago-Collazo et al., 2019; Bilskie et al., 2014; Kumbier et al., 2018) showed that multivariate flood drivers have highly non-linear responses on output variables such as flood depth and flood extent (Serafin et al., 2019; Couasnon et al., 2019). Significant dependence has been found between extreme rainfall and storm surges (Svensson and Jones, 2002; Svensson and Jones, 2004; Zheng et al., 2013; Kumbier et al., 2018) and between storm tides and riverine flooding (IPCC, 2014; Leonard et al., 2014; Moftakhari et al., 2019) in estuarine environments. A study by Bevacqua et al. (2017) in Ravenna, Italy suggested that underestimating the dependence between the ocean and river levels may lead to an underestimation of actual flood risk by increasing the return period from 20 years to 32 years.

A major issue of flood risk management is the analysis of flood hazards (Blumenthal et al., 2018; Dhote et al., 2018) considering the present and future

conditions. Future climate projections indicate an increasing probability of compound floods along parts of the European (Bevacqua et al., 2019) and the US coasts (Wahl et al., 2015) bringing additional challenges for the cities, their critical ecosystems, and the livelihoods (Cortès et al., 2019; Dickson et al., 2012). Accelerated sea-level rise (SLR) in the US East Coast, north of Cape Hatteras, will result in accelerated flooding (Ezer and Atkinson, 2014) and the flood risk will be greater under higher SLR and stream flow conditions (Feng and Brubaker, 2016). While the Intergovernmental Panel on Climate Change (IPCC) reported that the global average SLR during the 20th century was 1.7 mm/year (ACSM Bulletin, 2008), local rates and resulting impacts can be much higher.

Over the past decade, major hurricanes and extreme storm events have impacted several urban areas throughout the US. Metropolitan cities, like Washington, DC, that are concentrated along coastlines, are exposed to a diverse type of flood hazards which may overlap spatially and temporally (Depietri et al., 2018). Similar to New York City (NYC Emergency Management, 2015), Baltimore also experiences riverine, coastal, and inland flooding (National Academies of Sciences, 2019). On the other hand, Houston (from Gulf of Mexico) and Chicago (from Great lakes) are hit by coastal and inland flooding every year (National Academies of Sciences, 2019). While riverine and coastal floods are the major threats to communities across the US, urban floods can also cause billion-dollar losses every year (University of Maryland and Texas A&M University, 2018; Hecht and Vogel, 2020). Quantifying the actual compound flood impacts in estuarine urban areas presents challenges due to the complex mechanisms of the flood drivers. Compound flood hotspots can be identified from extreme flow and storm surge variables but there is

greater uncertainty on how the compound flood will propagate into inland flooding (Couasnon et al., 2019; Noh et al., 2016). Therefore, compound urban flooding needs to be studied and modeled locally due to its limited geographical extent and the physical interactions involved (Paprotny et al., 2018; Saleh et al., 2017).

The objective of this study is to investigate the spatial and temporal variability of the compound urban flooding in Washington, DC resulting from multiple flood drivers: riverine flow, coastal storm surges, and urban rainfall/runoff. We assessed the impacts of the flood drivers in different urban locations along the tidal Potomac River, analyzed the flood characteristics of the adjacent small streams, identified the hotspots of compound urban flooding, explored how the compound flood propagates into inland flooding, and investigated the impact of sea-level rise on the study area. A 2D hydrodynamic model was used with a set of possible storm surges and river discharges that are representative of the low-probability high-impact (extreme events) and high-probability low-impact (non-extreme/frequent) flood events induced by riverine flow, coastal surges, rainfall or a combination of all these drivers. While the results are specific to the Washington, DC metropolitan region, it provides insights on other metropolitan areas along tidal estuaries; therefore, this scenario-based methodology can be used for the flood analysis of any coastal metropolitan cities based on the relevant flood drivers.

2.2 Methodology

A modeling framework was developed in this study focusing extensively on the compound urban flooding with multiple flood drivers. The Washington, DC metropolitan region is used as a study area representing coastal metropolitan cities in the US. We used

five main steps to construct the flood modeling: i) implementing a hydrodynamic model for the region ii) selecting historical extreme flood events to calibrate and validate the model iii) producing synthetic time series of riverine flow, surges, and design rainfall iv) generating a set of runoff data from rainfall depth, and v) scenario-based simulations representing a range of combinations of high and low flow and surges with rainfall induced runoff and SLR. Finally, the synthetic events were evaluated for investigating the spatio-temporal patterns of flood inundation extent, flood duration, and flood depth.

2.2.1 Study Area

The Washington, DC metropolitan region has experienced severe floods and losses in the past decades: the Great Flood of 1889, Chesapeake-Potomac Hurricane of 1933, Great Potomac Flood of 1936, and Hurricane Agnes in 1972. The area is vulnerable to multiple future challenges like rapidly increasing population, climate change-driven sea level rise, increased runoff driven by imperviousness, and changing pattern of extreme rainfall due to climate change (Huong and Pathirana, 2013). This urbanized area is often affected by riverine flow, inland rainfall, and coastal storm surges. The topography varies widely in elevations ranging from sea level along the tidal Potomac and Anacostia Rivers, to approximately 414m above North American Vertical Datum of 1988 (Federal Emergency Management Agency, 2010). The urbanized portion of the area is centered on Washington, DC and includes Montgomery and Prince George's County in Maryland, Fairfax County, Falls Church city, Arlington County, and Alexandria city in Virginia. Urban areas surrounding Washington, DC have expanded at a rate of ~22 km^2 per year during 1973-1996, and even at a higher rate after that period

(Masek et al., 2000). Only about 19% of the area was found to be relatively undisturbed during 2010, which were mostly concentrated in the public parks, memorials, and national historic sites (Federal Emergency Management Agency, 2010).

The Potomac River is located within the Mid-Atlantic region of the US and flows from the Potomac River Highlands (i.e., Allegheny Mountains of West Virginia and the hills of Virginia and Maryland) to the Chesapeake Bay, the largest bay in the US with a length of 320km (Cho et al., 2012). The drainage area of the Potomac River is approximately 30,000 km^2, while that of the Anacostia River is 315km^2 and Rock Creek is 160km^2 (Huanxin et al., 1997). The tides in the 183km long tidal Potomac River originates from the Atlantic Ocean and propagates into the river through the Chesapeake Bay (Wang et al., 2015). The study area is bounded by the Potomac River and its tributary, the Anacostia River, and includes several urban and sub-urban watersheds such as the Rock Creek Park, Four Mile Run, Cameron Run, Oxon Run and some other small watersheds (Figure 16) This area includes several historically important infrastructures, federal buildings, defense facilities, monuments, and airports which are at high risk of flooding (Federal Emergency Management Agency, 2010). Figure 16 shows the study area, the streams inside the study area, and the important locations considered for flood depth analysis. Table 5 shows the name and ID of the locations selected within the study area. The streams considered in this study are located in three river reaches: i) Pimmit Run, Little Falls (LF) Branch, Gulf Branch, Donaldson Run, Windy Run, Spout Run, Maddox Branch, and Rock Creek along the *Upper Potomac River* reach, ii) Four Mile Run, Cameron Run, and Oxon Run along *Lower Potomac River* reach, and iii) Pope

Branch, Watts Branch, Hickey Run, Beaverdam Creek, Quincy Run, and Dueling Creek along *Anacostia River* reach. Besides these streams, Location ID-6 (Pentagon Lagoon) and ID-7 (Gravelly Point) are two water bodies near Washington DC which were also used to analyze the impact of flow and surges. A total of 11 important inland locations were mainly used for flood depth analysis along Potomac River starting from Georgetown Waterfront to National Harbor. One location at Navy Yard and one near Washington Channel were also considered for flood analysis.

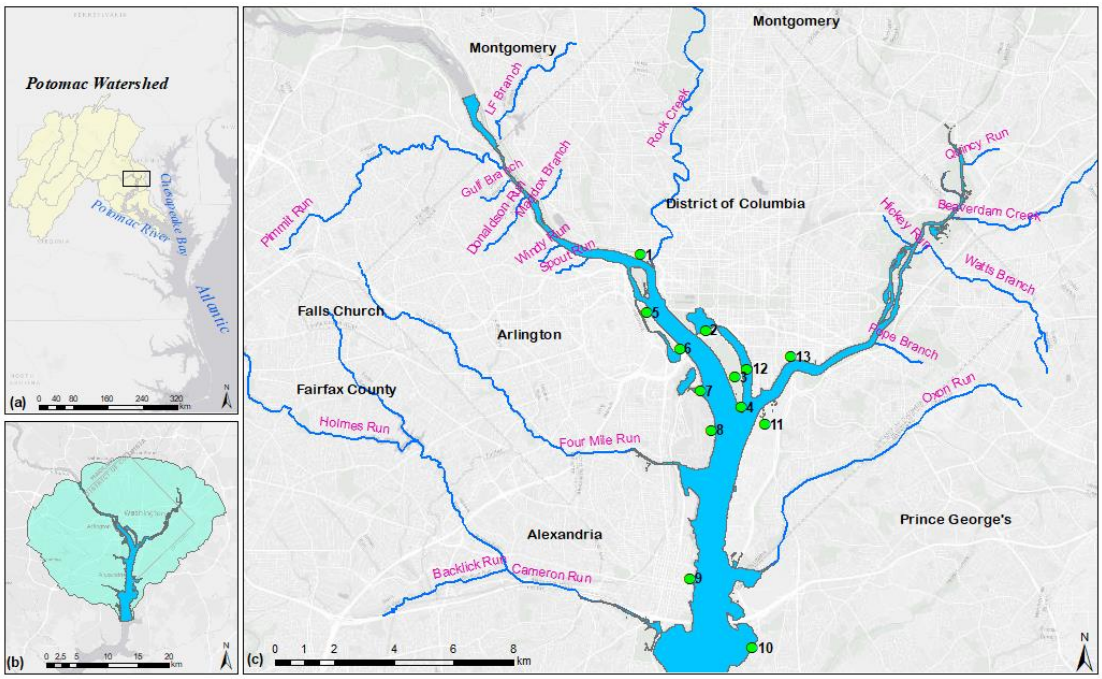

Figure 16 Study area with streams and different flooding location

Table 5 Flood location ID and location names

ID	Location	ID	Location
1	Georgetown Waterfront	8	Ronald Reagan Airport
2	Thomas Jeff Memorial	9	Old Town Alexandria
3	East Potomac Park	10	National Harbor
4	Haines Point	11	Dept. of Defense
5	Potomac Park	12	Washington DC
6	Pentagon Lagoon	13	Navy Yard
7	Gravelly Point		

2.2.2 Model Setup

This study implemented a 2D hydrodynamic flood model using the capabilities of the Hydrologic Engineering Center's (HEC) River Analysis System (HEC-RAS) for flood simulation in the locations around Potomac River. The hydraulic model, developed by the U.S. Army Corps of Engineers (USACE), has proved to be an efficient tool for flood modeling (Hicks and Peacock, 2005; Brunner et al., 2015; Cadavid et al., 2016; Quirogaa et al., 2016; Adams et al., 2018; Pasquier et al., 2018) and studying the interaction of riverine freshwater and coastal storm surges (Mashriqui et al., 2014; Feng and Brubaker, 2016).

2.2.2.1 Model Inputs

The hydraulic properties of the model are based on the terrain data, roughness values, and land cover grids. A well-developed topo-bathy was used for the model setup. DEM from USGS and bathymetry from NOAA was combined to create a topo-bathy with varying resolution (1m to 200m) and the datum of North American Vertical Datum

of 1988 (NAVD88). In order to study the compound flooding effects, the model requires upstream and downstream boundary conditions, i.e., streamflow and water level data respectively for this study. In Figure 17, UP1 is the upstream boundary at Little Falls, DC, UP2 is the boundary at Anacostia River, and LOW is the downstream boundary near Alexandria, VA. Coastal water from the Atlantic Ocean enters the Potomac River near Lewsietta, VA, and then travels towards Washington, DC. The surge propagation from Lewisetta (mouth of the Potomac River in the Chesapeake Bay) to the upstream is studied widely (Mashriqui et al., 2014; Feng et al., 2017; Khalid and Ferreira, 2020). Moreover, Mashriqui et al. (2014) found that the Washington, DC station has significantly higher tidal influence compared to the other station at Wisconsin Avenue located in close proximity to DC. Wind and surge propagation from the Chesapeake Bay also have optimal conditions to propagate water towards DC (Mashriqui et al., 2014). Moreover, Feng and Brubaker (2016) concluded that using the DC station data as a proxy for the annual peaks at their Washington, DC inland site proved to be a reasonable approach as it covers all the possible upstream and downstream events that cause the annual peak in the study site (Feng and Brubaker, 2016).

The major parameters associated with model simulations were channel roughness coefficient (Manning's n), theta weighing factor (0.6), computational time steps (hourly), and the number of iterations (default). A spatially varying Land Use classification (MRLC, 2020) was used to generate Manning's n grids. However, default Manning's n values can be used for the cells with missing land cover types. Based on literature (Chow, 1959; Bhandari et al., 2017), values of Manning's n were set as shown in Table 6. The

hydraulic system was provided with rain on grid to simulate the effect of urban flooding in the region. A hot start file was used to set the initial condition of the system for subsequent runs. The hot start simulation included running the model 15days prior to the event at 1hour interval.

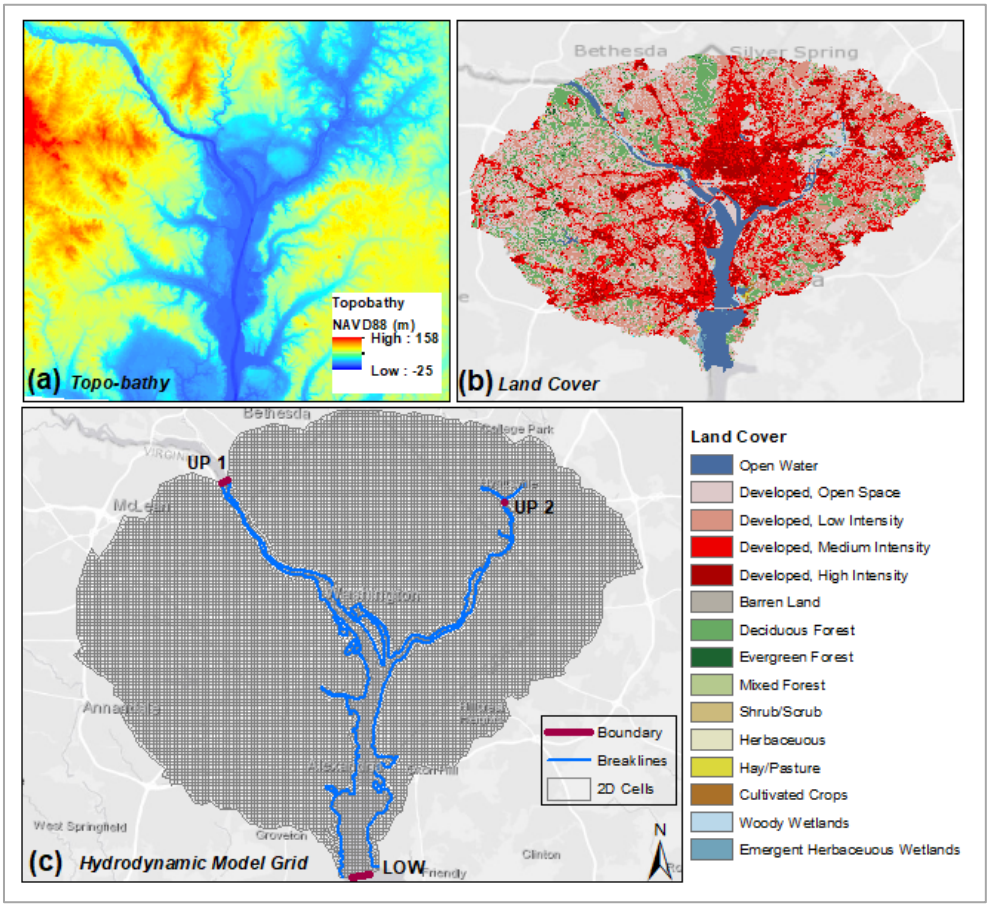

Figure 17 Model setup with (a) topo-bathy, (b) land cover, and (c) model grids

Table 6 Manning's n

Land Cover	Manning's n	Land Cover	Manning's n
Barren Land Rock/Sand/Clay	0.025	Evergreen Forest	0.160
Cultivated Crops	0.035	Grassland/Herbaceous	0.035
Deciduous Forest	0.160	Mixed Forest	0.160
Developed, High Intensity	0.150	Open Water	0.015
Developed, Low Intensity	0.100	Pasture/Hay	0.030
Developed, Medium Intensity	0.080	Shrub/Scrub	0.100
Developed, Open Space	0.040	Woody Wetlands	0.120
Emergent Herbaceous Wetlands	0.070		

2.2.2.2 Numerical Mesh and Model Domain

The underlying terrain information available from the topo-bathy was used to generate the two-dimensional (2D) flow area. HEC-RAS 2D implements either the full 2D Saint Venant equations or the 2D Diffusion Wave equations based on user needs and we selected the later equation for this study. In most of the flood analysis, 2D Diffusion Wave equation set works efficiently, runs faster, and are inherently more stable (USACE Hydrologic Engineering Center, 2016). Cells and cell face of the computational mesh are pre-processed to develop hydraulic property tables (elevation versus, wetted perimeter, area, and roughness) based on the terrain used in the modeling process. This property allows the use of larger computational cells, without losing the detail of the underlying terrain. A nominal grid size of 100m x 100m was used for the inland area (Figure 17). However, the water bodies (rivers, lakes, and some streams) in the study area were defined by breaklines. The mesh generation tools were enforced to align the computational cell faces along these lines. Cells around the breaklines and the 2D flow area boundary were irregular in shape to conform to the user specified break lines and boundary polygon. The mesh generation tools utilize the irregular boundary. Cell centers

are the points where water surface elevations are computed. The cell center does not necessarily correspond to the exact cell centroid (Brunner et al., 2015). The computational mesh controls the movement of water through the 2D flow area and the computational cell faces control the flow movement from cell to cell.

2.2.2.3 Rainfall to Runoff

The Soil Conservation Service (SCS) curve number (CN) method is one of the most common methods for estimating storm runoff in engineering design. It has been applied for runoff calculations ranging from small watersheds to comprehensive hydrologic models (Kim et al., 2002). CN is a dimensionless number ranging from minimum value of 0, when runoff = 0 to maximum of 100, when runoff = rainfall (USDA, 1986). The Natural Resources Conservation Service (NRCS) provides runoff curve number tables depending on land cover types, hydrologic conditions and the soil group A, B, C, and D (Hernández-Guzmán and Ruiz-Luna, 2013). Land use data from National Land Cover Database 2011 (MRLC, 2020) and soil data from Natural Resources Conservation Service (NRCS, 2020) were used for the CN grid (Figure 18) generation in ArcGIS to estimate the runoff. Urbanization effects can be simulated by changing the CN to represent increased impervious area. The equation used for estimating runoff (mm) is as follows:

Equation 3

$$Q = \frac{(P - 0.2S)^2}{P + 0.8S}, \quad P > I_a$$

where, P = Precipitation, $I_a = 0.2S$ = Initial abstraction, and S = Potential water retention after runoff begins. S depends on the soil capacity for water runoff or infiltration and is estimated based on the CN (Hernández-Guzmán and Ruiz-Luna, 2013):

Equation 4

$$S = \frac{25400}{CN} - 254$$

The 2D hydrodynamic model used in this study could only be forced with one uniform runoff grid for one watershed. Therefore, after generating the actual CN grid based on soil type and land cover, area averaged values of CN were generated to select relevant CN for the model simulation. Average or composite CN has been implemented in different studies (USDA, 1986; Reistetter and Russell, 2011) by assuming the percentages of impervious area. Based on the minimum value (blue box in Figure 18b) and maximum area coverage (yellow box in Figure 18b) of the averaged CN grid, we selected CN 65 and CN 85 for this study. The minimum and maximum CN values were used to represent a scenario with the highest and lowest runoff generation. The intent was to evaluate the influence of different drivers rather than precisely hindcast the historical events. However, we did not choose CN higher than 85 because a uniform value of such high CN will generate excessive runoff.

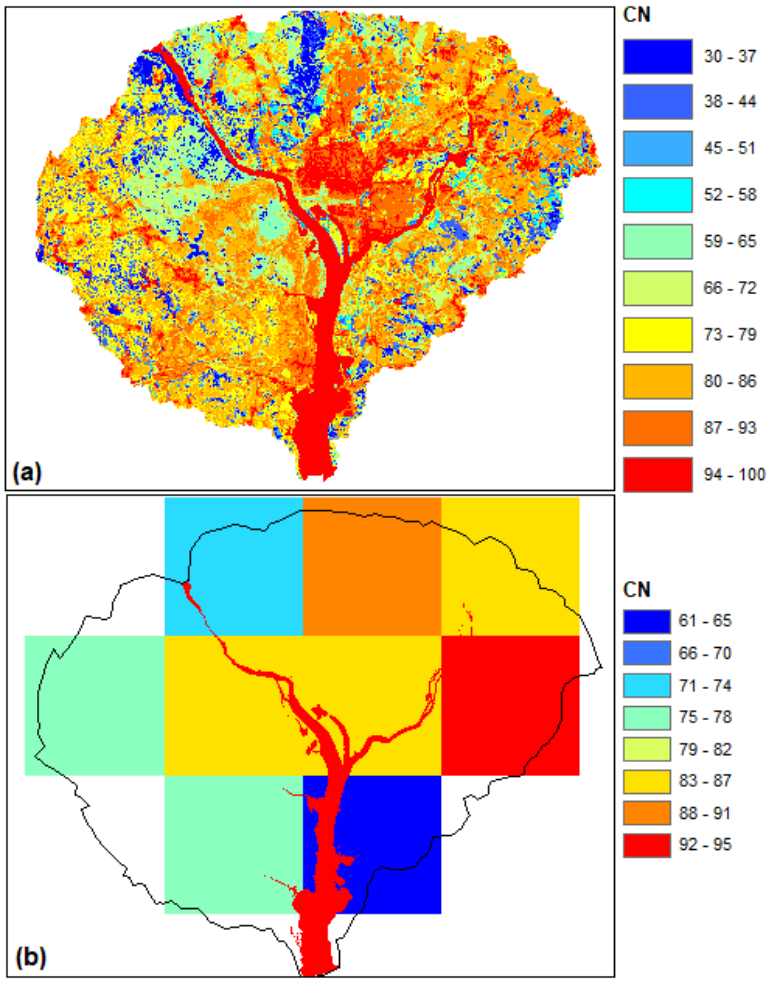

Figure 18 CN grid for the study area: (a) actual CN grid and b) area averaged CN grid

2.2.3 Historical Data for the Hydrodynamic Model

The hydrodynamic model was simulated with four historical events: Hurricanes Isabel 2003, Ernesto 2006, Sandy 2012, and the Flood of Jan 1996. Hurricane Ernesto was a coastal flood event driven only by storm surges coming from Lewisetta (LWT), while Jan 1996 flood was driven entirely by riverine flow from Little Falls (LF) station (Figure 19). Hurricanes Isabel 2003 and Sandy 2012 were compound flood events driven by riverine flow, coastal surges, and rainfall (Figure 20). Historical streamflow and water

level data were collected from the United States Geological Survey (USGS, 2017) and National Oceanic and Atmospheric Administration (NOAA, 2020a). Potomac River flow at LF gage station (USGS gage: 01646500) was used as UP1 boundary. We used the combined flow data from two Anacostia River stations at Northeast Anacostia (NE) and Northwest Anacostia (NW) as UP2 boundary (USGS gage: 01651000 and 01649500). In order to evaluate the impacts of storm surges or coastal effects, we relied on a downstream boundary condition at Alexandria (ALX), VA (USGS station: 0165258890) that would represent the influence of the coastal water levels from the Chesapeake Bay near Lewisetta, VA (NOAA station: 8635750) towards flooding in Washington, DC. Water level for DC was collected from another NOAA station (NOAA station: 8594900). Historical precipitation data was collected from National Climate Data Center (NCDC) at Washington Reagan National Airport, VA Station ID- COOP: 448906. Validation data for flood depths was collected from the NWS (National Weather Service, 2020c).

Historical rainfall for Hurricanes Sandy, Isabel, Ernesto, and the Jan 1996 flood are presented in Figure 21. Intense rainfall was observed during Hurricane Isabel and the Jan 1996 flood with depths of approximately 160mm and 155mm respectively. Hurricanes Sandy and Ernesto had comparatively lower amount of rainfall, 70mm and 20mm respectively. We used time series data of 15days for any flood events simulated in this study. For some events, the full time series at ALX was missing, where we estimated the time series based on peak values at Washington, DC. A regression equation (Eqn 5) was developed using ALX and DC peak water level from the historical observations during the period of 2010-2017. The regression equation showed an R^2 value of 0.98. R^2

describes the degree of collinearity between simulated and measured data and ranges from 0 to 1. Estimated values with $R^2 > 0.5$ significantly represents the observed values (Moriasi et al., 2007). Time lags between ALX and DC water level peaks were found to be approximately 15-20 minutes and that of LF and DC were less than 1 minute. Time lag between the rainfall event and rainfall induced flow in the streams were different for the streams. We considered the rainfall few hours before the surges and flow peaks to allow sufficient time for the catchment to accumulate the runoff. However, observed flood depth data was unavailable for the urban areas limiting the scope for validation of urban flood depths. We used the Advanced Hydrologic Prediction Service (AHPS) flood depths from NWS for the urban flood validation. AHPS or NWS inundation boundary covers 8.9 km of the tidal Potomac River and approximately 13.7 km of the Anacostia River along the western border of Washington, DC. The inland flood depths are based on the AHPS water level at Washington, DC recording station which are classified as *Action, Minor, Moderate,* and *Major* (National Weather Service, 2020c).

Equation 5

$$Y = 0.3X + 0.11$$

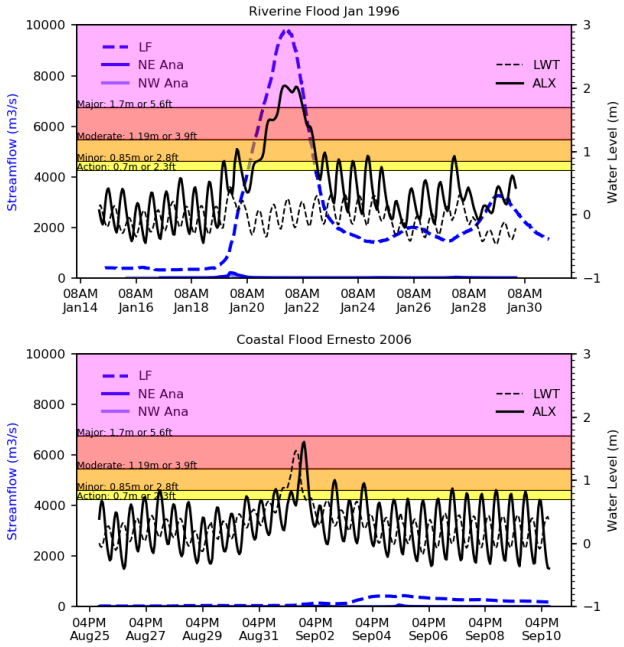

Figure 19 Riverine and coastal floods for historical simulations (blue dashed line = Little Falls (LF), blue firm line = Northeast Anacostia (NE), and purple line = Northwest Anacostia (NW) streamflow; black firm line = Alexandria (ALX) and black dashed line = Washington DC (DC) water level)

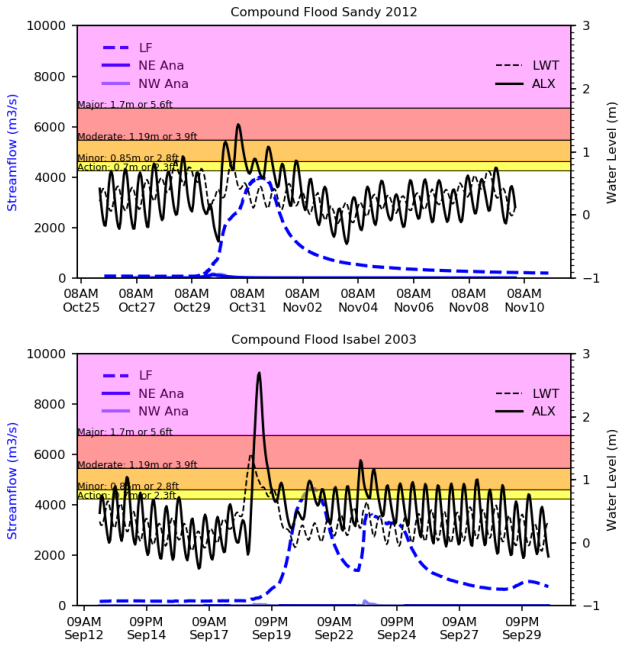

Figure 20 Compound floods for historical simulations (blue dashed line = Little Falls (LF), blue firm line = Northeast Anacostia (NE), and purple line = Northwest Anacostia (NW) streamflow; black firm line = Alexandria (ALX) and black dashed line = Washington DC (DC) water level)

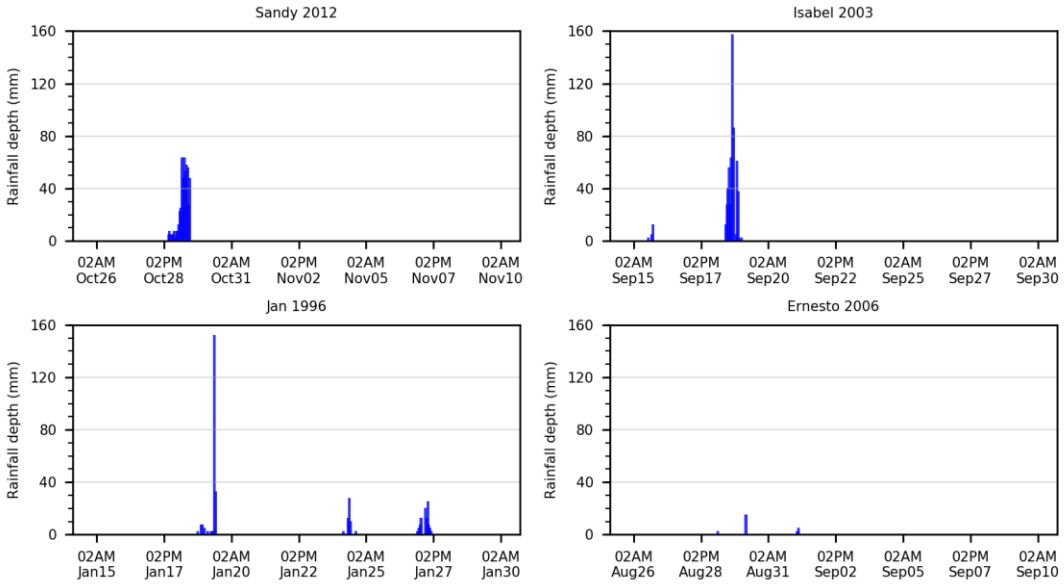

Figure 21 Historical rainfall depths for the four storms

2.2.4 Synthetic Data for the Hydrodynamic Model

In order to study the variability of compound flood in the region, flow, surge, and rainfall induced synthetic events were generated and forced into the hydrodynamic model. While this approach can have uncertainty in the magnitude, timing, and spatial distribution of the corresponding flood inundation outputs, it can provide a range of possible flooding variability expected in the region. Maximum riverine flow recorded in LF during 1980-2020 was 9,800m^3/s and maximum water level in ALX was ~2.7m (Figure 22). A number of scenarios were developed based on these historical extremes and the usual non extreme values of flow and surges. For the synthetic events, 100-year, 25-year and 5-year 6hour design rainfall duration were used to generate storm runoffs and implemented in the urban flood model. Runoffs were generated for each rainfall based on CN 65 and CN 85. The data set of 28 synthetic storms comprises the following

criteria: i) High Flow Low Surge - Riverine flood ii) Low Flow High Surge - Coastal flood iii) High Flow High Surge - Compound Flood iv) Low Flow Low Surge - Minor or No Flood.

Each of the flooding scenarios was simulated with and without the design rainfall induced runoff. Therefore, the compound floods were of two types: compound flood from riverine flow and coastal surges and compound flood from riverine flow, coastal surges, and rainfall. The impact of flow, surges, and rainfall were analyzed along the rivers and also along the small streams. We also identified the distance towards the upstream boundary of local streams where the impact of surge and flow becomes negligible and runoff dominates the flooding. This length is referred hereafter as the distance of influence for surge and flow. In order to account for the effect of increased sea level, a 0.34m SLR projected for the next 100 year was used in the model in addition to the existing surges downstream. The SLR value was obtained from NOAA Tides and Currents (NOAA, 2020a) for DC station and was used in the ALX station.

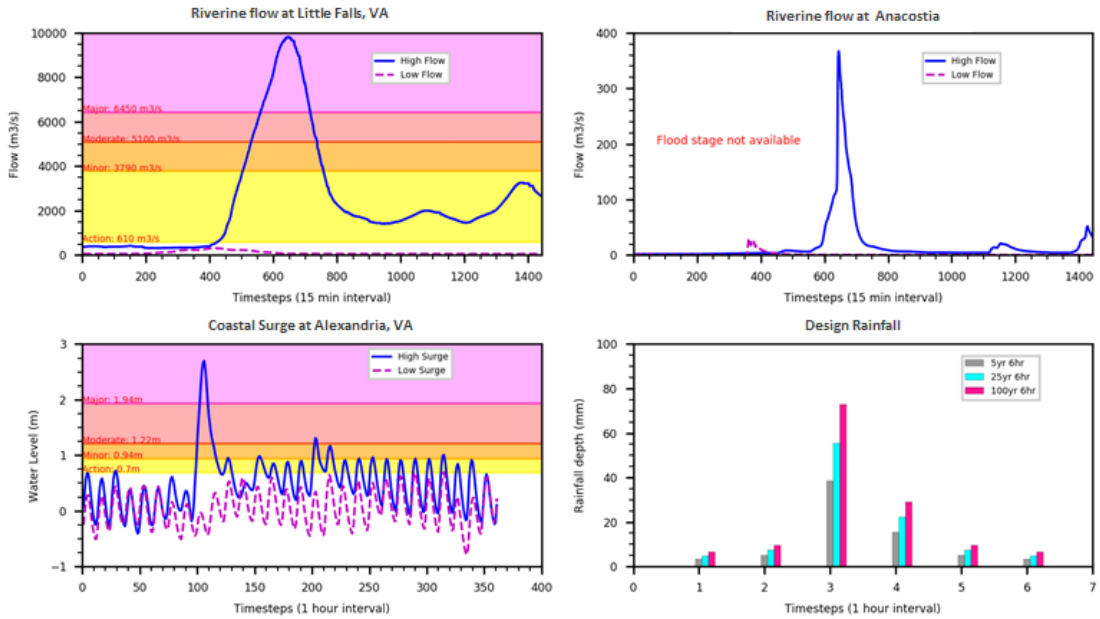

Figure 22 Synthetic storm inputs of flow, surges, and design rainfall

2.2.5 Validation of Simulated Flood Events

The model simulations were validated for historical storms based on the water level at the DC station and the inland flood depths at some specified locations near the Potomac River. These events were selected because the flood water during those events affected Washington, DC, The Tidal Basin, Old Town Alexandria, and the other surrounding areas. We considered uniform CN (either CN 65 or CN85) for the runoff in the full domain. The time series of simulated water levels had R^2 values in the range of 0.96-0.98 (Figure 23). R^2 values greater than 0.5 are considered acceptable (Moriasi et al., 2007). Such high collinearity between the model and the observed results demonstrated the similarity between the meteorological and hydrological characteristics of downstream boundary at ALX and the station at DC.

The bias in the flood depth results from the CN 65 or CN 85 scenarios varied for different inland locations (Figure 24). However, most of the simulated maximum flood depths were within the range of NWS or AHPS flood depths. These flood depth layers (NWS, 2020) were developed for the Flood Inundation Map Library displayed in the NWS's AHPS database. The flood depths represent potential flood extent for specific water levels as recorded at the Potomac River gages. These layers were created to correlate observed and forecasted flood levels with a visual representation of the areas impacted by floods. Depth grids for the inundation were simulated by USACE-Baltimore District. Flood depth locations were matched by selecting exactly the same point based on latitude and longitude. Results showed that urban flood depths with Curve Number (CN) 65 during Hurricanes Sandy and Ernesto were more representative of the flood depth provided by NWS. On the other hand, flood depths obtained from the CN 85 grid were more representative of the NWS flood depths for Hurricane Isabel and Jan 1996 flood. The results can be attributed to the lower rainfall (less than 70mm) during Hurricanes Sandy and Ernesto and higher rainfall (more than 150mm) during Hurricanes Isabel and Jan 1996 flood. Flood depths in Hains Point and East Potomac Park were in good agreement with the NWS depth for all the four events because CNs could represent the less imperviousness of those areas. Flood depths in Reagan Airport, Navy Yard, and Department of Defense varied from NWS data due to the higher impervious area.

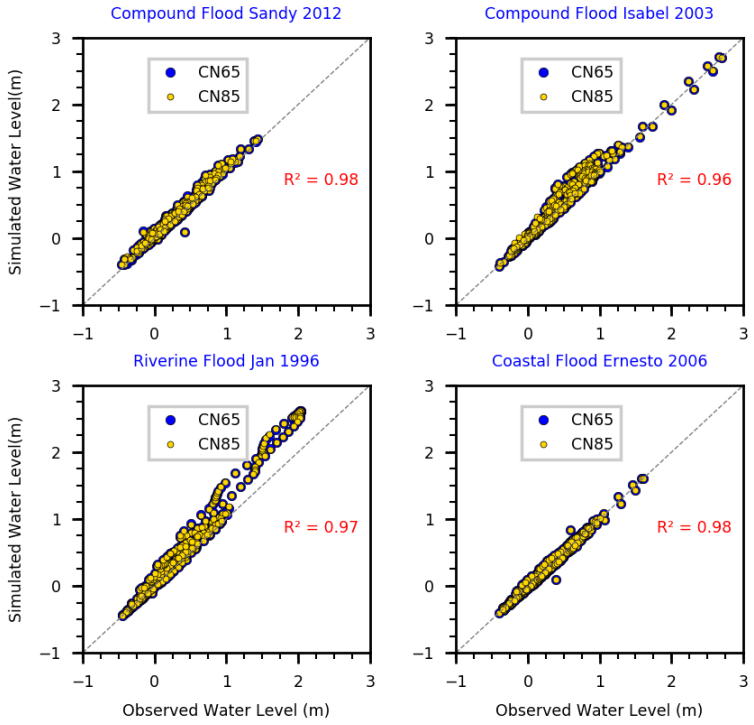

Figure 23 Validation of simulated water level at Washington DC station

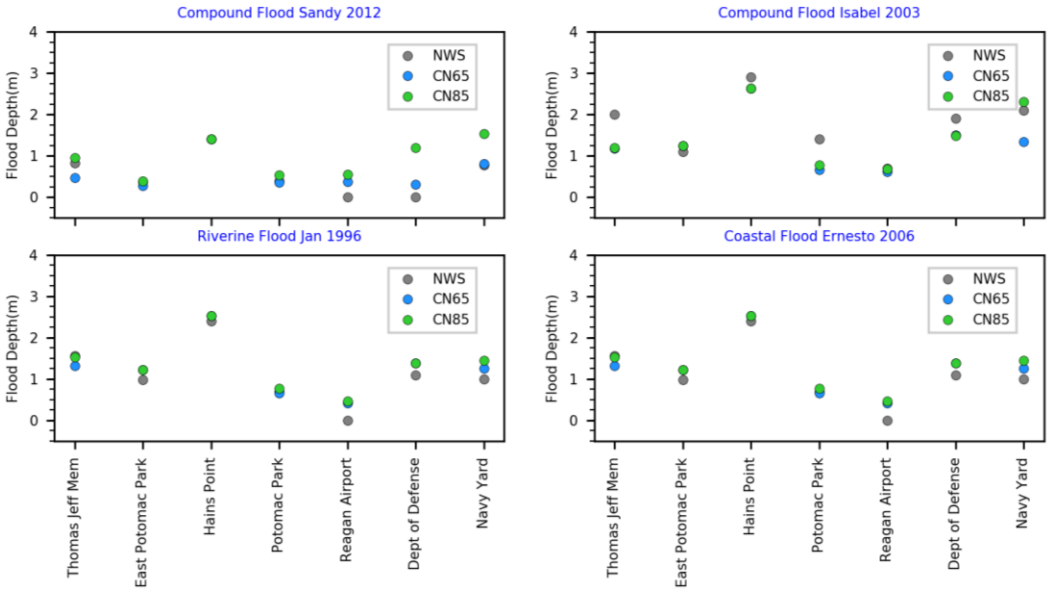

Figure 24 Validation of inland flood depth (NWS=National Weather Service simulated flood depth, CN65 = Depth using runoff scenario of CN 65, and CN85 = Depth using runoff scenario of CN 85)

2.3 Results and Discussions

This study has assessed compound flood variability driven by multiple factors in spatial and temporal dimensions. Results from this study include analysis on i) how different locations in the metropolitan area adjacent to Potomac River experienced variability in flood depth and extent ii) variation of flood characteristics from upstream to downstream iii) impact of compound flood drivers on the urban streams drainage iii) identifying the hotspots of compound urban flooding both along the river banks and inland and iv) the impact of SLR scenario on compound flooding. Detailed outcomes of all the scenarios are discussed in this section.

2.3.1 Flooding in the Metropolitan Area

The flood maps derived from the 28 synthetic events provided an indication of the sensitivity of our study area to different types of flooding. Results demonstrated larger differences in flood extents and inundation depths considering the low flow and low surge scenario vs the high flow and high surge scenario (Figure 25). In addition, the simulation provided information on temporal variation of the flood events, which is another important parameter of urban flooding. It was observed that during the first ten days of the 15 day events, flood extent increased rapidly. As expected, the duration of flood also increased with the increase in CN or rainfall depth (Figure 26). Some of the highly urbanized areas and lakes within the study area had longer flood duration as shown within the yellow colored locations. It was observed that higher runoff (100-year rainfall) dominated flooding had longer duration than only flow or surge dominated flooding, mainly, due to the water trapped inland. The second highest duration was

observed during high surge induced floods (Figure 27). In this intertidal zone, high surge events with extreme precipitation and high river flows lead to increased flood severity and duration as concluded by the previous compound flood studies (Svensson and Jones, 2002; Svensson and Jones, 2004). As suggested by Kundzewicz et al. (2019), our analysis also showed that the nature of flooding changes with increasing amplitude of rainfall induced runoff, as well as extreme riverine and coastal flooding. For instance, considering only coastal storm surges would have underestimated the flood extent by 10% and average depth by up to 1.1m locally (Figure 28). A similar study (Kumbier et al., 2018) showed an underestimation of those outputs by 40% and 1.5m respectively. The total inundation area varied from about 50km^2 to 175km^2 depending on the flow, surges, and rainfall inputs. Although rainfall was the dominant factor for increased inland flood inundation, flow and surge plays an important role in increasing the flood depth close to the river. A high flow scenario inundates significantly less amount of area compared to the high surge scenario. In order to compare the increase in flood inundation area for each rainfall condition, low flow low surge scenario with no rainfall, 25-yr, 50-yr, and 100-yr rainfall was each considered a base case scenario. The percent increase in area from the base case scenario (with no runoff) to high flow and high surge scenario (with no runoff) shows that inundation area depends significantly on coastal surges. Moreover, as the precipitation increases, the impact of compound flood and surge driven flood becomes very similar. With no runoff scenarios, the compound flood inundation is much higher than the flow dominated flood. Although we have used uniform runoff and synthetic flow or surge scenarios, the spatio-temporal variability results of this model

aligns with recent findings (Kumbier et al., 2018; Kundzewicz et al., 2019) on compound flood variability.

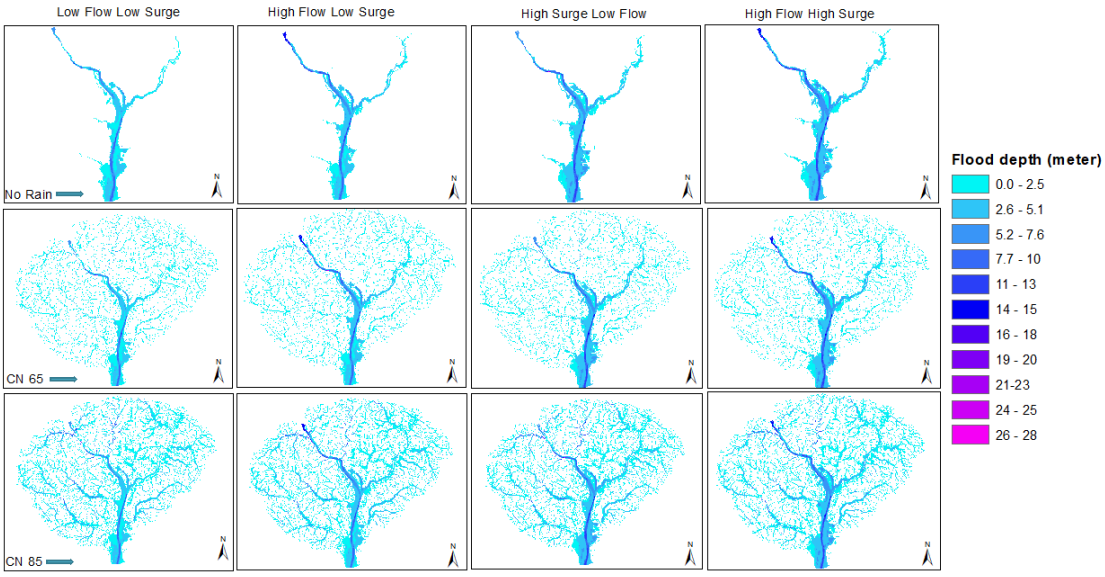

Figure 25 Maximum flood depth using 25 year rainfall

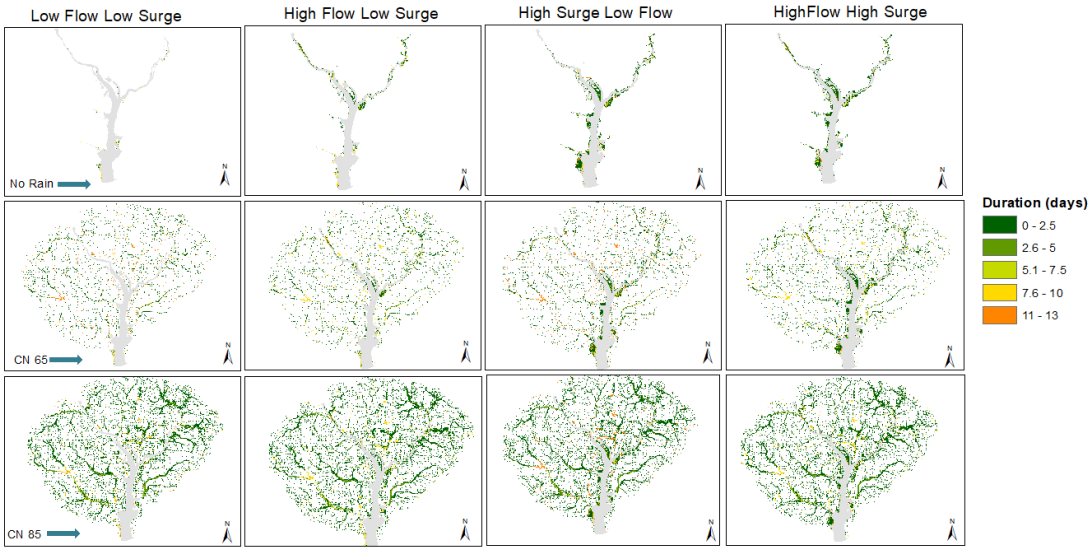

Figure 26 Total Flood Duration with 25 year 6 hour rainfall

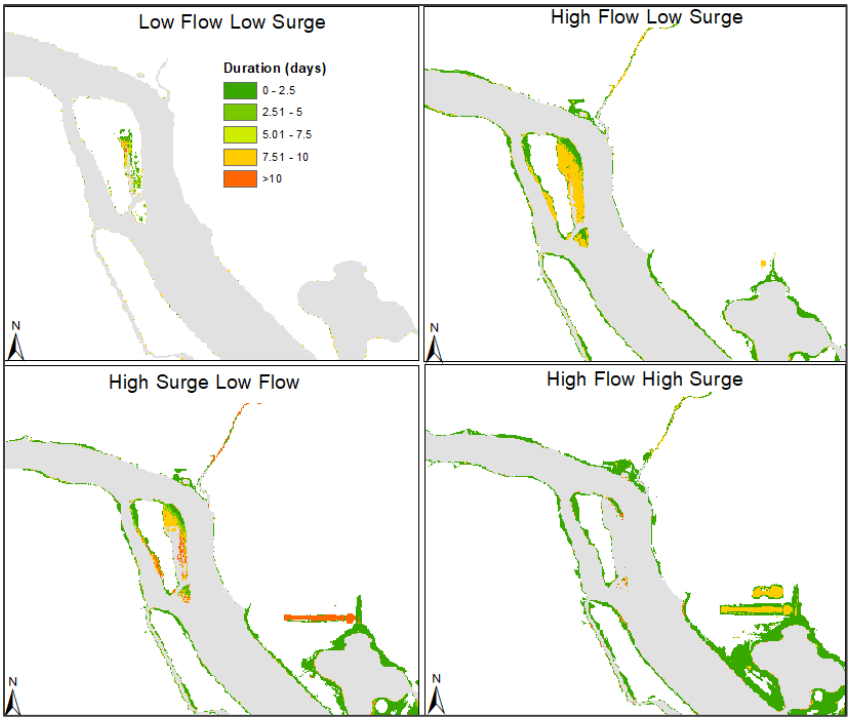

Figure 27 Duration of different types of floods with no rainfall scenario (zoomed in near Tidal Basin)

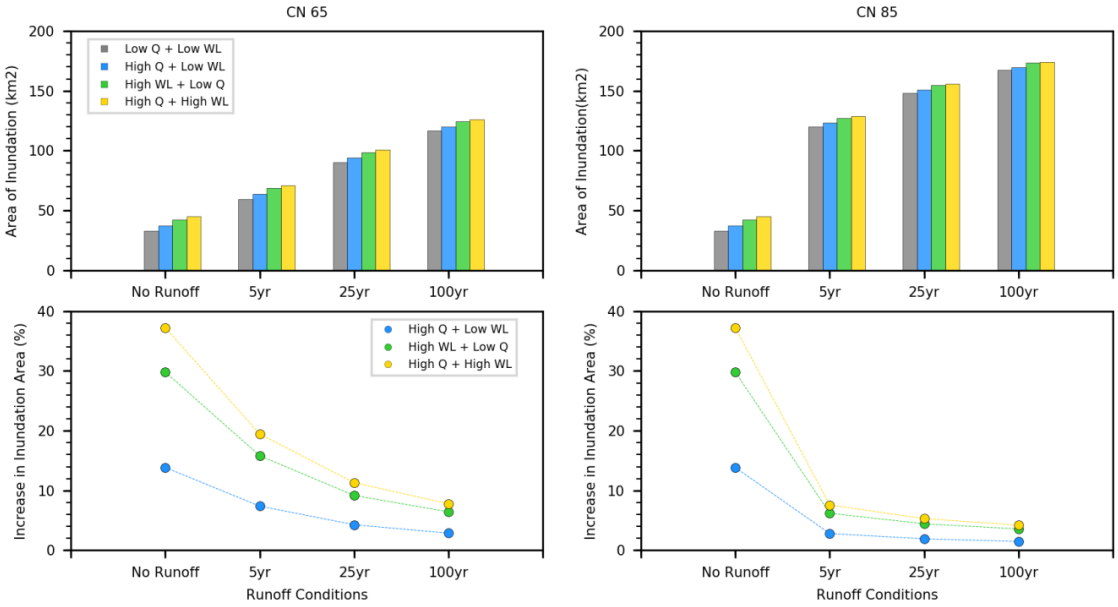

Figure 28 Total flood inundation area and the increase in flood inundation compared to low flow low surge 5, 25, and 100 year rainfall scenarios

2.3.2 Variation of Flood Characteristics from Upstream to Downstream

Identifying the flood locations and understanding the flood characteristics in those locations are very important to support the flood management strategies in urban areas (Depietri et al., 2018). In this study, we analyzed the impact of flow and surge at different locations along the Potomac River as shown in (Figure 29) and (Figure 30). The flow dominated region extended up to John F Kennedy Center while moving from upstream to downstream (Figure 29a and Figure 30a). From Ohio Drive SW1 to the George Washington Parkway Lower point, surge started to become more important compared to flow (Figure 29b and Figure 30b). After the Ohio Drive SW1 location, surges became the dominating factor for flooding as we moved towards downstream. All the locations along the Lower Potomac River were highly influenced by surges (Figure 29(d,e) and Figure 30(d,e)). In Old Town Alexandria and National Harbor, surge dominated flood depths were almost twice the flow dominated depths. Floods around Washington DC continued for several days affecting the important landmarks like the Seafood Market, Thomas Jefferson Memorial, Lincoln Memorial, Navy Yard, Reagan National Airport, Pentagon Parking, East Potomac Park, and East Potomac Golf Club and inundating other parts of this highly urbanized area. Flood depths in the urban locations adjacent to the Potomac River were not significantly sensitive to rainfall as shown in Figure 30 with no rainfall and 25-year rainfall results. From this analysis, we found that the study area can be divided into three zones: flow dominated upstream zones, flow and surge dominated transition zone, and surge dominated downstream zone.

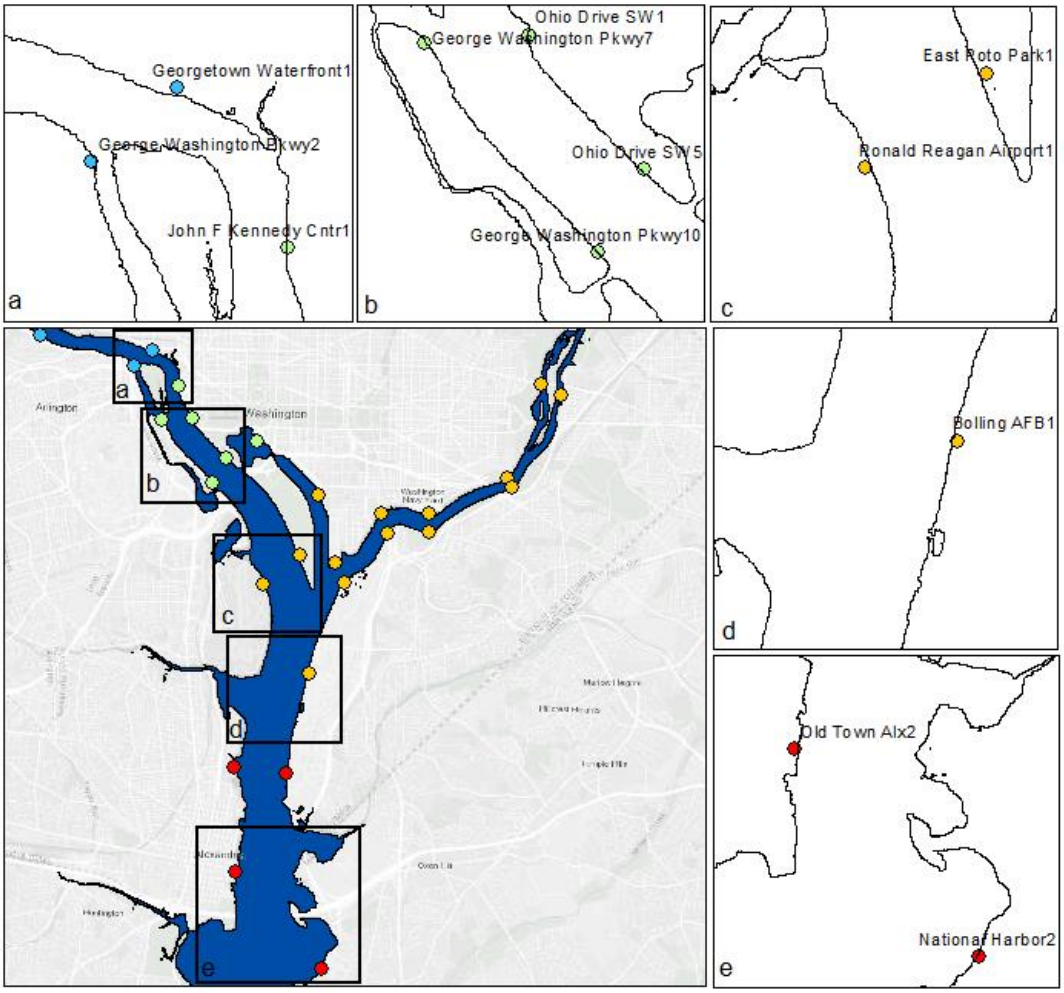

Figure 29 Selected locations for flooding along Potomac River (blue points are highly dominated by flow, green points are dominated by either flow or surge, orange points are surge dominated, and red points are extremely sensitive to surge dominated floods)

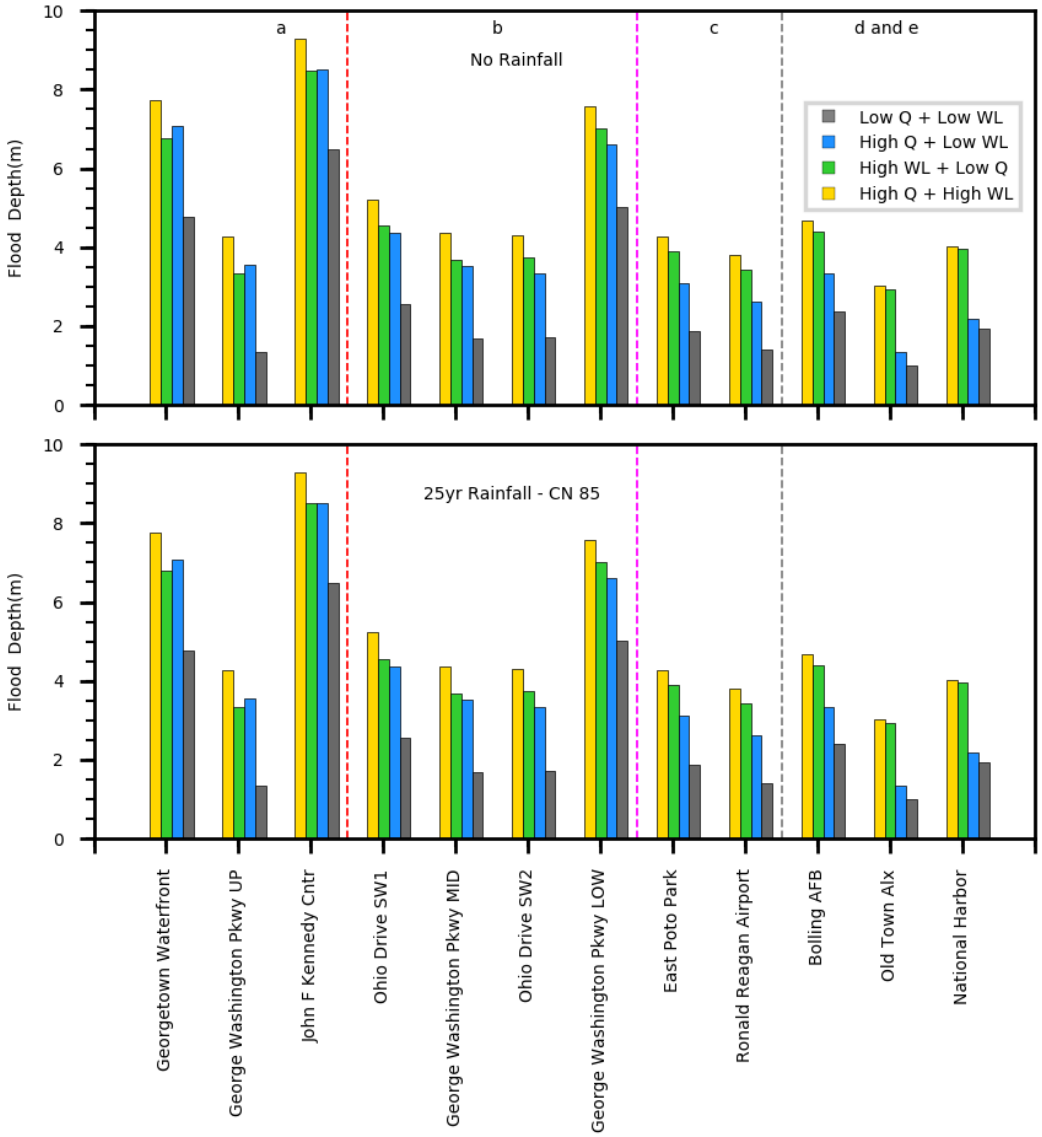

Figure 30 Impact of flow and surge from upstream to downstream of Potomac River without and with 25-year rainfall

Different flooding events in the same area can inundate different locations depending on the characteristics of the flood drivers. We selected two locations, Old Town Alexandria (ALX) and Reagan Airport (RR), with four points each (ALX1, ALX2, ALX3, and ALX4; RR1, RR2, RR3, and RR4) in order to analyze the variable impact of

flood drivers from river banks towards inland (Figure 31) maintaining the order of location numbers. It was found that the floods that threatened the city of Old Town Alexandria were mostly runoff induced floods towards inland (ALX3 or ALX4) with approximately 0m, 0.9m and 1.2m depth due to no rainfall, 25-year rainfall, and 100-year rainfall respectively, and surge induced floods close to the river with 3m (ALX1) and 2m (ALX2) depths based on any rainfall scenario (

Figure 32). This concludes that ALX1 and ALX2 were less impacted by rainfall depth, while ALX3 and ALX4 were significantly sensitive to any value of rainfall. The worst case was observed when high surge from downstream and high flow from upstream occurred together around this developed area obstructing the urban water to flow towards the river, similar to the findings of compound flood impacts studied by Huong and Pathirana (2013). Another study also suggested similar outcomes with an additional high runoff trapped upstream due to high surges (Van Den Hurk et al., 2015). Rainfall had significant impacts on flooding in Reagan National Airport as well. Inland flooding was increased by rainfall to a greater extent, about 0.5m increase in maximum depth compared to no runoff scenario at RR3 and RR4. Without rainfall, surge was the dominating factor generating a depth of 0.75m at RR1 located near the river bank.

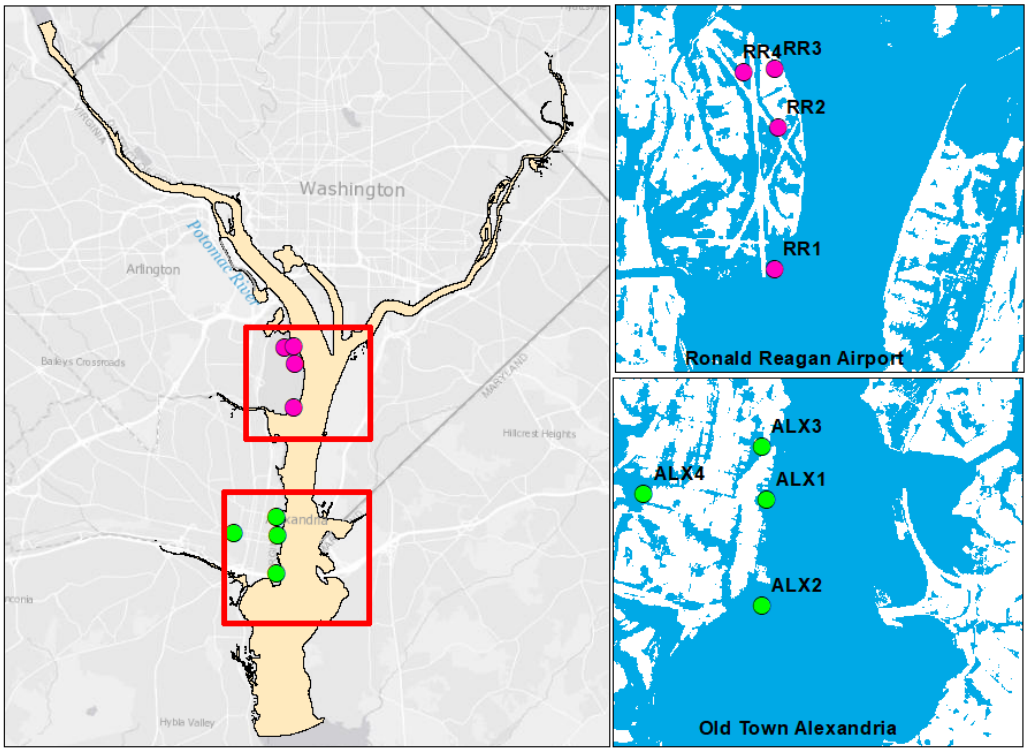

Figure 31 Flood depth locations towards inland

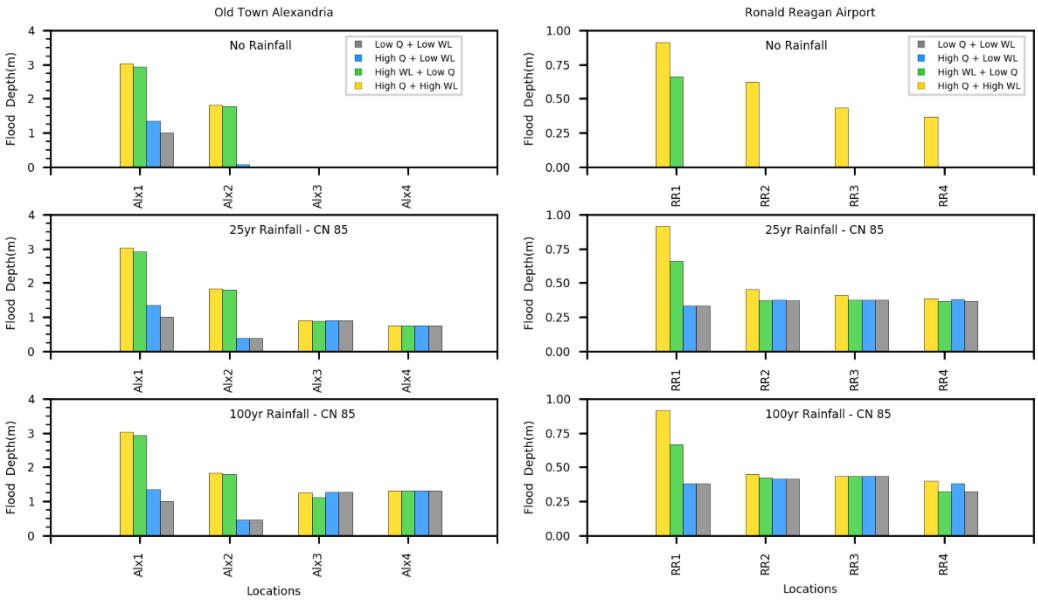

Figure 32 Change due to the impact of rainfall, flow and surge at the inland locations

2.3.3 Impact of Compound Flood Drivers on the Urban Streams Drainage

2.3.3.1 Impacts on Local Stream Water Levels

We evaluated the impact of the flood drivers on the downstream water level of local streams which affects its drainage capacity during rain fall events in the urban watersheds. Few points were selected to investigate the impact of flood drivers on the mouth of the streams and small water bodies where the river connects. Rock Creek was one of the most important streams for flooding in the Washington, DC area as significant amount of the urban runoff drains into this stream throughout its length. Rock Creek was impacted both by flow and surges, flow being slightly more dominant. According to FEMA, Rock Creek can significantly inundate the surrounding areas with a 100-year design rainfall induced runoff (Federal Emergency Management Agency, 2010) which was evident form the results. The analysis on the small streams showed that riverine flood and compound flood had almost similar impact on the streams at the Upper Potomac River (upstream to Rock Creek), such as Pimmit Run (Figure 33), because the Potomac River near LF Pumping Station (USGS Station No. 01646500) is not influenced by tides. The other streams downstream of Rock Creek were highly dominated by coastal surges. The two points near Pentagon Lagoon and Gravelly Point were dominated by surges as well. Streams at Lower Potomac and Anacostia responded in the similar pattern during surge dominated events.

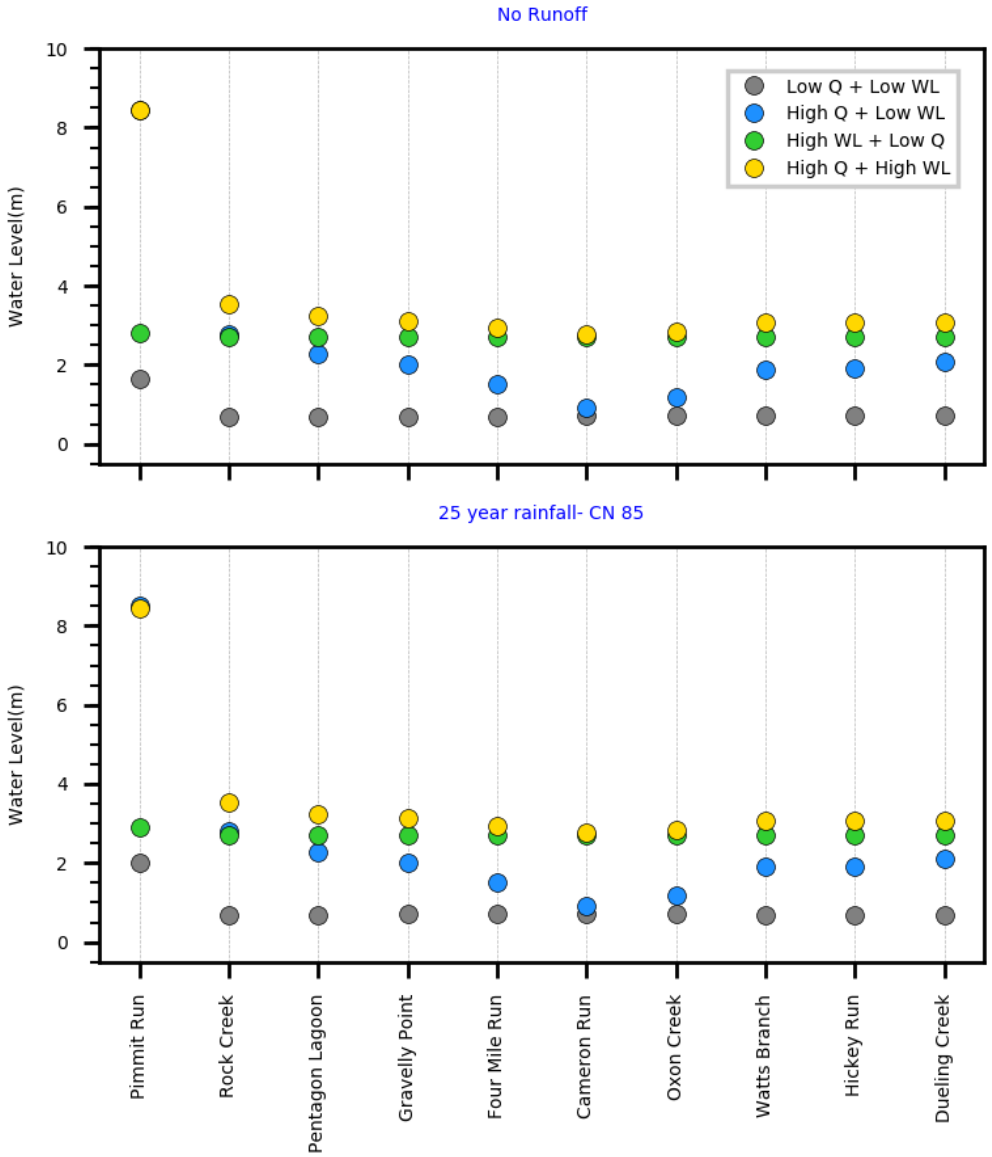

Figure 33 Water levels in streams with and without runoff

2.3.3.2 Distance of Influence

Riverine flow and coastal surges had a minor impact on the overall urban flooding of the National Capital Region. However, these drivers significantly impacted the regions along the main river and the small streams with its impacts propagating up to 8km

upstream for some small streams. If there is no rainfall, the flood depth will be zero at this point, irrespective of high or low flow and surge values. We analyzed the distance of influence for all the streams in the study area (Figure 34). The distance of influence was higher for the streams along Lower Potomac River. However, Rock Creek had the highest distance of influence among all the streams. The lowest distances of influence were found for the smaller streams around Upper Potomac River. As expected, the slope of the streams played a significant role in the distance of influence. Streams can be categorized based on the slopes (S): very steep ($S > 0.1$), steep ($0.04 < S < 0.1$), moderate gradient ($0.02 < S < 0.039$), and low gradient ($S < 0.02$) streams (Rosgen, 1994). The streams that had lower distance of influence also had steeper slopes in the analysis (Figure 35). Those streams were the smallest in length among all the streams considered in this study. The distances of influence increased with the increase in rainfall, as the rainfall accumulated in the streams and transported the impact of riverine flow more towards upstream of the small streams.

Detailed information about the streams is presented in Table 7. Rock Creek, Four Mile Run, Cameron Run, and Oxon Creek had higher distances of influence which were classified as low gradient streams. However, although many streams fall in the same classification, there are differences in the distance of influences based on the actual value of slope. For example, Rock Creek and Four Mile Run are both low gradient streams but the slope of Rock Creek (0.003m/m) is smaller than Four mile Run slope of 0.0074m/m. Therefore, Rock Creek had a higher distance of influence than Four Mile Run. This

analysis showed that the low gradient streams are more susceptible to the impacts of high flow and high surge on urban flooding.

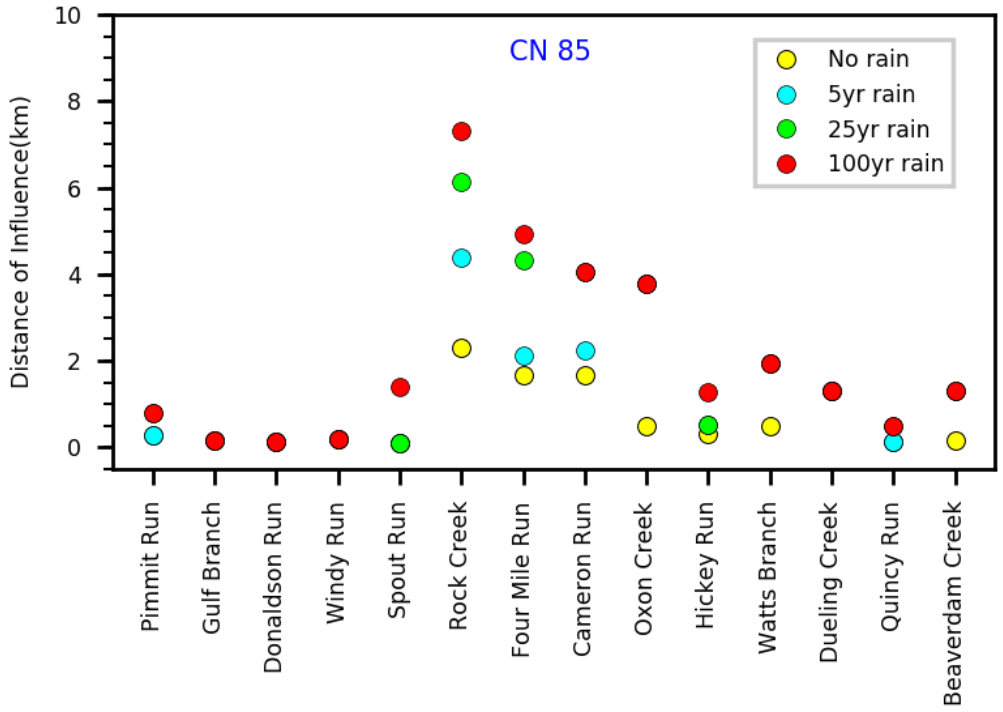

Figure 34 Distance of influence for surge and flow in the streams

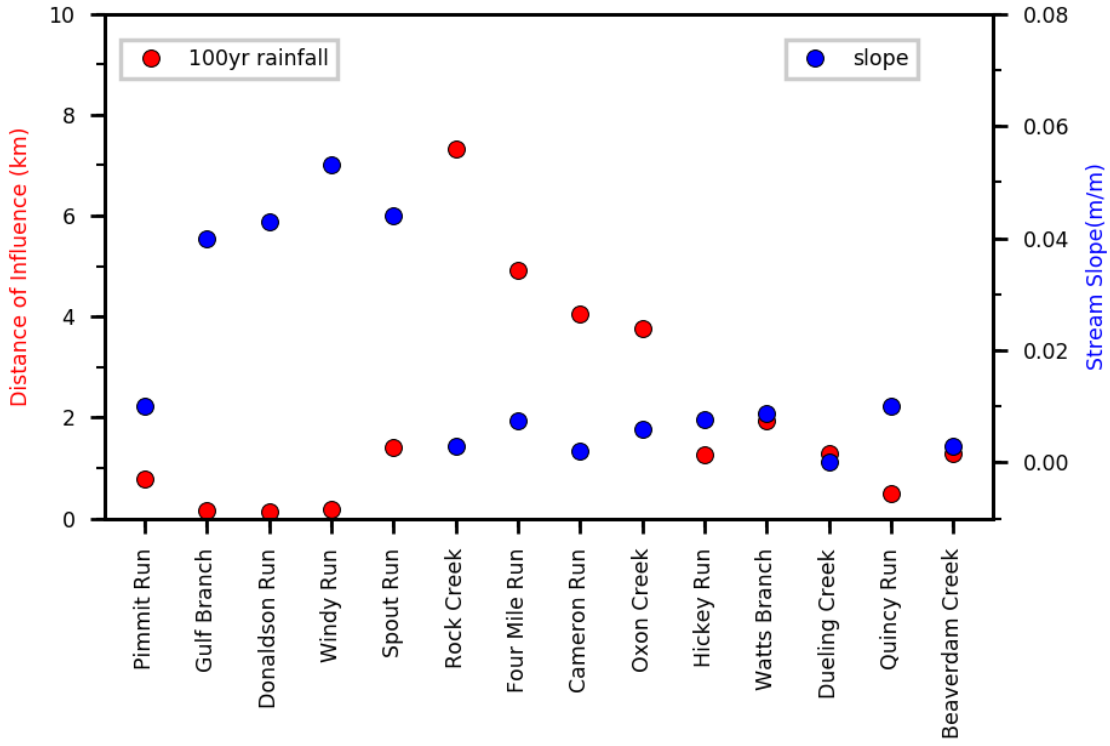

Figure 35 Impact of stream slope on distance of influence

Table 7 Stream properties with slope classification based on Rosgen (1994)

Streams	Length(km)	Width(m)	Slope(m/m)	Slope type
Pimmit Run	8.43	1.2	0.01	low gradient
Gulf Branch	1.4	1.78	0.04	steep
Donaldson Run	2.48	1.7	0.043	steep
Windy Run	0.99	1.5	0.053	steep
Spout Run	1.36	2.13	0.044	steep
Rock Creek	15	25	0.003	low gradient
Four Mile Run	14	93	0.0074	low gradient
Cameron Run	5.34	43	0.002	low gradient
Oxon Creek/Run	12.28	62	0.006	low gradient
Hickey Run	1.51	15	0.0077	low gradient
Watts Branch	7.66	33	0.0088	low gradient
Dueling Creek	1.21	45	2.40E-05	low gradient
Quincy Run	1.538	1	0.01	low gradient
Beaverdam Creek	7.527	33	0.003	low gradient

2.3.4 Hotspots of Compound Flooding

Most of the low-lying locations along the Potomac River are hotspots of compound flooding (Figure 36). In our study, the area between the Washington Channel and Ohio Drive Southwest, especially the Haines Point, East Potomac Park, and East Potomac Golf Course were highly exposed to the compound floods driven by the riverine flow and surges or riverine flow, surges, and rainfall. The low lying areas near Four Mile Run, Cameron Run, and Oxon Run were highly inundated by compound flooding events. Locations near Department of Defense and Anacostia Park also showed significant compound flooding. Moreover, some locations in the upstream area, close to Little Falls, were also inundated by compound floods. Without rainfall, locations only in the close proximity of the Potomac River and Anacostia River were flooded by compound flood drivers. When rainfall was forced in the model, small areas along the streams showed compound flooding depths as well, which can be found in (Figure 36b) with very small orange dots. These orange flooding locations were at the same distance where we estimated the distance of influence for different streams discussed previously and represents compound flood locations inundated due to river flow, coastal surge, and rainfall.

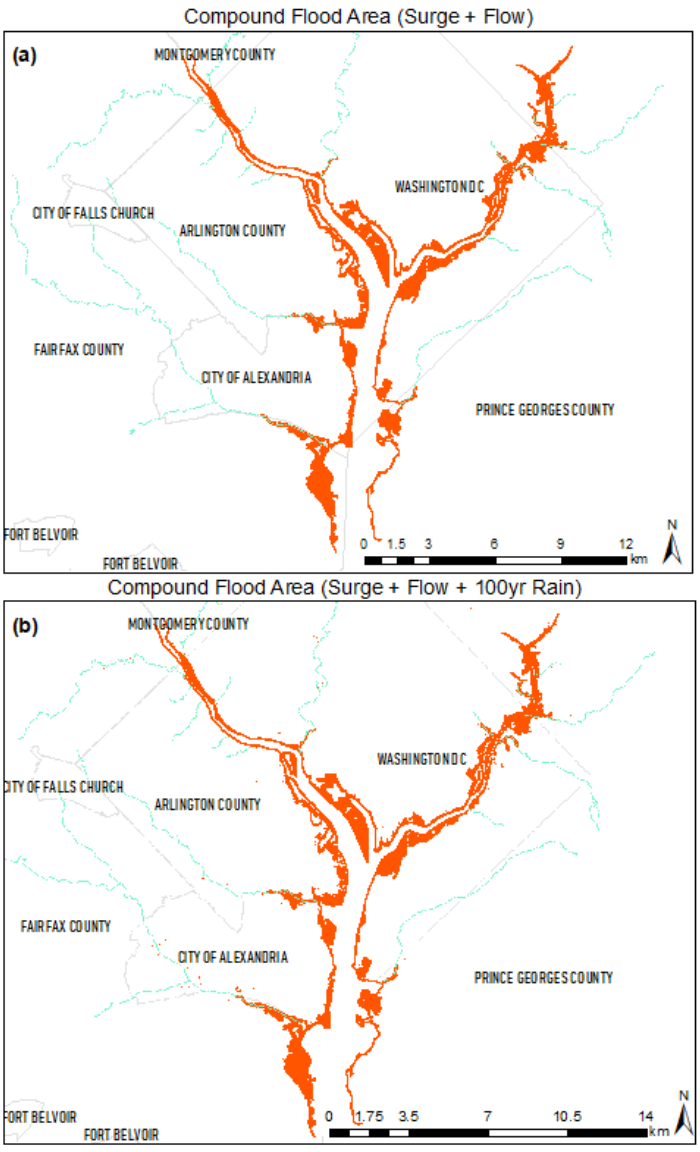

Figure 36 Locations of compound flood along the rivers and the streams

2.3.5 Impact of Sea Level Rise on the Compound Flooding

Washington, DC will face flooding, and eventual geographic changes in the long term because of increased sea level (Ayyub et al., 2012). Increase in minor flooding along the coasts of the US is also expected due to the SLR (Moftakhari et al., 2015). The highest impact of SLR was on the inundation area of Low Flow and High Surge Scenario

(5% increase) and the lowest impact was on the High Flow and Low Surge scenario with 2% increase in inundation area (Figure 37). However, the increase in flood depth was only visible in the locations adjacent to the river. Model simulations with SLR showed that new locations around the Potomac River and Anacostia River will become vulnerable to flooding and areas that were already flooded in current scenarios may experience increase in both flood extent and depth (Figure 38). This is because the SLR will increase the flood depths in the surrounding areas. For example, a flood stage at DC, which is less than 0.7m (no flood), can increase to more than 0.7m leading to possible *Action*, *Minor*, *Moderate*, or *Major* floods. The red and orange points will be impacted the most due to SLR in all the four scenarios. Increased flood water from SLR and high surge can reach Little Falls, which is not impacted by surge at present. It was also observed that a low surge and high flow scenario, along with SLR, will have much less impact among all the scenarios. The reason could be that the increased depth throughout the river reduces frictional resistance, thereby reducing the water level slope and the water level as well (Orton et al., 2018).

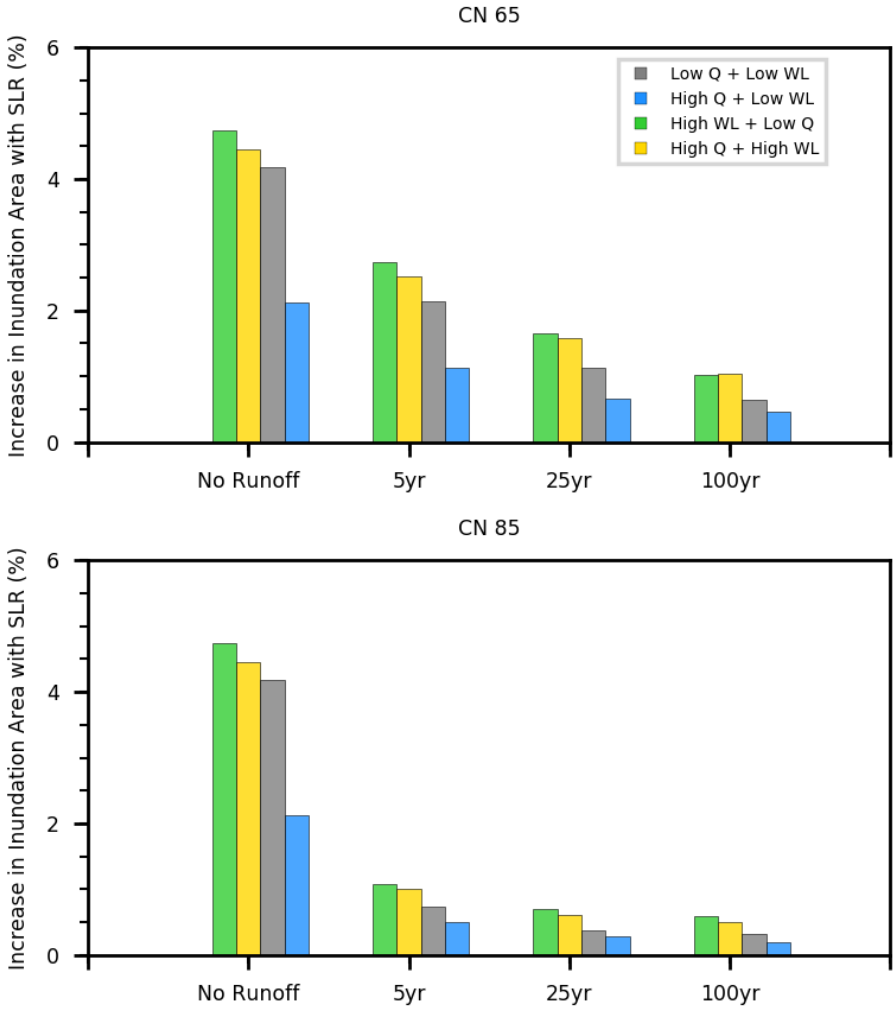

Figure 37 Increase in inundation area due to SLR

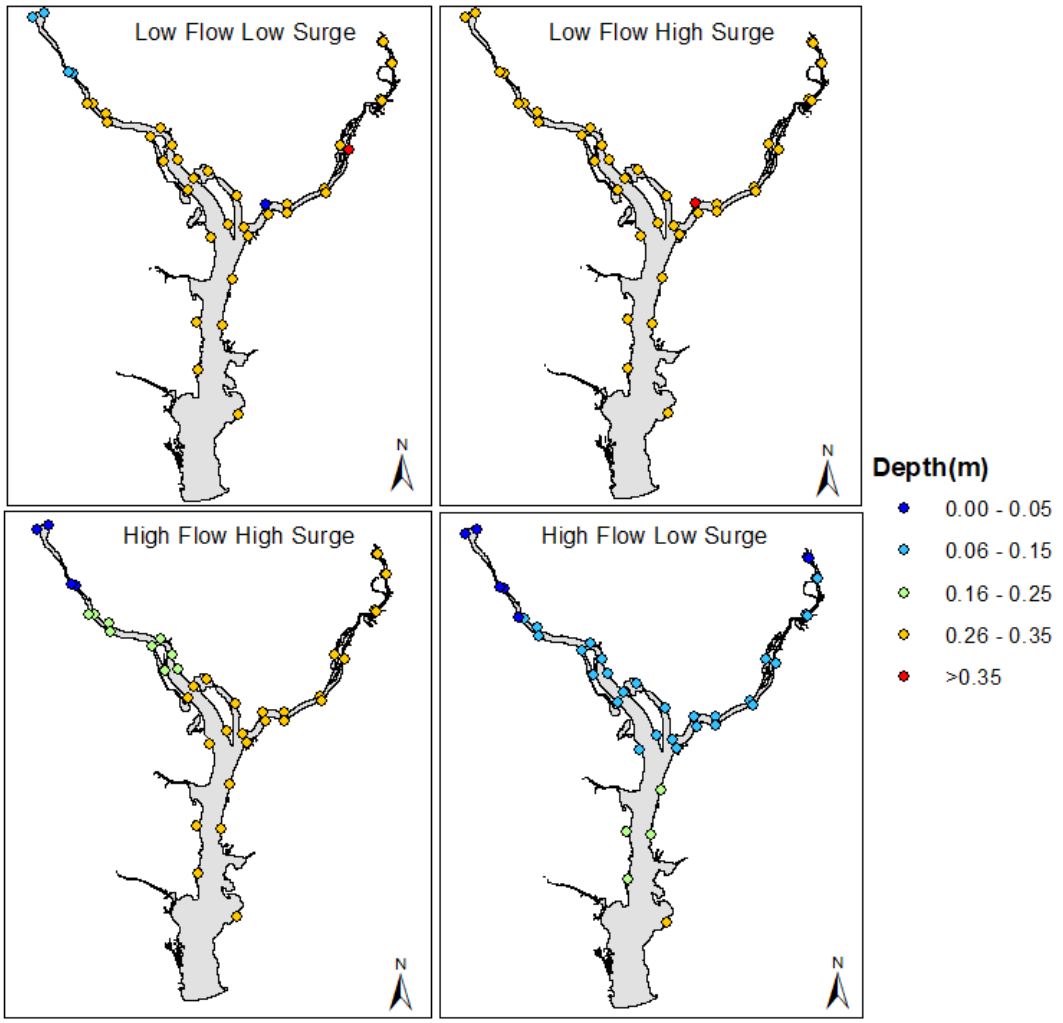

Figure 38 Increase in flood depth due to SLR with no runoff

2.4 Conclusions

A larger part of the Washington DC metropolitan area is in floodplain areas of the tidal Potomac River, as are many of the tidal cities of the US. Furthermore, Washington DC is exposed to different hazards including coastal surges, riverine flow, and intense runoff due to rapid urbanization. The goal of this study was to assess compound flood variability in space and time driven by multiple factors. The results from our study

suggested that, in the highly urbanized DC area, inundation extent increased by 10% with high surges and flow. While flooding driven by a single variable (high surge or high flow) also caused flooding in the region, multiple factors associated with the event (i.e. compound scenario) increased the flood extent and water depth, in some cases doubling the inland flood depths. The dominating factors of the flood scenario helped to understand the flooding properties along the Potomac River: i) riverine flood impacted mostly in the upstream part of the river, ii) both riverine and coastal boundaries dominated the flood along the middle part of the river, and iii) the lower part was highly influenced by surge only. The area at the confluence between the Potomac and Anacostia Rivers was highly exposed to the compound floods driven by the riverine flow and surges or riverine flow, surges, and rainfall.

Surge induced floods inundated most of the areas close to the Lower Potomac River. On the other hand, intense runoff generated greater flood inundation in the urban areas located far from the rivers but adjacent to the streams. Low gradient streams were mainly responsible for urban or inland compound flooding due to the impact of flow and surge being present at a longer distance from the stream mouth. High flow and surge did not have significant impact on the streams with steeper slopes mainly located on the Upper Potomac region. To incorporate the effects of climate change, 0.34m SLR were implemented on the model which showed that locations adjacent to the Potomac and Anacostia River banks will become more vulnerable to flooding, especially during high surge events, and some areas may even experience increase in both inundation extent and depth.

Few assumptions in the modeling and averaged inputs may lead to a relatively increased bias or uncertainty in the outcomes of this study. We estimated area averaged CN (CN 65 and CN 85) to generate uniform runoff for the study area, while accurate flood modeling requires a storm-runoff model and an inundation model to generate the area specific runoff as input. Furthermore, meteorological factors, such as the timing and distribution of rainfall, may cause change in actual streamflow along the modeled reach leading to variations in the water-surface elevations and inundation boundaries. However, the methodology and outcomes from this study can be implemented in other metropolitan areas to understand the flood variability in terms of depth and extent, stream flood characteristics during different events, and change in flood duration due to the change in flood drivers along the urban areas located along tidal rivers and estuaries.

3 REAL-TIME COMPOUND FLOOD FORECASTING IN URBANIZED AREAS OF THE WASHINGTON METROPOLITAN REGION

Abstract

Flooding is the most frequent natural disaster impacting the economy, environment, and societies. Like many coastal cities in the United States (US), extreme flooding in the Washington, DC metropolitan region is generated by the co-occurrence of multiple flood drivers such as riverine flow, coastal surges, and intense rainfall-induced runoff. This study has developed a compound urban flood forecast system based on a 2-dimensional (2D) hydrodynamic model that incorporates all the flood drivers associated with flooding in the region. Forecasting the compound urban flood events encompasses the complex dynamics between the flood drivers in the urban watershed. Moreover, data scarcity on the urban flood depths and extents during extreme events is another challenge to validate the urban flood forecast system. Therefore, the forecasted flood depths and extents along the rivers and the adjacent areas are compared to the available information, videos, and photos from newspapers and social media. The use of such crowdsourced data has made it possible to validate any real-time forecasts in the urban locations of the study area. The system was run by forcing the model with the forecasted river flow and coastal water level from the Advanced Hydrologic Predictions Service (AHPS), flow from the National Water Model (NWM), and coastal water level from the Integrated Flood (iFLOOD) system, and precipitation dataset from High-Resolution Rapid Refresh

(HRRR) database. Multiple forecasts are generated for each location with the variable inputs of flow, surge, and runoff. The optimum flood depth is selected based on the characteristics of the location, i.e., whether the location is urbanized or not. This modeling framework has highlighted the importance of total water level forecast resulting from compound floods in large metropolitan areas like Washington, DC. The forecast methodology developed in this study can be used for other coastal cities located along major rivers and estuaries.

3.1 Introduction

Compound floods from multiple flood drivers bring substantial impacts to human lives and properties around the world. High runoff and surges can cause compound flooding in the low-lying coasts and estuaries (Bevacqua et al., 2020; Ben Daoued et al., 2020; Fang et al., 2020). Storm surges alone are often the greatest threat to communities along the coasts of the US. Furthermore, these coastal areas are often prone to compound flood hazards from inland flow, rainfall, and sea-level rise (Wang et al., 2015; Kundzewicz et al., 2018). Hurricanes Isabel in 2003 (Sheng et al., 2010), Joaquin in 2015, Matthew in 2016 (Ezer et al., 2017), and Harvey in 2017 (Thyng et al., 2020) demonstrated the unprecedented damage caused by compound floods in the coastal cities. In 2016, two flood events in Louisiana inundated the rural, coastal, and urban watersheds due to the combined impact from river, coast and urban runoff (Laska, 2020).

Urbanization combined with rainfall, coastal surges, and riverine impact have increased the threat of large unprecedented floods in populated areas near coastal regions (Laudan et al., 2020). River floods increase water levels slowly after accumulating flood

water from the watershed, but urban floods are generated within small catchments leading to rapid and unpredictable flow (Kumbier et al., 2018; Laudan et al., 2020). However, flood modeling with only runoff, riverine flow or coastal surges can underestimate the compound flooding risk (Kumbier et al., 2018) in urban areas. Studies have performed global scale analysis of compound flooding from four types of flood drivers: surge-dominant, discharge-dominant, compound-dominant or insignificant drivers (Gallien et al., 2018; Eilander et al., 2020). Total water levels in the estuarine areas vary significantly due to the interaction of these variables which should be captured well through the flood modeling tools (Gallien et al., 2018). Therefore, the compound urban flooding needs to be studied and modeled locally due to its limited geographical extent and the physical interactions involved (Paprotny et al., 2018; Saleh et al., 2017).

An accurate and timely flood forecast system is an important tool to protect the people and infrastructures in flood-prone areas. National Weather Service (NWS) has adapted advanced techniques for simulating streamflow, flash-flood events, flood plain maps, and ensemble prediction for streamflow (Mcenery et al., 2005) through the Advanced Hydrologic Prediction Service (AHPS). However, there is greater uncertainty on how the compound flood will propagate into inland flooding (Couasnon et al., 2019), especially, in a real-time forecast system. An improved 1D or 2D model is needed to study the complex flooding in the urban areas (Barthélémy et al., 2018). Advanced multi-dimensional (2D-3D) models have a higher accuracy rate but it comes with a cost of higher simulation time, input data, and computational expenses (Contreras et al., 2020), which is a limitation for regional or local scale study.

The predictive skill of a real-time forecast system needs to be evaluated for implementing in decision making strategies. Although urban flood data is not available officially, advanced technologies have provided public access on large number of observations shared through social media, online news sites, and newspapers on any flood incident. The hydraulic data, such as flood depth and extent, can be easily extracted from photos and videos produced by the citizens on social media (Le Coz et al., 2016). Few studies have already evaluated the use of crowdsourced data for model validation in the areas where data is unavailable (Allaire, 2016; Poblet et al., 2018; Wang et al., 2018; Ogie et al., 2019; Yagoub et al., 2020).

The region along the tidal Potomac River is prone to riverine flooding like 1996 January, coastal flooding like Ernesto 2006, and at times a combined flooding from both river and coast. Washington, DC and the surrounding areas of Maryland and Virginia are hit by multi-flood hazards every year. The non-linear relation between the flood drivers causes the total water level to rise to an unprecedented level and cause severe damages. Therefore, an efficient urban flood forecast system is required for the region with accurate information ahead of any severe flood event. Our study has developed a real-time system with a 2D hydrodynamic model in the tidal Potomac River to generate forecast for the rivers, streams, and urban areas. The goal is to understand the physical characteristics of the flood drivers that generate compound flooding in the region and implement the outcomes for developing a real-time flood forecast system.

3.2 Methodology

3.2.1 Study Area

The study area is located at the junction of the Potomac and Anacostia rivers, and a small stream, the Rock Creek. Anacostia River is connected to the tidal Potomac River near Washington DC. Drainage area of the Anacostia River is 315 km^2 and the Rock Creek is 160 km^2 which are very small compared to the Potomac River drainage area of 30,000 km^2 (Huanxin et al., 1997). The upstream boundary begins at Little Falls, Washington DC and ends near Alexandria, VA. The tidal portion of the Potomac River includes Anacostia River, Roosevelt Island Channel, Washington Channel, Tidal Basin, Broad Creek, Piscataway Creek, Dogue Creek, Gunston Cove, Pohick Bay, and Accotink Bay tidal inlets (Schaffranek, 1987). There are several adjacent streams in the study area such as Pimmit Run, Rock Creek, Four Mile Run, Cameron Run, Oxon Run, Watts Branch, etc. The cities around Washington, DC are highly urbanized and experienced several flood over the years. The areas adjacent to Washington DC have extended at a higher rate (~22 km^2 per year) after 1972 (Masek et al., 2000). It has multiple future challenges: dense population, old sewer system, location at the confluence of two major rivers, increased runoff driven by imperviousness, and changing pattern of extreme rainfall and sea level rise due to climate change (Huong and Pathirana, 2013). Study area for compound urban flooding includes the urbanized portion of the Washington, DC Metropolitan Area, Montgomery and Prince George's county in Maryland, Fairfax county, Falls Church city, Arlington county, and Alexandria city in Virginia. Figure 39 shows the study area with the surrounding streams and land use types.

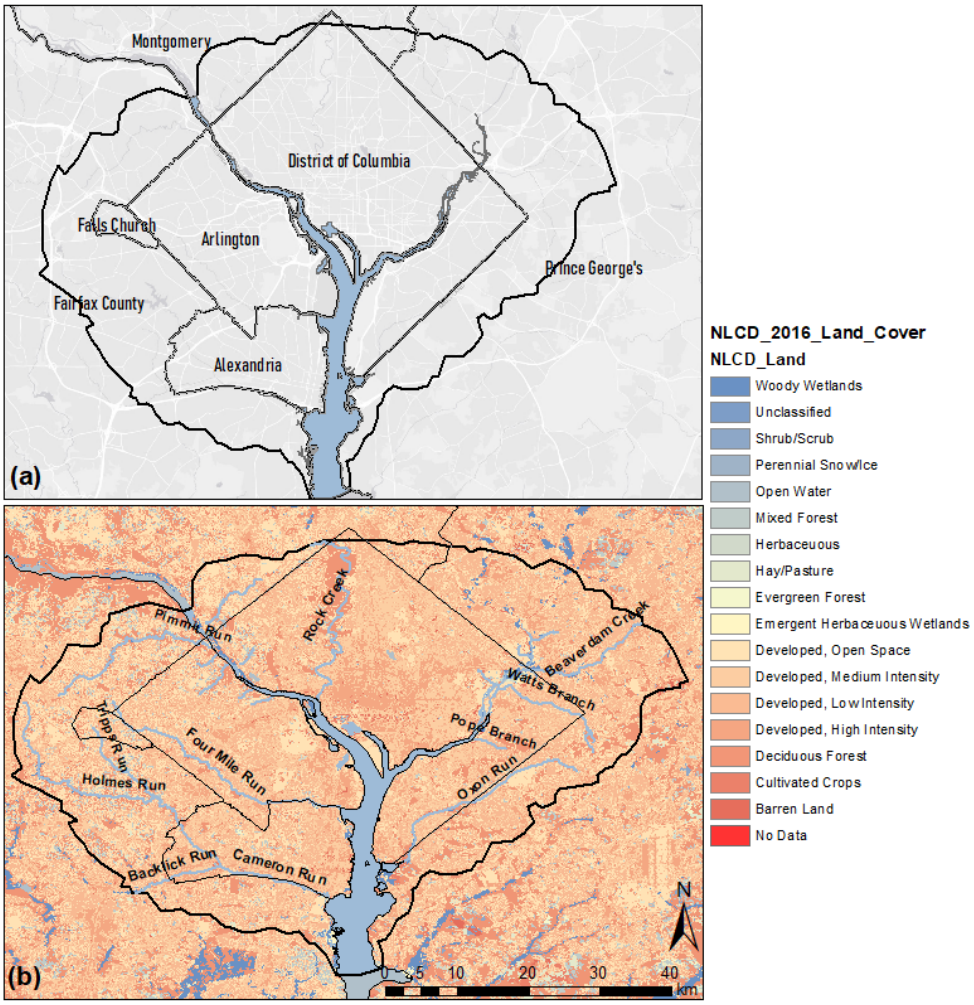

Figure 39 Study area showing a) cities and counties and b) land use type and streams

3.2.2 Model Setup

Our flood forecast system is developed using the Hydrologic Engineering Center's River Analysis System (HEC-RAS). This model allows 1D and 2D unsteady flow calculations for natural or constructed channels and the adjacent floodplain areas (Brunner, 2016). The upstream boundaries of the system are located in the flow dominated regions of Little Falls, DC and at the junction of Northwest and Northeast

Branch of Anacostia River. The downstream boundary is in a highly tide-dominated region at Alexandria, VA. A high resolution topo-bathy was generated for the model simulation using Digital Elevation Model (DEM) and NOAA Nautical Charts for the entire area along tidal Potomac River. The topo-bathy for our study area was then clipped from the entire topo-bathy. The DEMs were obtained from the United States Geological Survey (USGS, 2016), and the bathymetry data was collected from the NOAA Electronic Navigational Charts (ENC), a dataset prepared for supporting all types of marine navigation (NOAA, 2018b). NOAA ENC charts use tidal datum of mean lower low water (MLLW) and the DEM from USGS uses North American Vertical Datum of 1988 (NAVD88). The ENC datum was converted from MLLW to NAVD88 for the full model domain. The combined topo-bathy is shown in Figure 40 and the model boundaries for our forecast system are presented in Figure 41. Manning's roughness coefficient was estimated from literature (Bhandari et al., 2017), ranging from 0.015 to 0.16 depending on the land cover types shown in Figure 39.

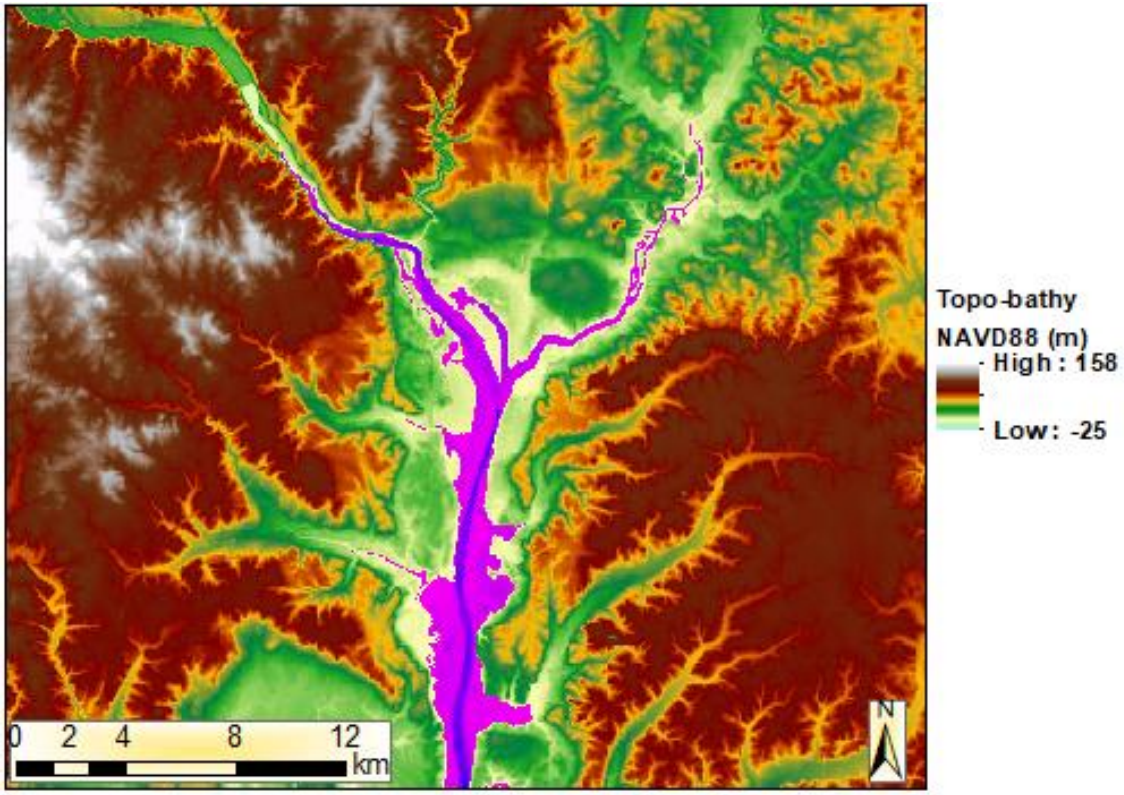

Figure 40 Topo-bathy for 2D grid generation in ArcGIS (blue and pink: river bathymetry, green and brown: inland topography)

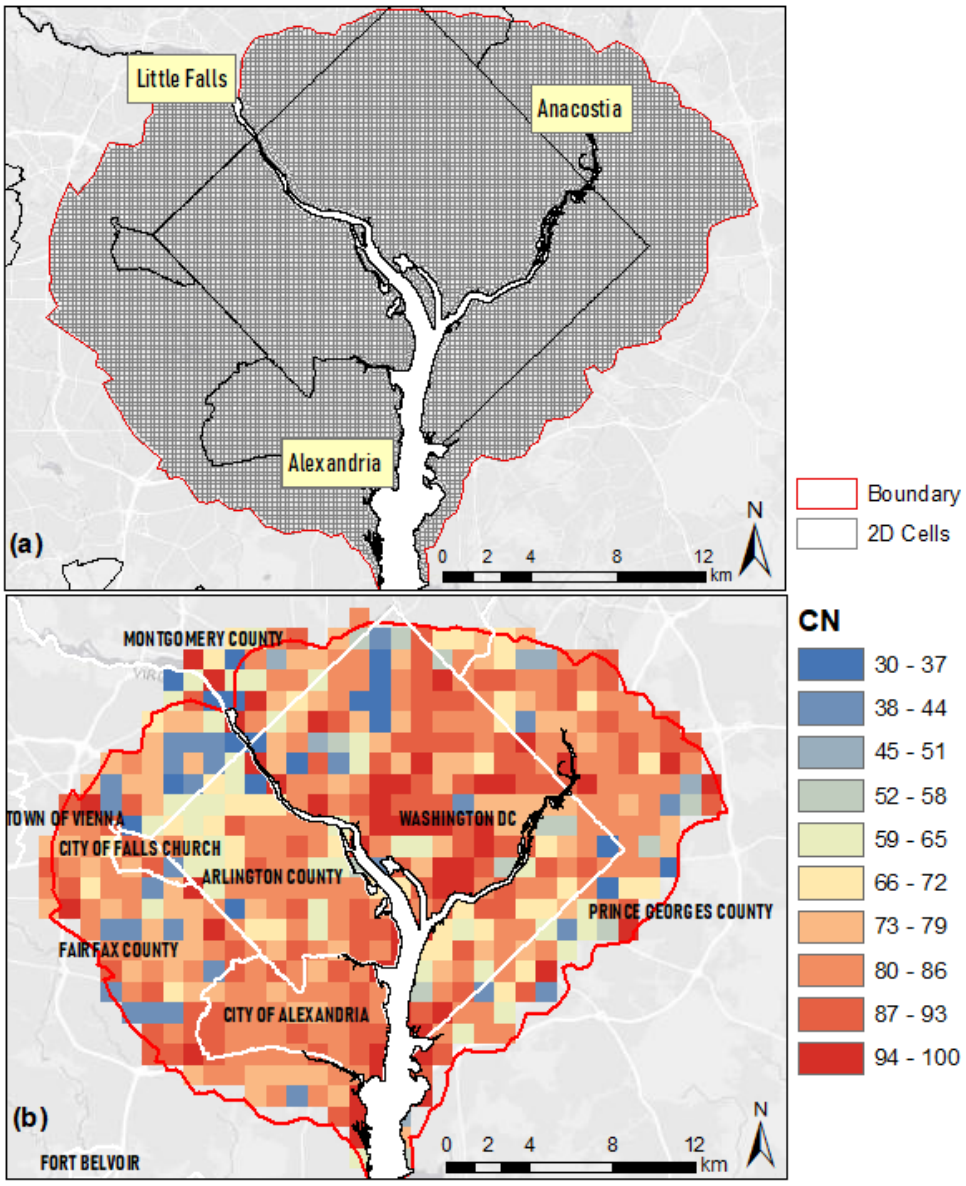

Figure 41 Model setup with a) 2D computational grids and b) CN grids

3.2.3 Runoff Estimation

The rainfall data was converted to runoff for generating forecasts using the Soil Conservation Service (SCS) curve number (CN) method, the most widely used method for predicting storm runoff. This method has been extensively applied in runoff

calculations for small watersheds and comprehensive hydrologic models (Kim et al., 2002). CN is a dimensionless number ranging from 0 to 100. The value is 0 when runoff = 0 to 100 when runoff equals rainfall (USDA, 1986). Natural Resources Conservation Service (NRCS) provides runoff curve number tables depending on land cover types, hydrologic conditions, and the soil groups (Hernández-Guzmán & Ruiz-Luna, 2013). Land use data from National Land Cover Database 2016 (Figure 39) and soil data from Natural Resources Conservation Service (NRCS) were used for the CN grid generation in ArcGIS. Average CN has been developed based on the methodology used for calculating composite CN (USDA, 1986; Reistetter and Russell, 2011) by assuming the percentages of impervious area. We selected CN 35, 65, 85, and 95 for runoff estimation in this study to consider flooding in both impervious and pervious areas.

3.2.4 Observed Dataset and Forecast Boundaries

3.2.4.1 Observed Data

The proposed model was initially validated for the compound flood simulation with observed dataset (figure not shown). Observed streamflow and water level data were collected from the United States Geological Survey (USGS, 2017). Potomac River flow at Little Falls (LF) gage station (USGS gage: 01646500) and combined flow data from two Anacostia River stations at Northeast Anacostia (NE) and Northwest Anacostia (NW), i.e., USGS gages 01651000 and 01649500 respectively, were used as upstream boundaries. In order to evaluate the coastal effects, we used a downstream boundary

condition at Alexandria, VA (USGS station: 0165258890) to consider the influence of the coastal water levels from the Chesapeake Bay towards flooding in Washington, DC.

3.2.4.2 Advanced Hydrologic Prediction Service (AHPS)

The modeling system demonstrated in this research provides a 3-day flood forecast. Boundary conditions for flow and water level forecasts were collected from the NWS's AHPS database (NOAA NWS, 2018). AHPS provides magnitude and probability of floods for several days in advance (National Weather Service, 2020c). Potomac River forecasts by AHPS are available at several river stations in the study area: Little Falls pump station (BRKM2), Washington Channel (WASD2), Wisconsin Avenue/Georgetown (GTND2), and Alexandria (AXTV2). Anacostia River does not have any AHPS forecast at present. In order to quantify the forecast at Anacostia River, we estimated a relation between the flow at Little Falls, DC station and Anacostia NE and Anacostia NW combined streamflow using the data during 2010-2019 which is shown in Figure 42. It was estimated that daily peak of Anacostia river flow is about 2-6% of Potomac River daily peaks. We calculated 2% and 6% from LF daily peaks and then estimated the average of these values to use as Anacostia boundary.

3.2.4.3 National Water Model (NWM)

A set of streamflow input data was collected from the National Water Model (NWM) medium range dataset (Office of Water Prediction, 2018). The NWM is a hydrologic model that simulates observed and forecasted streamflow over the continental US. The NWM simulates the water cycle using mathematical representation of the processes involved and counterparts the current hydrologic modeling. It provides

forecasts for more than 2.7 million river reaches with very fine spatial and temporal resolution (Office of Water Prediction, 2018). National Water Model flow forecasts were evaluate by (Viterbo et al., 2020) during the flash flood event of May 2018 in Ellicott City, Maryland. This study has evaluated the HRRR precipitation data as an input to their forecast system across multiple spatial scales, from regional watershed-scale to local urban scale flooding. The forecast were evaluated by implementing the available footage from street cameras. For small watersheds, the NWM response was clearly linked to the meteorological forcing, but the response was very complex in larger basins (Viterbo et al., 2020).

3.2.4.4 Integrated Flood (iFLOOD)

Forecast from the recently developed iFlood guidance system was implemented in the downstream boundary of the model. iFLOOD is an operational real-time flood forecasting computational framework that integrates coastal and estuarine process in order to provide accurate water information. The system is based on a coupled surge-wave (ADCIRC + SWAN) model and provides water level forecasts in the Chesapeake Bay for a lead-time of 84 h twice a day. It has been operational for several years and has been validated for daily weather and extreme weather flood forecasts that showed competing performance against other NOAA existing operational guidance systems (Khalid and Ferreira, 2020).

3.2.4.5 High Resolution Rapid Refresh (HRRR)

HRRR rainfall data was used to generate storm runoff in the model. HRRR is an hourly updated real-time atmospheric model with 3-km resolution (NOAA, 2020d). The

accuracy of HRRR forecasts were evaluated for few extreme storms in the US by comparing with gauge corrected Multi-Radar/Multi-Sensor products (Yue and Gebremichael, 2020). In this study, a good agreement was found between the forecasted and observed precipitation on an hourly basis. However, the forecasts underestimated rainfall for tropical storms, and produced almost unbiased estimates for the other storms. Forecasts captured the spatial pattern of hurricanes but produced more localized, high-rain intensities compared to observation (Yue and Gebremichael, 2020). The unit for HRRR precipitation is $kgm^{-2}s^{-1}$ which is equal to 3,600 mm/hour. The data was converted to mm for implementing in this model.

3.2.4.6 AHPS Depth Grids

The model forecasts were validated by comparing with AHPS flood depth grids. AHPS grids provide inland flood depths based on the flood stages (*Action, Minor, Moderate,* and *Major*) at Washington, DC station. *Minor* flooding indicates there is possibility of some public threat. *Moderate* flooding may require evacuations of people to higher elevations, and *Major* flooding causes extensive inundations of structures and roads (National Weather Service, 2020c). AHPS inundation boundary includes approximately 8.9 km from the Main Stem Potomac River and approximately 13.7 km from the Anacostia River located along the western border of Washington, DC. The dataset is provided in raster format which has been reviewed in multiple steps to provide reliable depth values. LiDAR elevation data was used as the source to determine flood inundation level estimated by the constant tidal elevations used for mapping purposes. The Digital Elevation Model (DEM) used to generate the mapping products was

produced by the Army Geospatial Center and consists of a raster digital elevation model with a horizontal ground resolution of 1-meter (National Weather Service, 2020c). The downstream and upstream boundaries of our model are shown in Figure 43 and Figure 44. The rainfall input is shown in Figure 45 and the overall model setup with the forecast boundaries are presented in Figure 46. The outputs from the proposed urban flood forecast model are flood depths, duration, and flood extent.

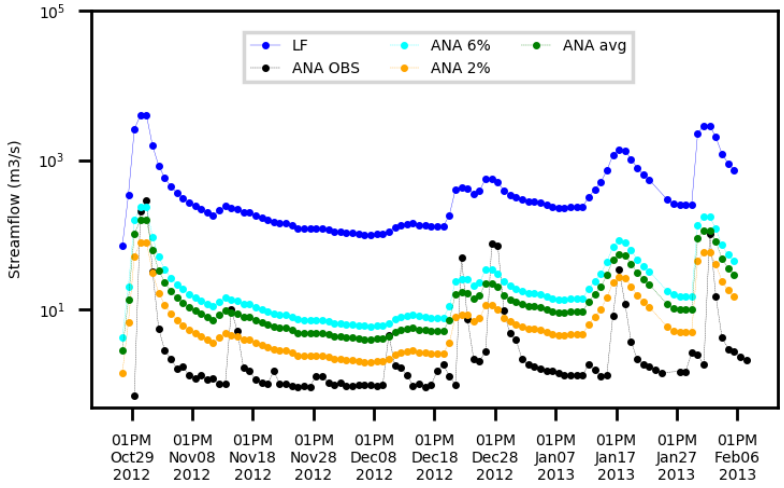

Figure 42 Estimated streamflow forecast at Anacostia River boundary calculated from Little Falls (LF) flow (y axis in log scale and time in UTC; ANA 6%, ANA 2%, and ANA avg are 6% and 2% of LF flow and average of the percentages respectively)

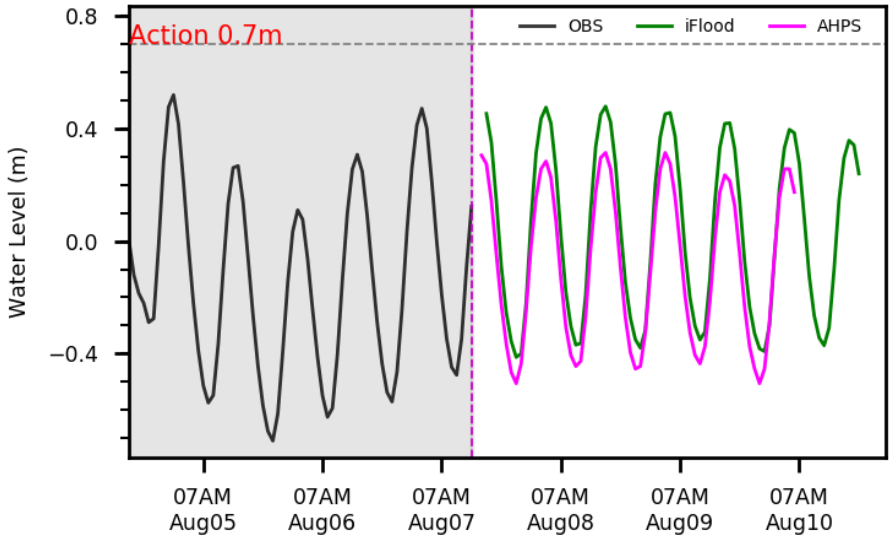

Figure 43 Water levels at downstream boundary of the proposed model obtained from observations (grey), forecasts at AHPS (pink) and iFLOOD (green). Grey shaded area indicates period with observed data

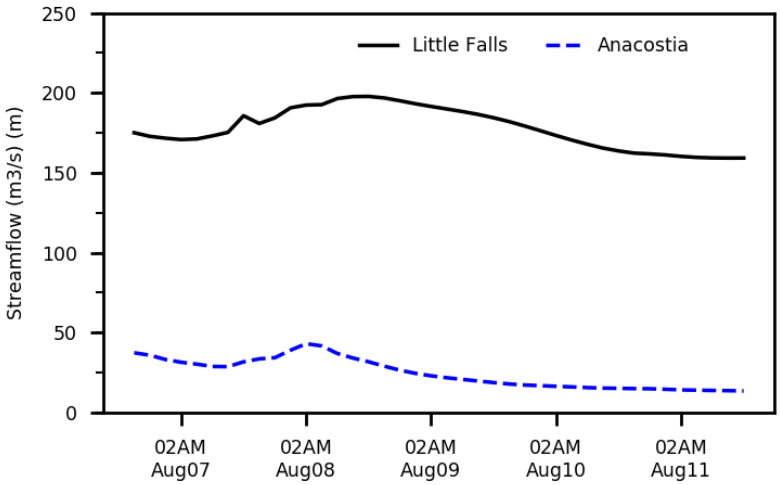

Figure 44 Upstream streamflow boundaries and Little Falls (LF) and Anacostia (ANA) obtained from the National Water Model forecast

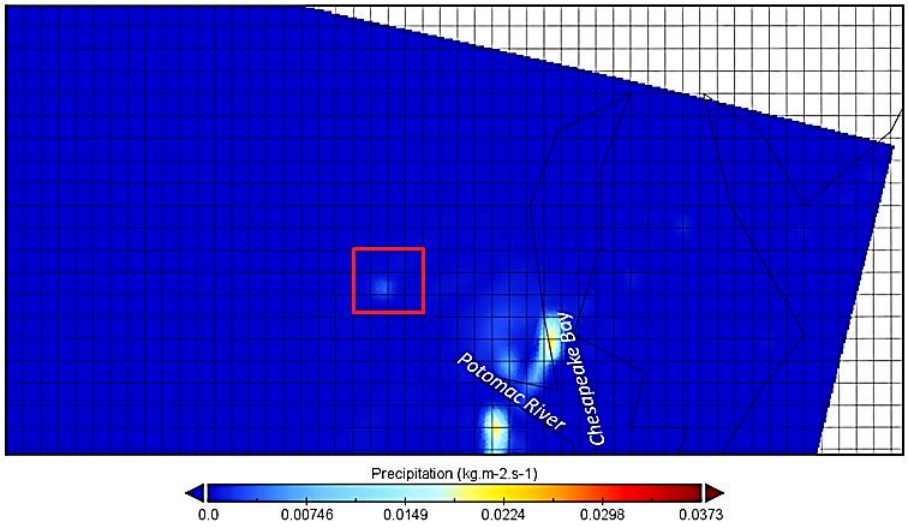

Figure 45 HRRR Precipitation forecast for August 04, 2020 (red box includes the study area)

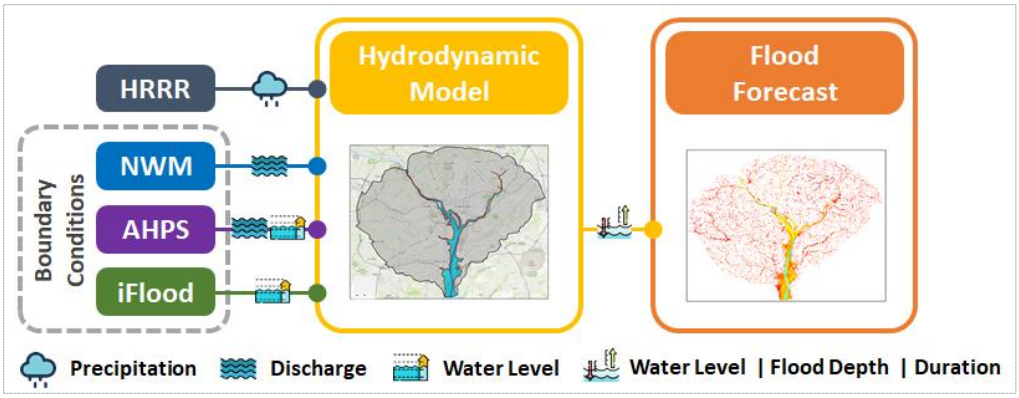

Figure 46 Multiple forecast inputs forced in the model

3.3 Results and Discussions

3.3.1 Forecast Validation

The model was validated based on NWS's AHPS forecasts at Washington, DC and Wisconsin Avenue stations, and the AHPS inland flood depth grids. We simulated recent water levels in DC from August 1, 2020 to August 7, 2020. There was a *Minor*

flooding in August 04 due to Hurricane Isaias (2020) and some *Action* stage flooding after August 05 in the region.

3.3.1.1 Validation for Potomac River Flood Stage

The forecast system outputs resulting from multiple inputs were compared to AHPS river forecasts to test the predictive skill of the model. In the figures of this section, three sets of outputs are presented: i) forecast from AHPS forced boundaries, ii) forecast from AHPS (downstream) and NWM (upstream) boundaries, and iii) forecast from iFlood (downstream) and NWM (upstream) boundaries. The water levels were simulated from August 06, two days after Hurricane Isaias. The simulated *Action* stage event was compared with AHPS forecasts at two stations (Washington, DC and Wisconsin Avenue); AHPS can be noted as the reference forecast for comparison (Figure 47). The difference between AHPS forecast and the proposed model forecasts range between 0.05 m to 0.30 m for the peak water levels (Figure 47). The reasons for the difference between the forecasts can be attributed to: i) model parameters or input values, and ii) the assumption that AHPS forecasts are accurate. In reality, there can be a difference between the observation and AHPS forecasts. To confirm this, forecasts from the last 2 days of this simulation period were archived to compare with the observed data. AHPS forecast were not accurate at all the times during the events and the peaks differ between 0.00 and 0.20 m. The results obtained from our model simulations were better than the AHPS forecast during some events analyzed in the validation process, and a bias is noted when compared to AHPS forecast results, most likely due to differences in the model input.

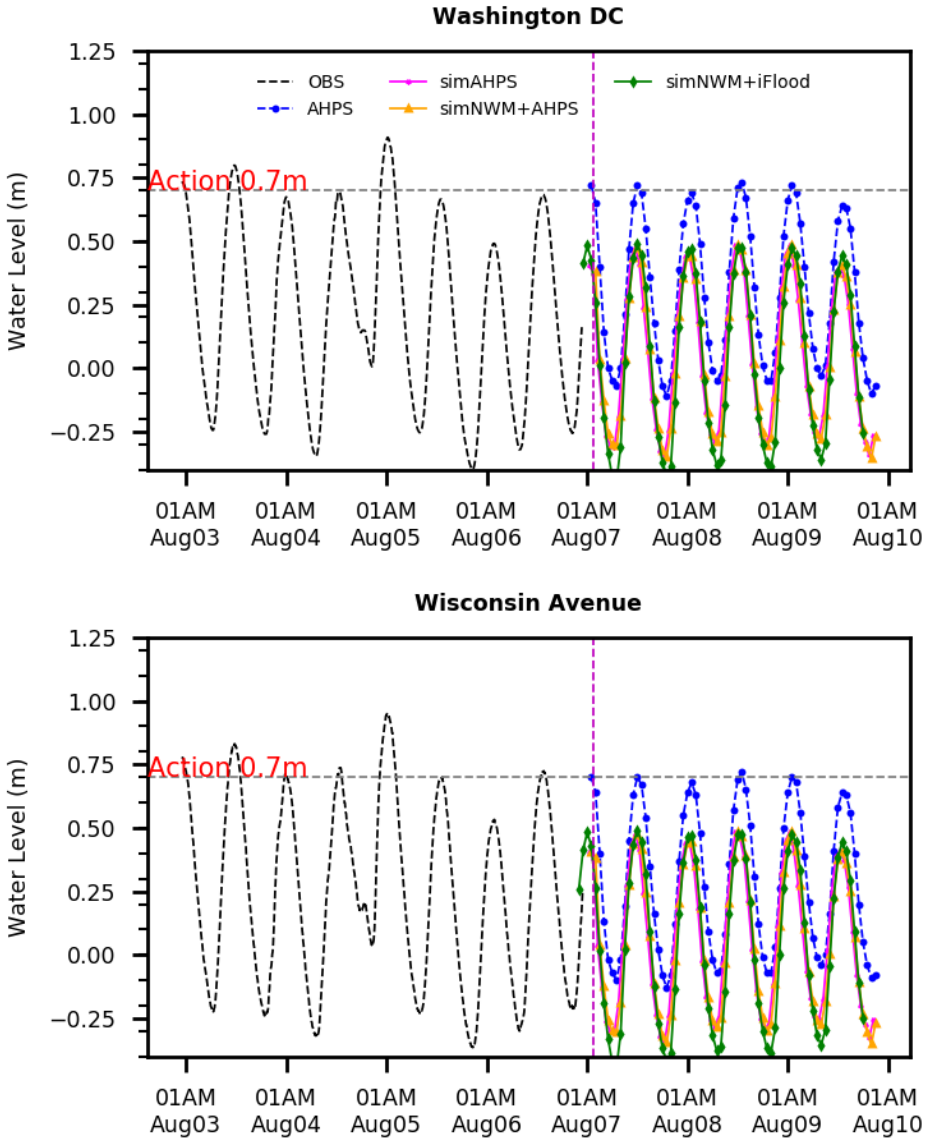

Figure 47 Water level forecasts at Washington DC and Wisconsin Avenue for different model boundaries and compared with AHPS forecasts (reference forecast)

3.3.1.2 Validation for Inland Flood Depth

AHPS provides inundation boundary around Washington, DC based on the flood water levels at the DC station (Figure 48). Model forecasts were compared with the flood depths from AHPS inundation grids. Although the AHPS depths are not in real time,

those values can provide significant information on the range of flood depths to be expected during any *Action*, *Minor*, *Moderate*, or *Major* floods. River depths between the model forecast and AHPS inundation grids have significantly higher bias (1.2m). A high resolution bathymetry (from NOAA nautical chart) was used in our urban flood model; therefore, it could represent the river depth more accurately than the AHPS grids. However, the inland flood depth forecast was very similar to the AHPS grids with minor bias at some locations.

There is no official source available to provide historical or real-time inland flood depths during different flood events. Therefore, we could not find any inland flood data for validating the model results. However, the available flood inundation and depth information from television and online news, newspapers, and social media photos proved to be good sources for the event validation. We simulated the recent flooding in DC, MD, and VA due to Hurricane Isaias on August 04, 2020. The storm moved northeast at approximately 44 km/h at 5 a.m. according to the NHC (National Hurricane Center, 2020). The winds and rain passed over the Washington, DC area during mid-morning (Patch, 2020). The observed water levels and streamflow at the upstream and downstream boundaries during the Hurricane Isaias, and the water level at DC are shown in Figure 49. From Figure 49 it was clear that there was *Action* and *Minor* stage flooding during the storm. We archived our model results to validate with the observed flooding conditions around the DC metropolitan area.

Newspapers and online news sources featured the flood event in the area. The flood depths at different locations could be determined from these photos. For example,

as shown from an online source in Figure 50(a) collected from Patch (2020), the Four Mile Run stream was full to its capacity which indicates that the *Action* stage (1.83 m) of the stream was exceeded at the location and areas nearby were flooded. Figure 50d shows that there was flooding in the adjacent trail of the stream. Moreover, from Figure 50(b) (NBC4 Washington, 2020) and Figure 50(c), it can be estimated that the flood depth in Old Town Alexandria streets was equivalent to ankle deep water. In addition, flood depths can be estimated by archiving photos with the height of the buildings inundated and later measuring the height physically. This will also help to delineate the boundary of the flooding around the area. Moreover, the twitter and facebook photos posted by the residents are very useful to estimate flood depths in any residential or commercial area.

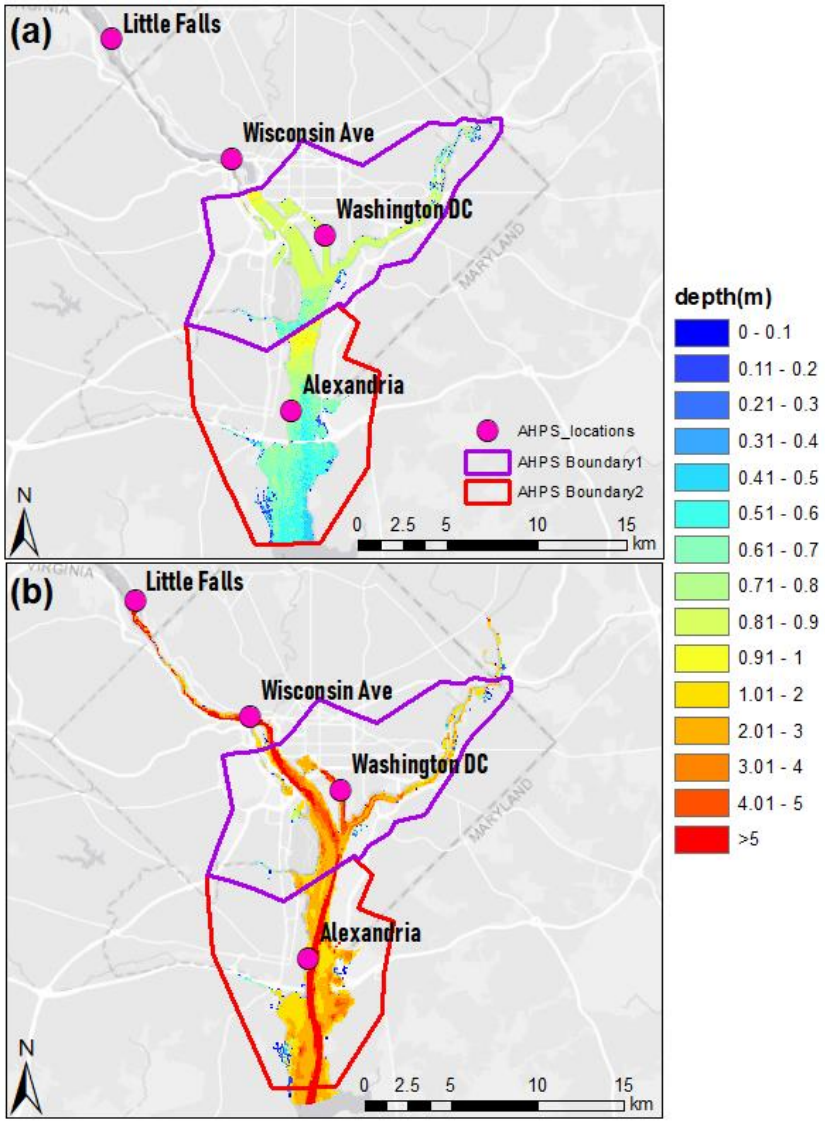

Figure 48 AHPS inundation grids (a) and proposed model forecasts (b)

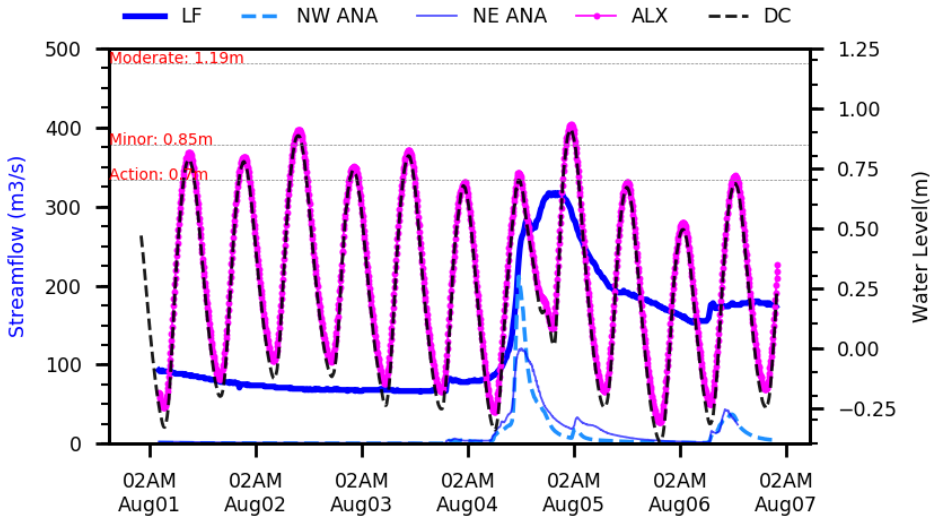

Figure 49 Observed boundaries during Hurricane Isaias

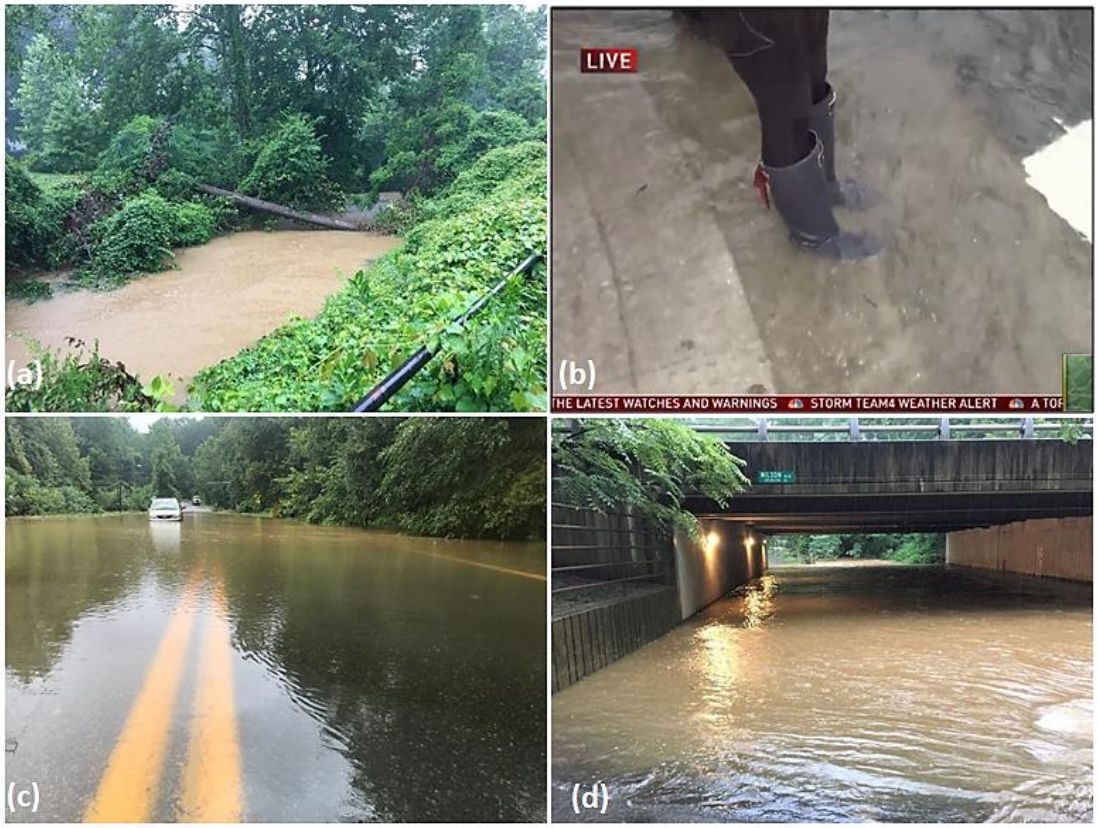

Figure 50 Flooding during Isaias on August 04, 2020; (a) Four Mile Run near Arlington, (b) Old Town Alexandria, (c) Woodburn Road Fairfax, VA, and (d) Washington and Old Dominion Trail along Four Mile Run

3.3.2 Impact of the Compound Flood Drivers in the Model Forecast

The forecasted results illustrated the effect of riverine flow, rainfall, and surges on inland flooding. Predicted inundation boundaries from our model provided valuable information on the flooding characteristics. Flooding near Washington, D.C. is caused by either tidal flooding from Chesapeake Bay, or flows from the upstream of Washington, D.C., or a combination of both. Riverine flow combined with high surges can also produce severe flooding in the region. However, the forecast on August 4, 2020 showed significant flooding in the region mainly due to rainfall (Figure 51). Coastal surge had some contribution to DC flooding and Little Falls flow was below *Action* stage of 1.52 m. Rainfall was the dominating factor for flooding which was evident from the forecast generated with and without rainfall showing significant difference in forecasted depths. NBC4 Washington reported several inches of rainfall and life-threatening flash flooding into the D.C. region (NBC4 Washington, 2020). The urban areas including Old Town Alexandria, Washington, DC, and Ellicott City was hit by flooding from this event. The forecasted flood duration was 1-3 days in the urban areas both with and without rain (Figure 52). The red colored region in the river boundary shows a duration of 4-5 days. Rainfall had significant impact on the duration of flooding in the urban areas located at the upstream.

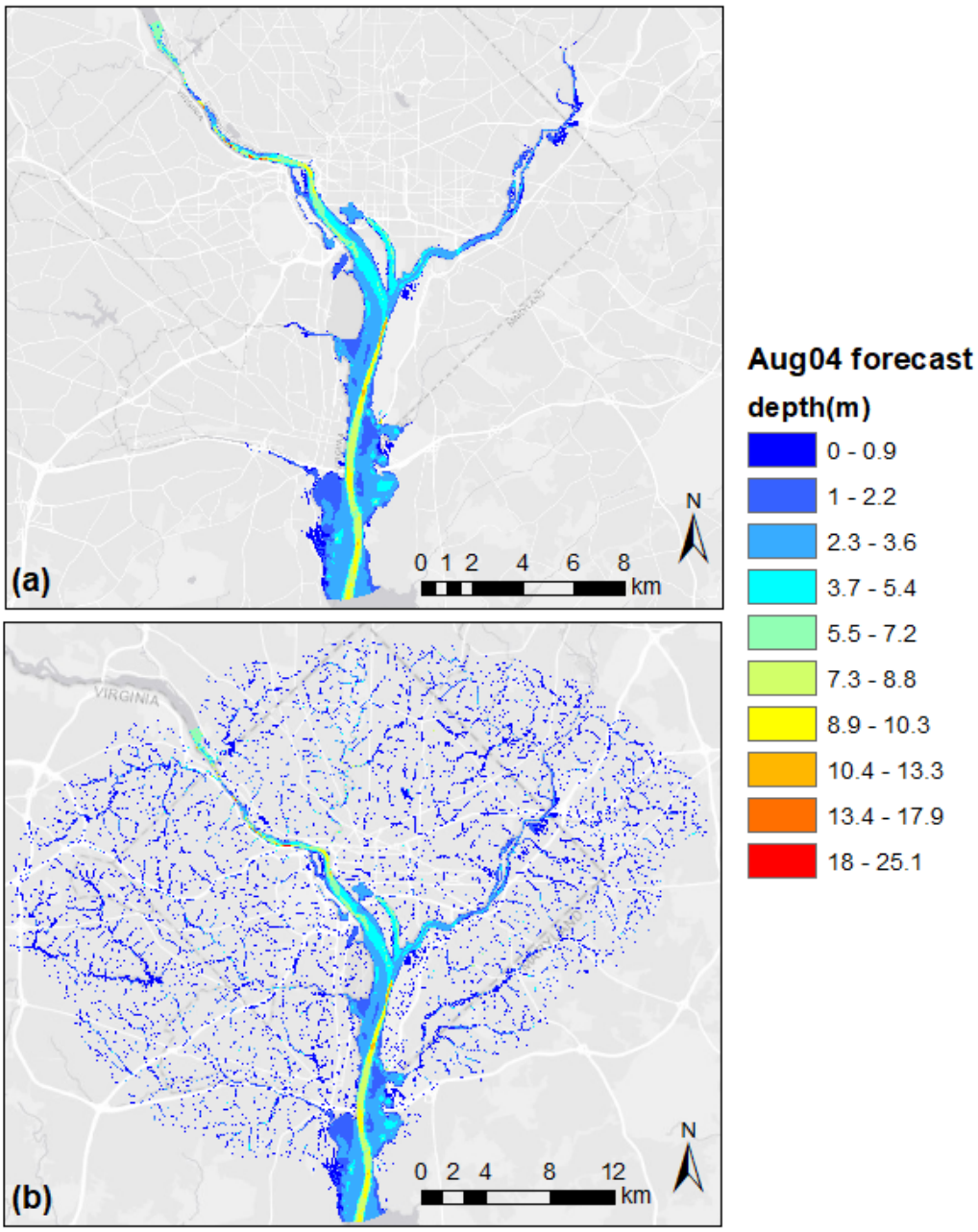

Figure 51 Floodplain map for maximum inundation (a) without and (b) with rain

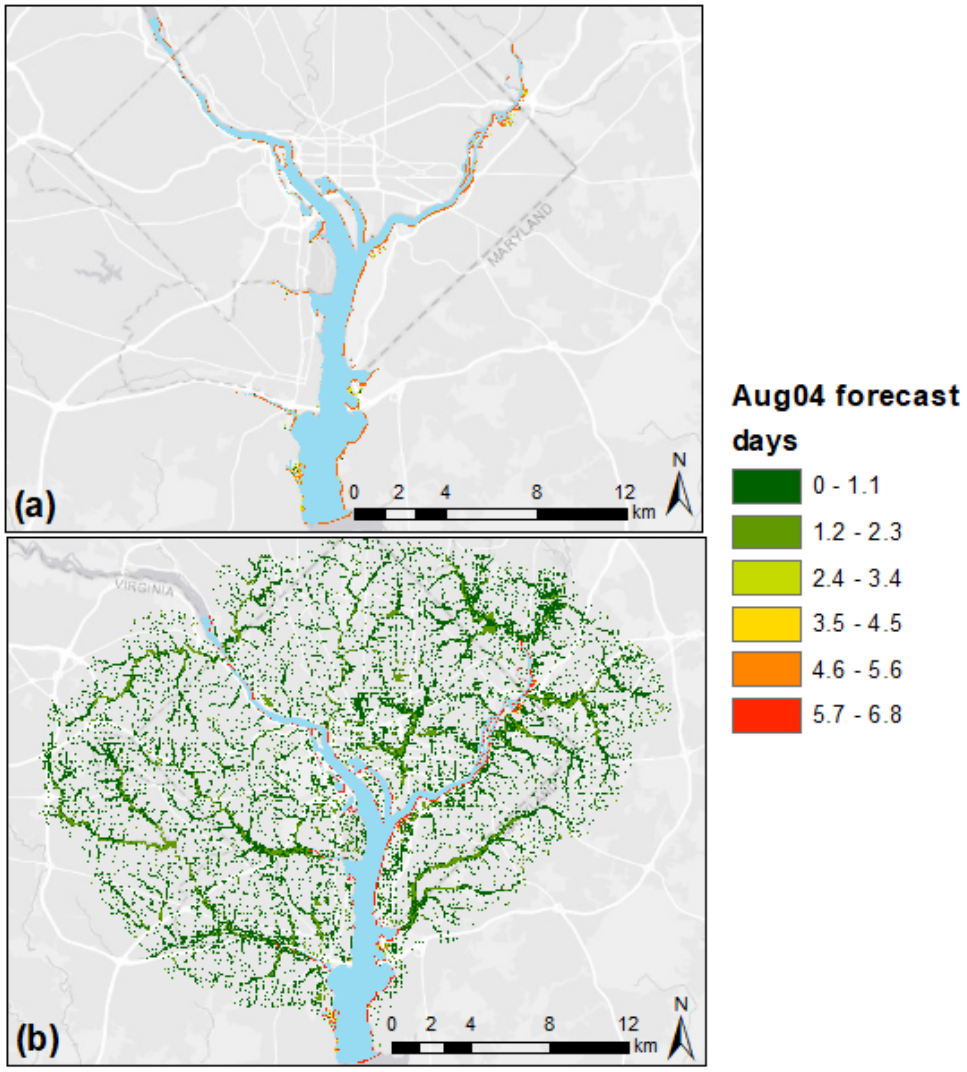

Figure 52 Forecasted flood duration (a) without and (b) with rain

3.3.3 Stream Water Level Forecast

The streams around Washington metropolitan region are also impacted by flooding from riverine flow, surges, and rainfall. The forecasts for the streams show very low to no flooding when rainfall is not considered. However, with even a small amount of rainfall, the stream forecasts show much higher water level. The Potomac River and

Anacostia River do not show such increase in water level due to rainfall. This indicates that rainfall is very important input for stream water level forecasts. Figure 53 shows water level forecasts in some of the streams in the area. In the forecasted period (August 4-5, 2020) there was a rainfall of maximum 50 mm and the streams showed higher peaks and fluctuations in water level. During the observed period there was negligible amount of rainfall (1-2 mm), and only the tidal impact was visible in the stream. Among the streams in the figure, Pimmit Run is in a flow dominated region, Rock Creek in a compound flood dominated region, and the other streams are located in the tide dominated region. Therefore, the runoff impact from rainfall is more prominent in the Pimmit Run stream. It is difficult to estimate flooding condition in the streams. While the streams are at lower than *Action* stages, it may reach the threshold values to generate flooding condition. Data analysis during the period of 2007-2019 showed that Rock Creek has an *Action* stage of 1.83 m although it can generate flooding condition with higher than 0.6m water level as shown in Figure 54. Moreover, any rainfall event near DC has impact to all the streams although the impact varies in characteristics and quantity. Rock Creek can be represented as a proxy to the urban flooding condition because when Rock Creek shows elevated water level, the same is observed in the surrounding streams of the area (Figure 54).

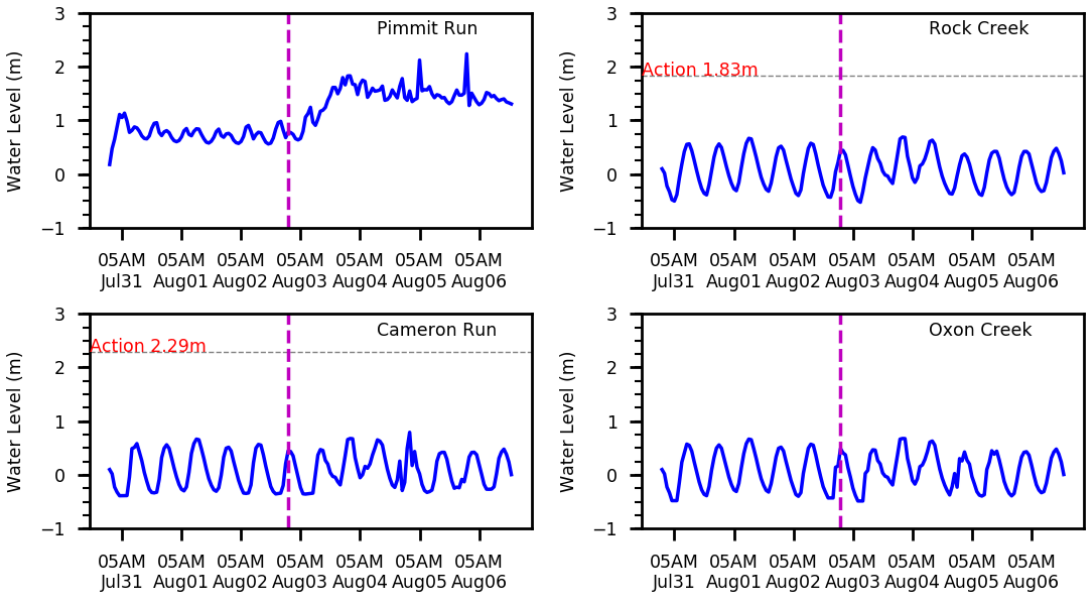

Figure 53 Water levels in the small streams (vertical magenta line indicates start of forecast period)

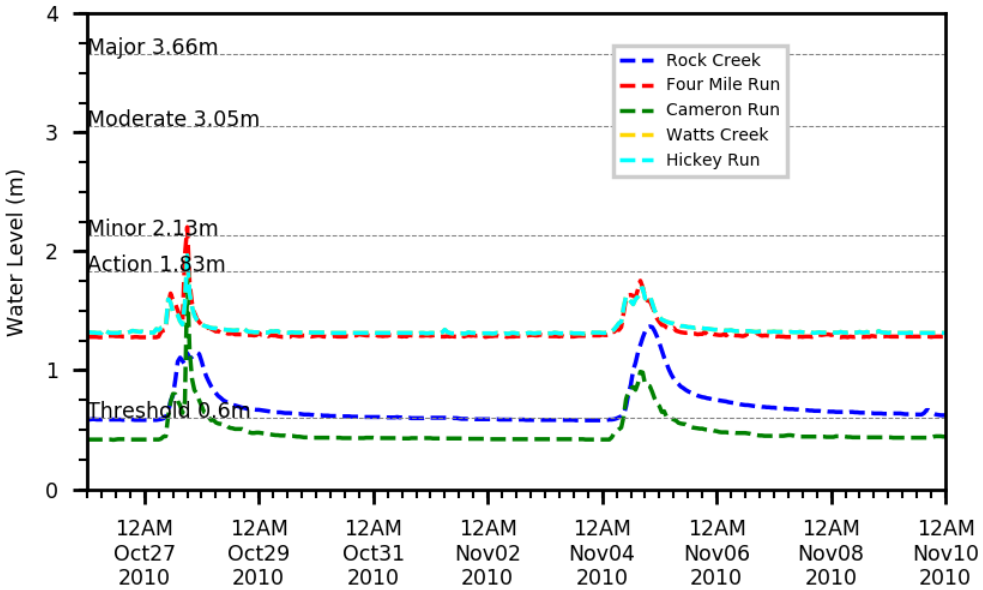

Figure 54 Historical water levels in the small streams (*Threshold, Action, Minor, Moderate,* and *Major* flood stages are for Rock Creek)

3.3.4 Forecast along the Potomac and Anacostia Rivers

Several inland locations very close to the rivers were selected to analyze and compare the flood depth (Figure 55). Location ID and names of those locations are shown in Table 8. These locations are impacted by compound flooding from coastal, riverine, and runoff impacts (Figure 56). However, locations adjacent to the Potomac River are not impacted much by rainfall compared to the inland locations in the urban areas far from the rivers. Without rainfall, the tides or flow did not have much impact in the inland water depths during the observed period from August 01 to August 03 (Figure 56). The impact of compound flood drivers varied on different locations In Reagan Airport and other locations close to the river, the rainfall did not have much impact. National Mall showed very high depth value when simulated with CN 85 because with such high CN, the area is assumed to be urban and the runoff is trapped in the area for a longer period. A single flood depth forecast is not sufficient to provide information on the flood events. Multiple simulations based on different runoff conditions are generated to provide an approximate flood depth value which is presented in the next section.

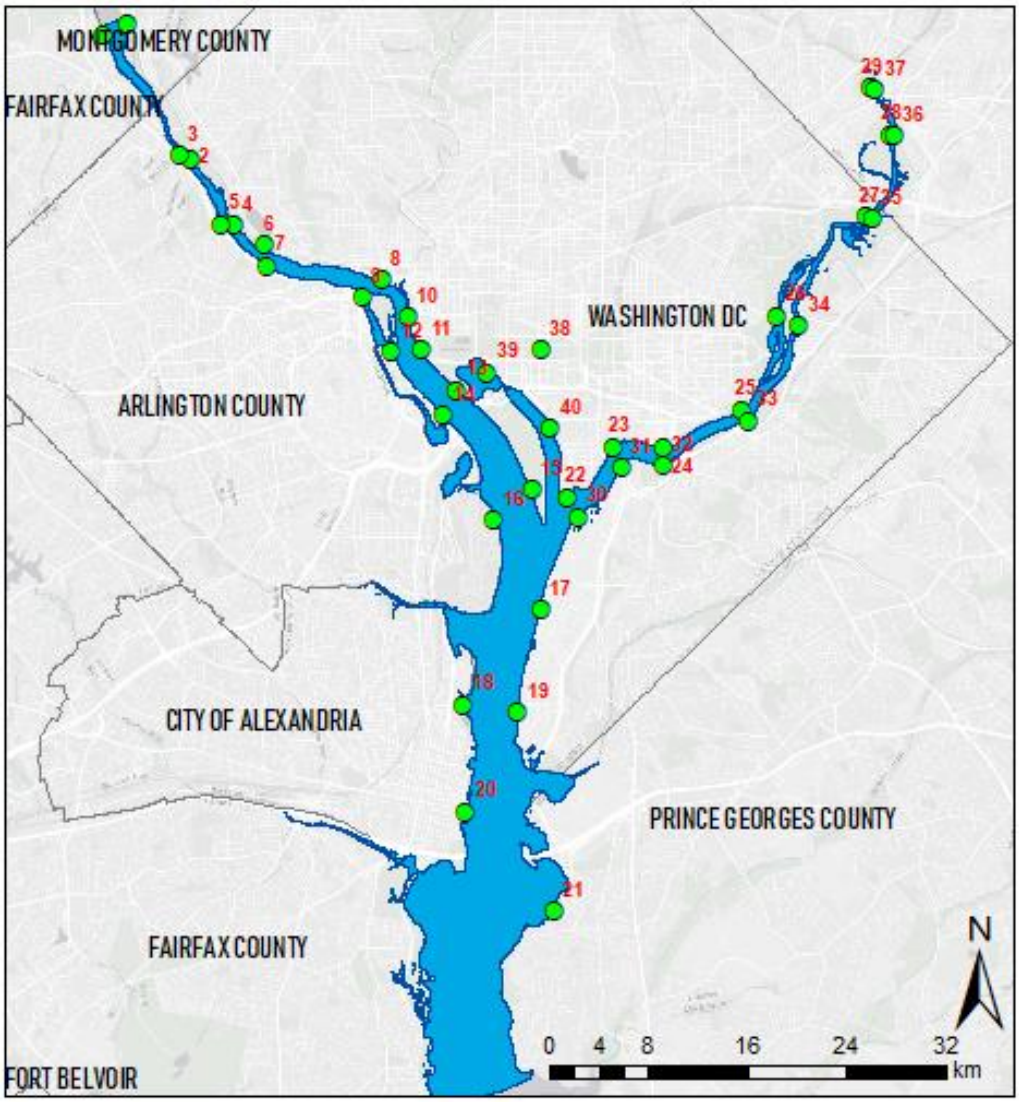

Figure 55 Flood depth analysis locations along the Potomac and Anacostia River

Table 8 Locations along the rivers

ID	Location	ID	Location
0	Crest Lane3	22	Anacostia L1
1	Clara Barton Pkwy2	23	Anacostia L2
2	Canal Road4	24	Anacostia L3
3	George Washington Pkwy311	25	Anacostia L4
4	Canal Road1	26	Anacostia L5
5	George Washington Pkwy211	27	Anacostia L6
6	Palisades Park1	28	Anacostia L7
7	George Washington Pkwy111	29	Anacostia L8
8	Georgetown Waterfront1	30	Anacostia R1
9	George Washington Pkwy2	31	Anacostia R2
10	John F Kennedy Cntr1	32	Anacostia R3
11	Ohio Drive SW1	33	Anacostia R4
12	George Washington Pkwy7	34	Anacostia R5
13	Ohio Drive SW5	35	Anacostia R6
14	George Washington Pkwy10	36	Anacostia R7
15	East Poto Park1	37	Anacostia R8
16	Ronald Reagan Airport1	38	Tidal Basin2
17	Bolling AFB1	39	Washington Channel2
18	Marina Tower2		
19	Smith Street1		
20	Old Town Alx2		
21	National Harbor2		

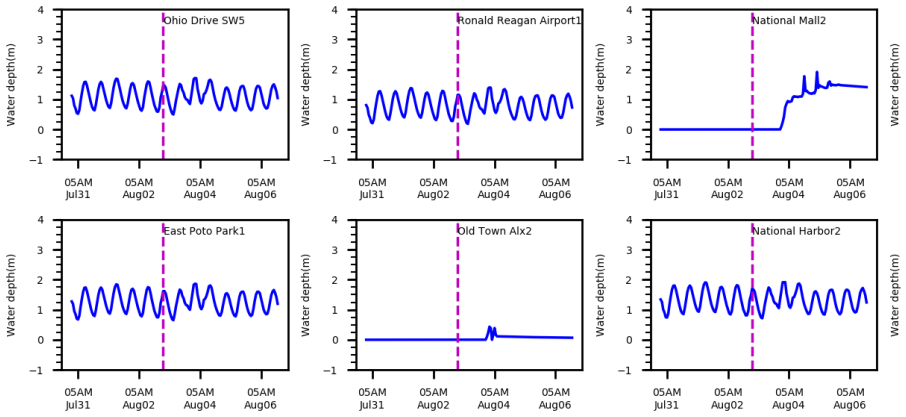

Figure 56 Flood depths near Potomac River with CN 85 (vertical magenta line indicates start of forecast time)

3.3.5 Multiple Forecasts from Variable Inputs

The goal for multiple flood forecasts is to choose the best forecast for each location based on the characteristics of the area. For example, if an area is highly urbanized, a CN 95 forecast will be more appropriate while for a less urbanized area, the forecast with CN 35 or CN 65 is suitable. Multiple forecast lines have been generated by changing the model inputs: flow, water level, and rainfall-runoff. The forecast lines vary widely due to the change in the flood drivers, particularly, due to the rainfall variation. Change in CN does not have significant impact on the river water level. The most impacted areas with the rainfall are the urbanized areas in the region. The difference in inundation depth due to rainfall intensity (i.e., CN 35, CN 65, CN 85, and CN 95) is estimated to show how the peak flood varies based on rainfall induced runoff (Figure 57). CN 35 did not generate any urban flood, therefore not presented in the figures.

The East Potomac Park location is a less urbanized area, and Old Town Alexandria is a highly urbanized area impacted by rainfall every year. These two locations are presented to provide an understanding on how the flood depth forecasts may vary due to the runoff input and the location types. Moreover, an urban location near Rock Creek is also selected to represent urban areas located far from the main rivers. The peak flood depths obtained by using CN 85 and CN 95 were very steep and went down abruptly compared to the ones representing CN 65. However, depths from CN 85 lines show that these are more representative of the flood depths observed in the urban areas like Old Town Alexandria. Urban floods are mostly small duration events which increase suddenly, like the steep increase for CN 85 or CN 95, and have the most destructive

impact within urban areas. According to the photos and information obtained from different online news portals, news channels, and social media, the water depth at Old Town Alexandria seems to be 0.30-0.6 m in the streets. The depths may vary from one location to another. Thus, a range of possible values should be indicated for the flood inundation while providing a forecast to stakeholders depending on the characteristics of the area.

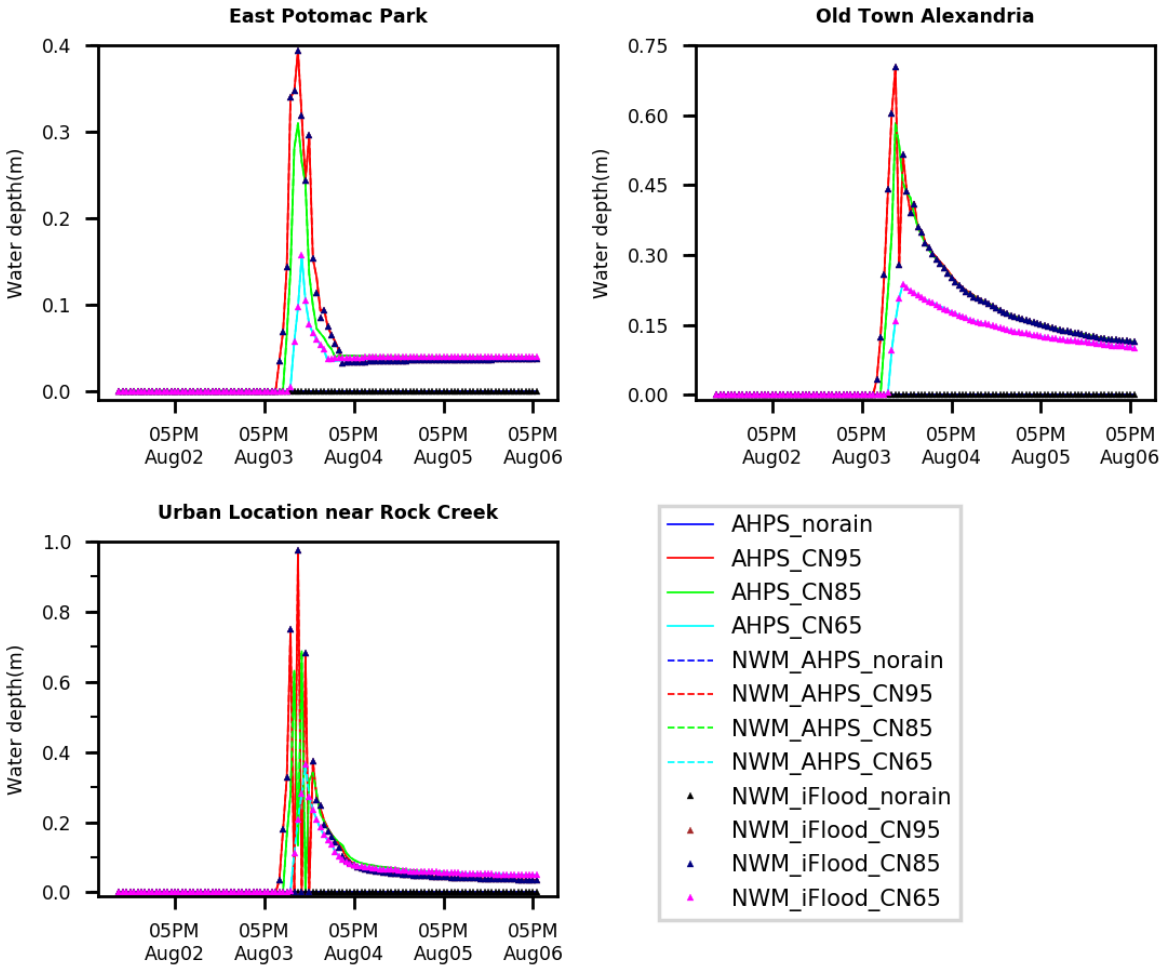

Figure 57 Flood depths from multiple forecast inputs

3.4 Conclusions

This study has explored and generated a platform for automating simulations and forecast of river water levels, inland depths, and floodplain maps during compound flooding at a faster rate. The validated hydraulic system was capable of representing past events with some bias depending on the flood drivers associated and enhanced the scientific understanding of the interactions between the flood drivers in the river, stream, and inland locations. It has provided acceptable results ahead of storm events in the region with minimum time and computational use. Moreover, spatial and temporal distribution of flooding during the events was significantly captured by the model. Outcomes from this study demonstrated that it is critical to consider the interactions between the processes that lead to major flood from river flow at the upstream boundary, and coastal flooding from downstream boundary. The importance of accurate rainfall input is evident from the analysis because some urban areas are impacted by runoff only.

The model has some limitations due to the use of CN for approximate estimation of runoff for the study area. Furthermore, the model parameters and inputs can also generate bias in the results. Biases in the results may occur partly due to the spatial resolution of the model and rainfall inputs. Existing models are not capable of providing reliable compound flood forecasts in coastal cities even though the compound urban flooding has been increasing rapidly. However, the relative contribution of each driving factor can be estimated in real-time through this system. Although the forecasts were not validated against observed flood records, the results were compared with available information from the local news and social media. This modeling approach can be used

in the coastal communities around the Washington, DC metropolitan area, and the application can be extended to other such areas around the globe.

The forecasted results have provided an improved understanding of the urban flood processes which would be helpful for the decision-making processes in flood risk management. A number of urban areas have similar flooding problems and share similar hydrological properties as this study area. Although the study is developed for a specific area, the knowledge from the application of this system can be scaled up to a broader watershed scale analysis and forecast.

CONCLUSIONS

Compound flooding results from the simultaneous occurrence of multiple flood drivers generating significantly higher peaks and longer durations when compared to single driver induced events. However, the interaction between these drivers is complex, and requires extensive local analysis based on their impact on the flood peaks and duration. The Washington, DC metropolitan region is exposed to compound flood hazards, as are many of the tidal cities of the US. This study has implemented a data driven analysis in DC from 1931 to 2019 to identify the major flood drivers, and investigated the spatial and temporal variability of flood depths and extents. We have also implemented a hydrodynamic model to generate flood forecast for this urban region based on the outcomes from the historical analysis. Results from this analysis have addressed the three science questions:

- *What are the major flood drivers that cause compound flooding in a river-estuarine transition zone? What is the impact of each flood drivers in generating the compound flood peaks in the tidal river?*

The magnitude and duration of floods in DC can be attributed to the impacts from different flood drivers including riverine flow, coastal water level or storm surge, urban runoff and local wind. The flood events were classified as *river*, *coastal*, *compound* , and *other* flood. Moreover, the flood days in DC were categorized as *Action*, *Minor*,

Moderate and *Major* flood days. During 1980-2019, four *Major* floods were observed in the DC station, three of which were *compound* floods (Nov 1985, hurricane Fran 1996, and hurricane Isabel 2003) and the other one was a *river* flood (Jan 1996). The *other* floods were mostly the result of low water level and high wind speed leading to *Action* or *Minor* flooding. In few cases, rainfall induced urban runoff events were responsible for floods in DC. *Moderate* and *Major* flood stages were mainly the result of *compound* floods. Results suggested that the coastal water level at LWT alone had the highest potential to create flood conditions in DC. Moreover, wind speed and direction affected the interaction between storm surges and riverine flow along the Tidal Potomac River. Sea-level rise can also have significant impacts on the flood peak at DC, by increased water levels in the Chesapeake Bay. The results from this study emphasized the need to refine the current forecast models in large estuaries by considering the potential complex interactions between the *compound* flood drivers.

- *How does the compound flood in a tidal river propagate into the spatial and temporal variability of flooding in an urban area? To what extent the compound flood drivers impact urban flooding?*

This study assessed compound flood variability in space and time driven by multiple flood drivers based on 28 scenarios of high and low flow and surges along with multiple design rainfalls. While flooding driven by any single variable can cause extensive inundation in the region, multiple factors associated with an inundation can generate even higher flood extent and depth. The dominating drivers (flow, surge, or rainfall) of the synthetic events helped to understand the flooding properties along the

Potomac River: riverine flood impacted mostly in the upstream part of the river, both riverine and coastal boundaries dominated the flood along the middle part of the river, and the lower part was highly influenced by surge only. The area at the confluence between the Potomac and Anacostia Rivers was the most exposed area to the compound floods driven by the riverine flow and surges or riverine flow, surges, and rainfall. Intense runoff generated greater flood inundation in the urban areas located far from the rivers but adjacent to the streams. Low gradient streams are mainly responsible for urban or inland compound flooding due to the impact of flow and surge being present at a longer distance from the stream mouth. In the future, SLR will flood new locations in the area and the already exposed areas will experience increase in both inundation extent and depth. The methodology and outcomes from this study can be implemented to the other US metropolitan cities like NYC, Baltimore, Houston, and Chicago as well as any coastal cities around the world which are impacted by compound floods.

- *Can an integrated state of the art modeling framework accurately forecast compound flooding conditions in real-time?*

This study has implemented a prototype for a real-time flood forecast system including the impacts from all the flood drivers associated with the flooding in the urban areas of Washington, DC. The real-time system also provides flood levels in the small streams adjacent to the Potomac River. Flood depths from the inundation grids of the National Weather Service are compared with the results. There is no other significant data available to validate real-time urban flooding in the region. However, information from newspapers can be a good source to compare the inundated locations, flood depths,

and extents. This study is critical to improve the understanding of the processes that lead to compound flooding in urban areas. Flood simulations by either riverine flow or coastal water levels cannot fully demonstrate the risk of flooding for decision support systems in this coastal-estuarine region. The local floodplain managers and decision makers can be benefited from these tools and methodologies developed for estimating and predicting compound flood in the river, small streams, and also in urbanized areas.

Single-hazard flooding analysis has become insufficient to account for extreme flooding events in estuarine urban areas. Compound events have a more devastating impact than their single-hazard equivalent, and pose higher threat to the low-lying areas prone to flooding every year. Furthermore, low probability or extreme flood peaks may be driven by events that are not extreme themselves. Therefore, local scale flood modeling and floodplain mapping in coastal urban environments with river flow, rainfall, and storm surge needs to be better understood and communicated. A detailed and comprehensive understanding of compound flood events at present and into the future will significantly increase communities' preparedness and response. Therefore, this study will lead to better understanding and modeling of the underlying compound flood characteristics in the coastal cities which is of utmost importance to support policymakers in making informed decisions and implementing effective protection measures.

APPENDIX

Appendix A - Model Calibration

The Delft 3D hydrodynamic model was used in our study, which is capable to simulate hurricanes, storm surges, water levels, detailed flows and morphology and also model the interactions between those processes (Deltares, 2019). This modeling tool was used to simulate the water levels at DC by considering the impacts from riverine, coastal, estuarine, and urban environments. A topo-bathy was generated by using the Digital Elevation Maps (DEM) from USGS (USGS, 2020) and bathymetry from NOAA nautical chart elevations (NOAA, 2018) with varying resolution (1m near DC to 200m near LWT in downstream) and the datum of North American Vertical Datum of 1988 (NAVD88). The topo-bathy is shown in Figure A.The model grid were generated with the RGFGRID tool (Deltares, 2019) and had about 40,000 node elements. A curvilinear grid was iteratively generated by drawing splines. The study area boundary mainly consisted of the river bathymetry but extended towards land with some buffer zone. The land boundary was used for the model grid generation and to further improve the model, the grids were converted from regular to irregular structure; therefore, the grids were unstructured (Figure A). Unstructured grids allowed local grid refinement in areas with large horizontal gradient. Figure A shows the study area with the boundaries and observation stations (DC and Dahlgren or DAHL).

The most important parameter for the modeling was calibrating the roughness coefficient Manning's n values. As suggested by previous flood modeling studies on the Potomac River (Mashriqui et al., 2014; (Wang et al., 2015) and the values from Chow (1959), a range of Manning's n of 0.021 and 0.015 were initially selected for simulating the water level in the Potomac River. Figure shows the water levels at DC and DAHL station with varying Manning's n values from 0.01 to 0.1. As the manning's n value increases from 0.015, the water level at DC loses its amplitude. However, in the downstream station at Dahlgren the impact of Manning's n in not as high as in DC. The hydrodynamic model boundary was within the rivers and the banks and did not include any urban areas. Therefore, a uniform value of 0.015 was used finally for the Potomac and Anacostia River. The flood stage of DC station can be translated into the flood inundation in the surrounding areas as provided by the NWS.

Other calibration parameters for the model were horizontal viscosity and diffusivity. These values were chosen such that they account for any coarse numerical grids. Delft3D was used in a study to simulate water level in a tidally influenced river, similar to our study area, with horizontal eddy viscosity of 10 $m^2 s^{-1}$(Buschman et al., 2010). As the modeling environment for this study was similar to our study, we used this value for our study. A report for the development of an Integrated Water Resources Management (IWRM) plan in Myanmar used horizontal eddy diffusivity of 20 $m^2 s^{-1}$ (Deltares and TU Delft, 2016). However, the study area was different than our study; therefore, we tested the model with multiple diffusivity values (20, 40, and 60 $m^2 s^{-1}$) and the value of 20 $m^2 s^{-1}$ showed the best result (Figure). The final model parameter values

were evaluated based on the bias and presented in Figure . The average bias in DC water level was 0.03m with n=0.015 and horizontal diffusivity of 20 $m^2 s^{-1}$; and bias was 0.07m with n=0.021 and horizontal diffusivity of 60 $m^2 s^{-1}$. The bias increases if Manning's n are increased further from 0.015.

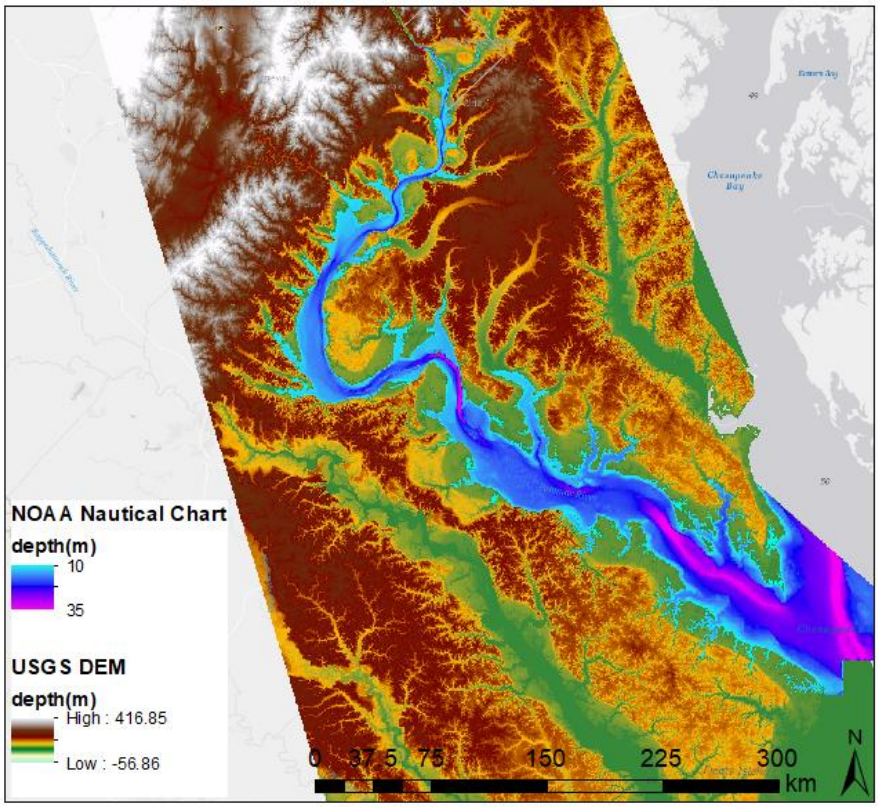

Figure A1 Topo-bathy for mesh generation in Delft3D (blue and pink: river bathymetry, green and brown: inland topography)

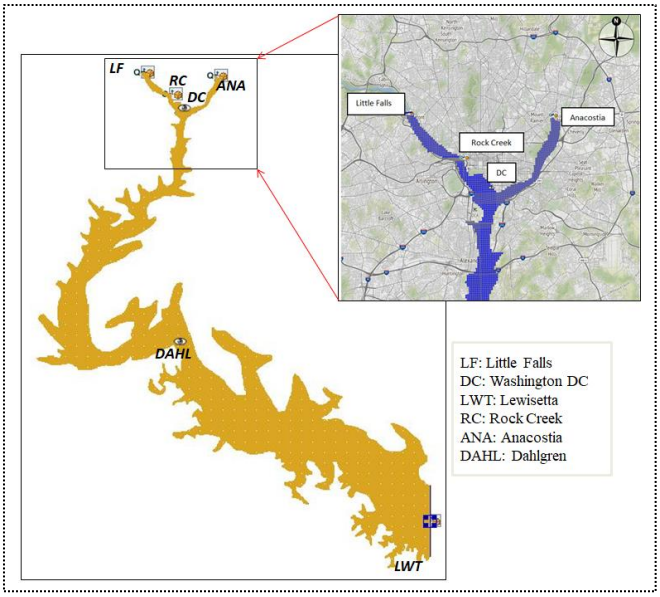

Figure A2 Delft3D model setup with boundary conditions

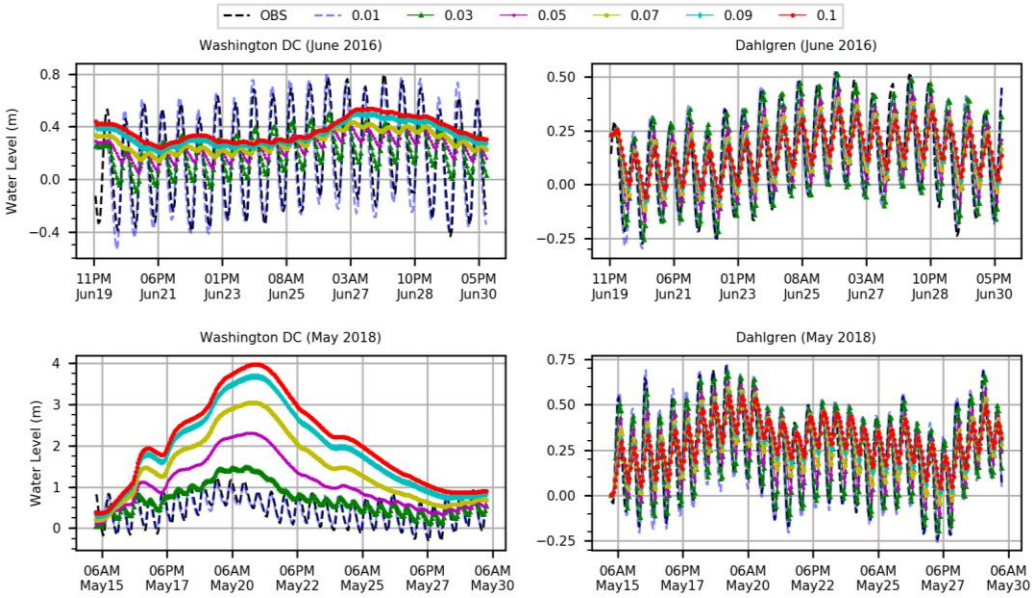

Figure A3 Manning's n calibration: Black line is observed and the colored lines are simulated water level with different Manning's n

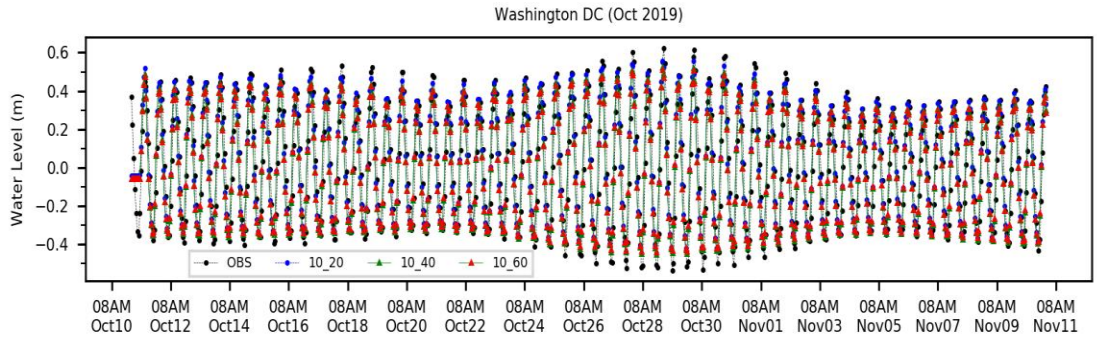

Figure A4 Model calibration for horizontal diffusivity (legend naming: viscosity_diffusivity): Black line is observed and the colored lines are simulated water level with different horizontal diffusivity

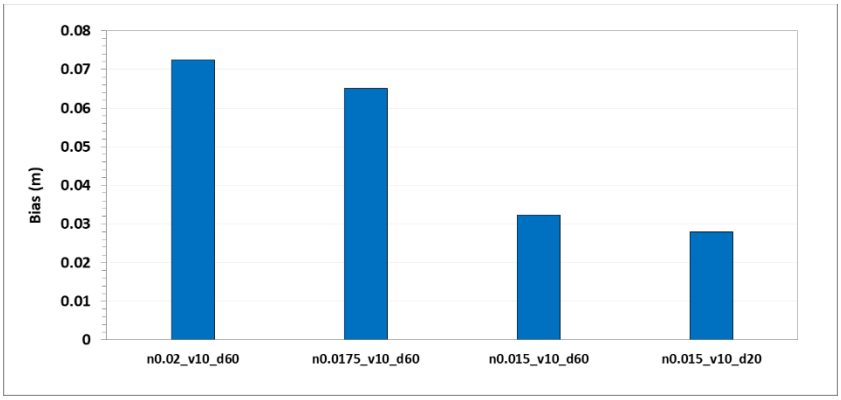

Figure A5 Final evaluation of model parameter (Manning's n_viscosity_diffusivity)

Appendix B - Compound Flood Drivers

During a compound flood event, different flood drivers may co-occur and generate a higher peak and longer flood durations. In Figure B1, the cyan colored line is the urban runoff or Rock Creek streamflow. The LWT water level is below action stage but LF and RC are above flood stage which means this a river flood.

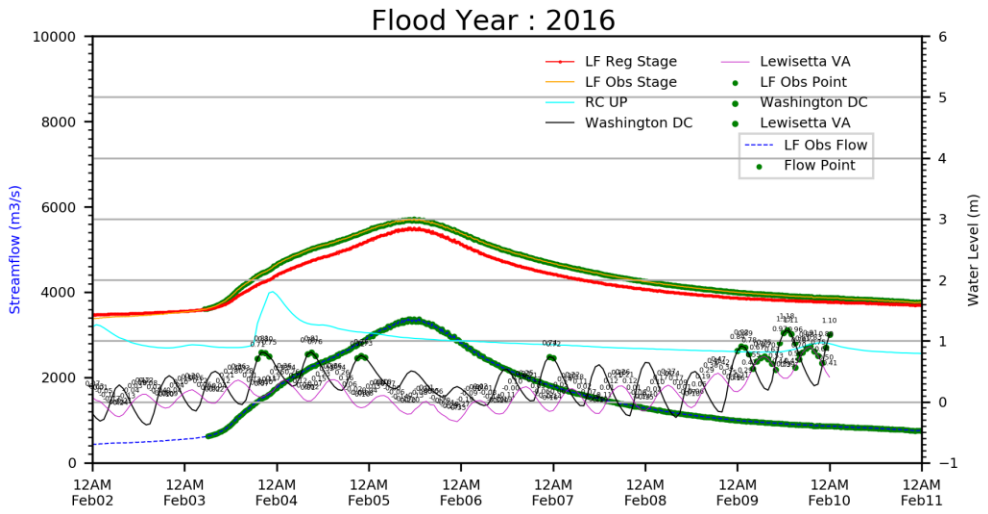

Figure B1 Compound flood drivers in Washington DC (green dots indicate flooded points for different drivers, LF Reg Stage: calculated regression, RC UP = Rock Creek)

There are few stations in between DC and LWT (Figure B2). However, as the previous studies suggested (Mashriqui et al., 2014; Feng et al., 2017; Khalid and Ferreira, 2020), the coastal surge from LWT has a significant impact in DC flooding and therefore we selected DC for our study. However, other stations also have impact from upstream and downstream but the best location to study the impact from both is DC. The water from Lewisetta travels to DC through Dahlgren and Alexandria. However, while the tidal

amplitude in DC and Alexandria changes, the tidal pattern remains the same. Furthermore, the impact of local winds in DC and Alexandria is similar. On the other hand, any increase or decrease in water level at Lewisetta will result in similar changes in Dahlgren. Therefore, using Alexandria or Dahlgren for the analysis will not provide any additional information. Moreover, we use the Lewisetta water levels for our analysis because water from the Chesapeake Bay is directly impacting this location. Therefore, we can expect certain changes in DC due to the ocean or bay water, which can be captured by Lewisetta water level.

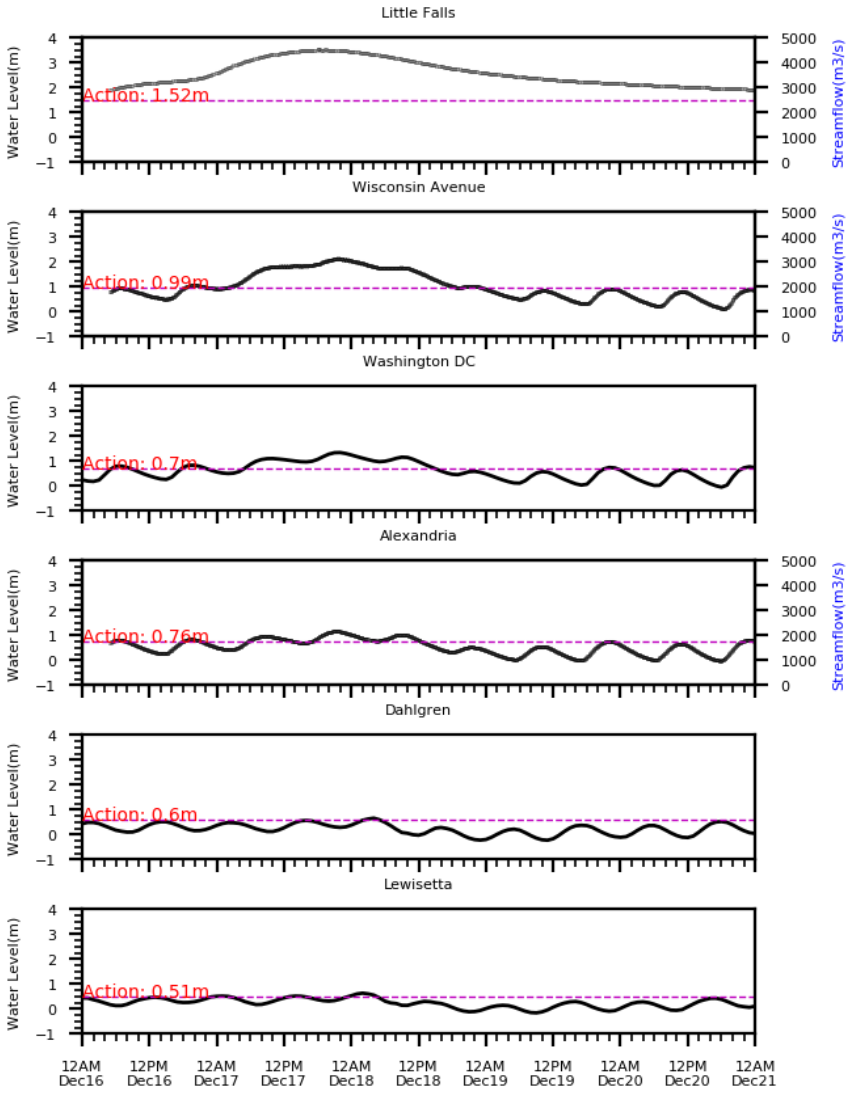

Figure B2 Water levels at different Potomac River stations in 2018

The time lags were measured for more than 30 storms during 1931-2019 by calculating and analyzing the time of peak for the flow and water levels at different stations. The time difference were calculated as shown in Table B1 and also plotted to check the values manually (Figure B3). It was observed that the peak at DC occurs 6-8 hours after the peaks at Lewisetta. However, the flow at Little Falls and water level at DC

start to increase almost at the same time and decrease also at the same time, therefore time lag is approximately zero for these two stations.

Table B1 Time of peak at DC and LWT

Storms	DC Peak time	DC	LWT Peak time	LWT	DC time – LWT time (dd:hh:mm)
Arthur	6/20/96 10:00	0.844601	6/20/96 4:00	0.433426	00:06:00
Bertha	7/13/96 7:00	0.881482	7/13/96 1:00	0.551383	00:06:00
Bonnie	6/4/16 7:00	0.887578	6/4/16 0:00	0.562356	00:07:00
Dennis	9/6/99 4:00	1.114654	9/5/99 22:00	0.81534	00:06:00
Helene	9/26/00 6:00	0.709574	9/26/00 0:00	0.545287	00:06:00
Isabel	9/19/03 4:00	2.652674	9/18/03 20:00	1.430426	00:08:00
Cindy	7/8/05 8:00	1.109472	7/8/05 2:00	0.678485	00:06:00
Alberto	6/8/06 5:00	0.824484	6/7/06 22:00	0.543458	00:07:00
Ernesto	9/2/06 1:00	1.56149	9/1/06 18:00	1.490472	00:07:00
Irene	9/2/11 23:00	0.864718	8/27/11 22:00	1.131418	06:01:00
Andrea	6/7/13 6:00	0.856488	6/7/13 0:00	0.470306	00:06:00
Arthur	6/28/14 8:00	0.795528	6/28/14 2:00	0.535534	00:06:00
Ana	5/3/15 7:00	0.756514	5/3/15 1:00	0.51755	00:06:00
Claudette	7/17/15 8:00	0.920496	7/17/15 2:00	0.589483	00:06:00
Hermine	9/3/16 21:00	0.975665	9/3/16 15:00	0.820522	00:06:00
Julia	9/16/16 19:00	0.892454	9/16/16 13:00	0.613562	00:06:00

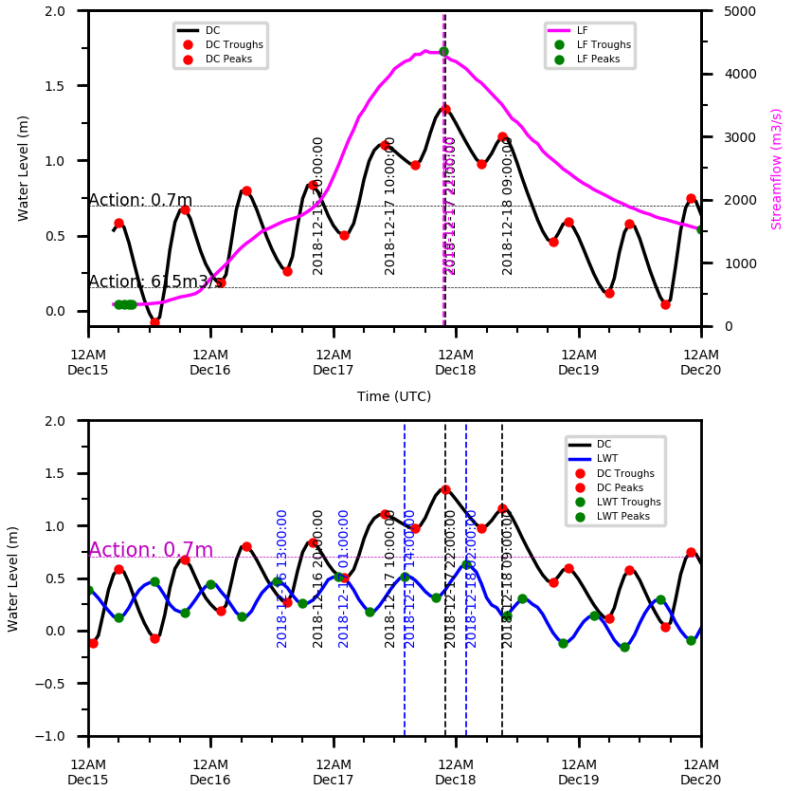

Figure B3 Time lags between the flood recording stations (blue lines for LWT peak and time, black line for DC peak and time)

There was only one rain gage available in this area (Ronald Reagan Airport) which is no longer available. However, we used the flow in different small streams connected to Potomac River which are close to Washington, DC, to estimate the local rainfall driven runoff in those locations. The flow in these small streams are assumed independent (correlation<0.37) from the riverine flow from the large watershed of the Potomac River. Finally, we selected one small stream, Rock Creek, as a proxy to represent all the water coming from the local urban streams due to rainfall. The rainfall from Ronald Reagan airport and the flow from adjacent streams during the same rainfall event are shown in Figure B4, B5, and B6. Although rainfall is a spatially variable driver,

the figure shows that all the local streamflow stations and the rainfall gage usually are affected by the same rainfall event.

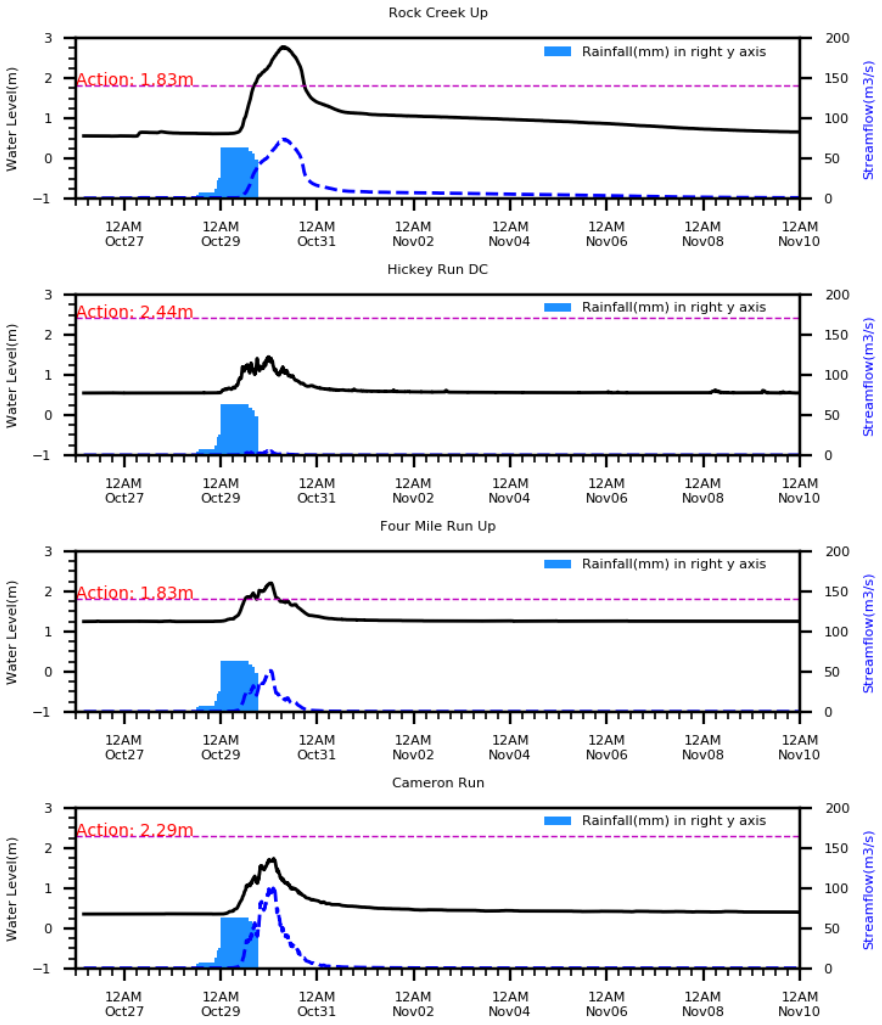

Figure B4 Flows in the streams and rainfall at Ronald Reagan Airport in 2012

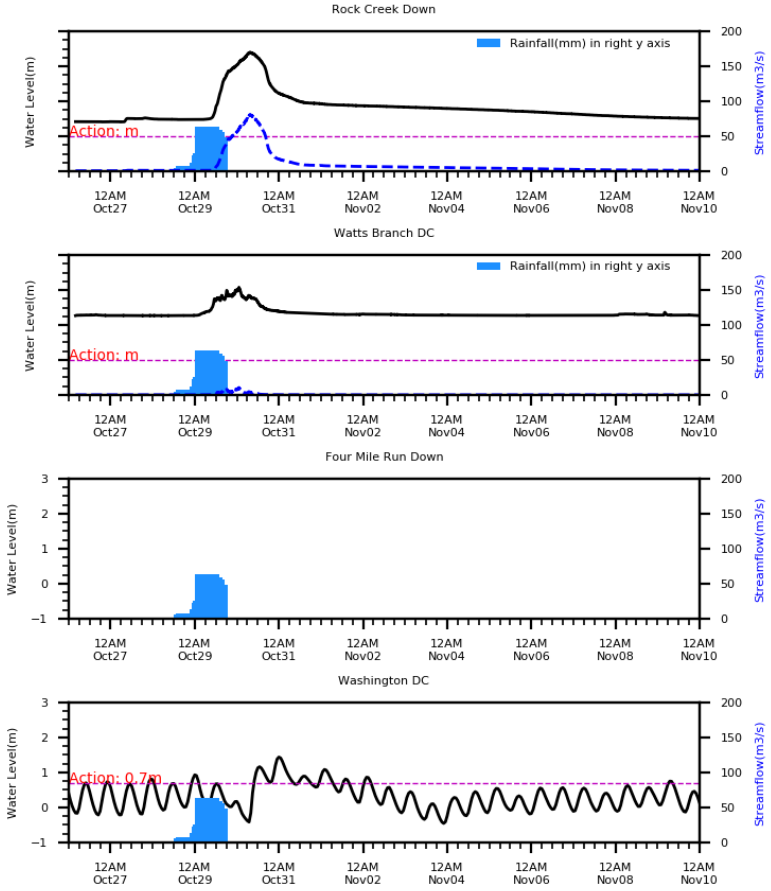

Figure B5 Flows in the streams and DC and rainfall at Ronald Reagan Airport in 2012

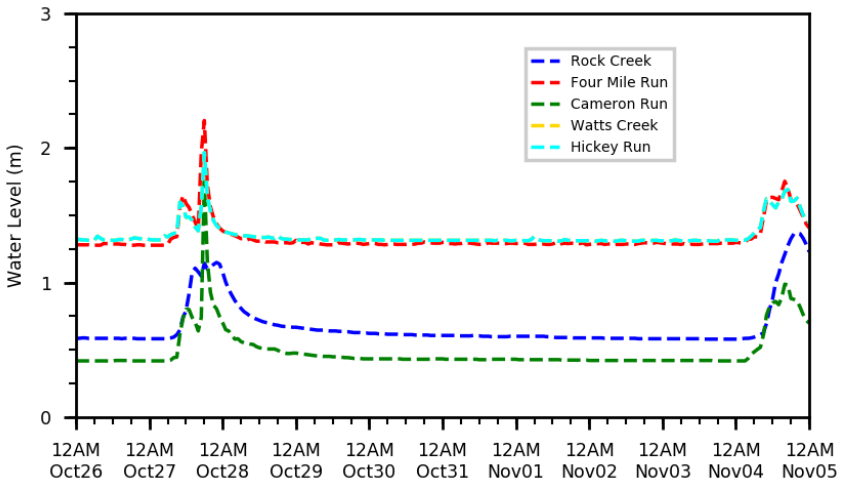

Figure B6 Streamflow in during a rainfall event in 2010

Appendix C - Test of Independence

For our study, DC water level is the dependent variable and all other variables are considered the independent variables. We generated correlation plots and scatter plots between each variable along with the R^2 values. The correlation co-efficient values were less than 0.37 (Figure C1) which is a low or weak correlation (Taylor, 1990) and R^2 values were less than 0.1 (Figure C2) which shows that there is very weak or no collinearity among the variables and therefore, we assume these variables as independent.

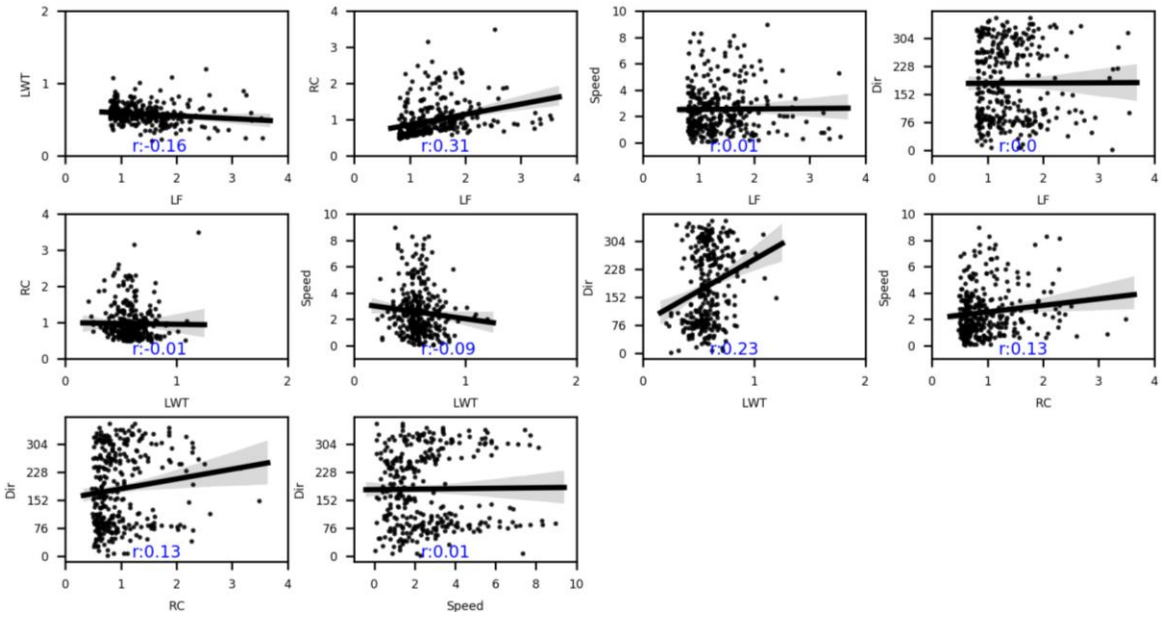

Figure C1 Independence: Correlation co-efficient(r) between the variables

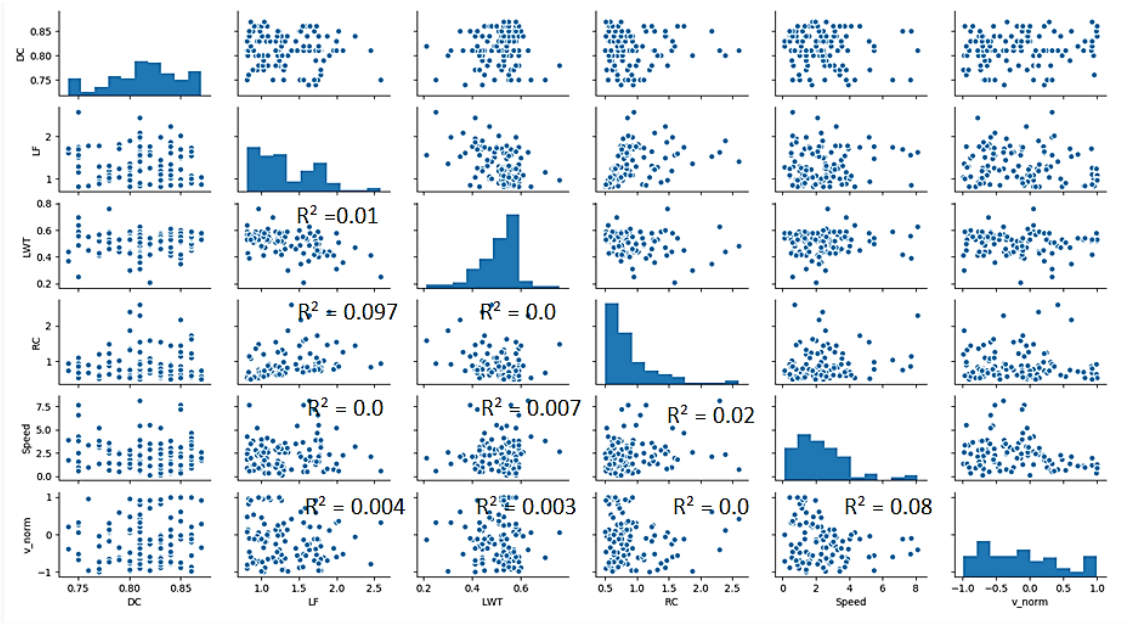

Figure C2 Independence: R^2 values between the variables

Appendix D - Data Availability and Pre-Processing

Little Falls station does not have 15-min or hourly flow data before 1980. During 1930-1980, the station only has daily average data. Therefore, we used the available daily average and 15-min data from 1990-2019 to generate a regression equation that would convert daily average to daily maximum values (Figure D1).

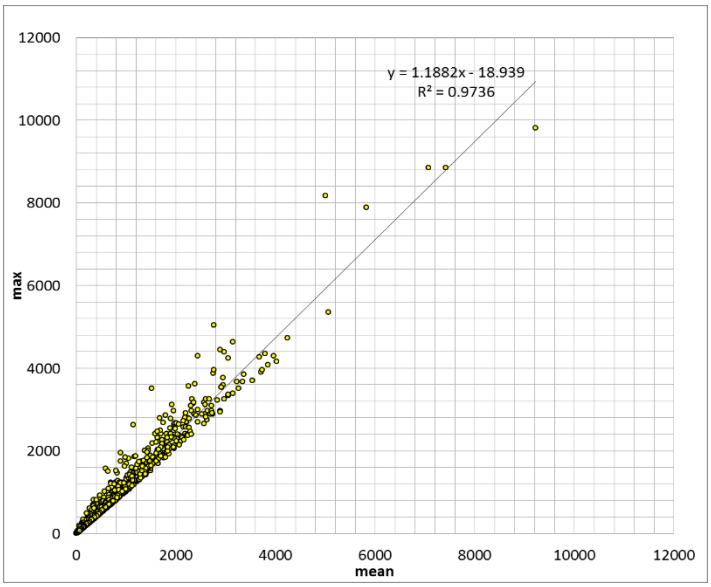

Figure D1 Little Falls Mean to Max

Equation D1

$$Y = 1.882X - 18.939$$

We used Sewells Point water level data as a proxy of LWT after calibrating and validating the available dataset. This is the only station that has available data with continuous time series for the study period and could represent the water level at Lewisetta with a R^2 value of 0.7, which is typically considered acceptable (Moriasi et al., 2007). We have collected historical data for both LWT and SWP when both of the

stations had available data (1980-2019). We generated a regression equation (Figure D2) to estimate LWT values from SWP values. After that, a 5 hour time lag was added to consider the timing difference between LWT and SWP peaks. The surge characteristics will be very different in DC than in Lewisetta or Sewells Point. However, tidal and surge propagation from Lewisetta (mouth of the Potomac River in the Chesapeake Bay) to upstream of the Potomac River is well studied (Mashriqui et al., 2014; Feng et al., 2017; Khalid and Ferreira, 2020).These studies demonstrate in details the propagation of both astronomical and storm tidal signals propagating upstream towards Washington DC. Astronomical tidal analyses along the tidal Potomac River also clearly demonstrated the tidal propagation from Lewisetta to Washington, DC. Lewisetta is actually the logical choice as it defines the boundary between the Chesapeake Bay and the Potomac River (as shown in the study area figure). Our goal is to investigate and quantify the impact of storm surges coming from Lewisetta (and therefore the Chesapeake Bay) on DC flood levels. This is indeed one of the objectives of the study and demonstrated in the results section. We believe that the results of the present study also support the selection of this station as a proxy for storm surge.

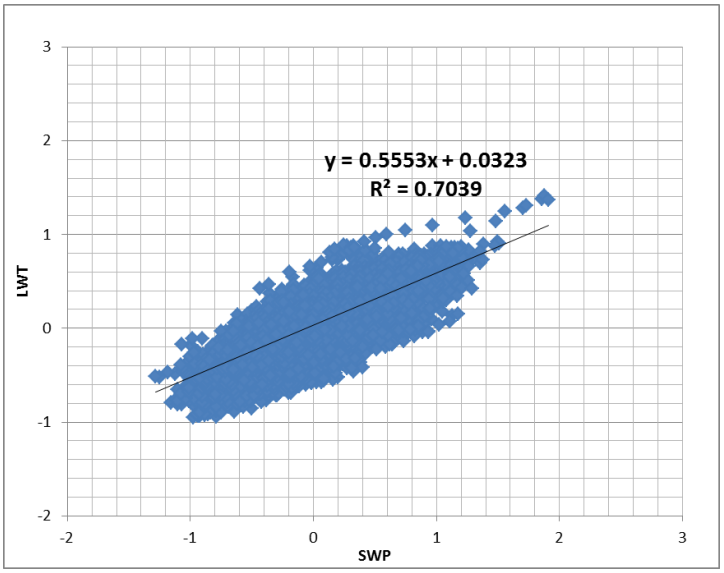

Figure D2 Sewells Point daily maximum water level and Lewisetta daily maximum water level from (2005-2019)

Equation D2

$$Y = 0.5553X + 0.0323$$

Validation was done by using the regression equation to generate LWT water level from SWP daily maximum water level during 1980 – 2004 (Figure D3). The focus was on determining the flood stages (*Action*, *Minor*, *Moderate*, and *Major*) correctly rather than estimating the actual flood peak.

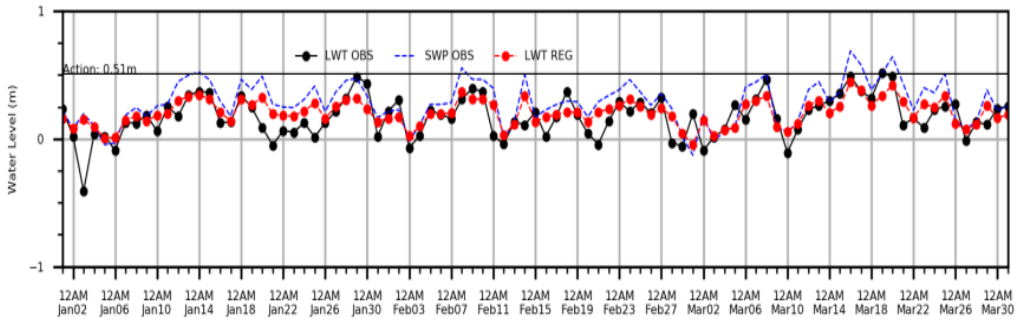

Figure D3 Validation of Sewells Point data to use as proxy of Lewisetta data

Daily max SWP to daily max LWT:

LWT flood days from observed data: 550 days

LWT flood days from regression equation: 552 days

LWT Error mean: -0.0072 days

A flowchart is presented to summarize the processing of the data to use in the analysis (Figure D4). The flowchart shows which equations were used for calculating the missing values of each variable. Moreover, we used the daily maximum values of the drivers to analyze any event by selecting the peak from 24hours data for LWT, LF, and RC.

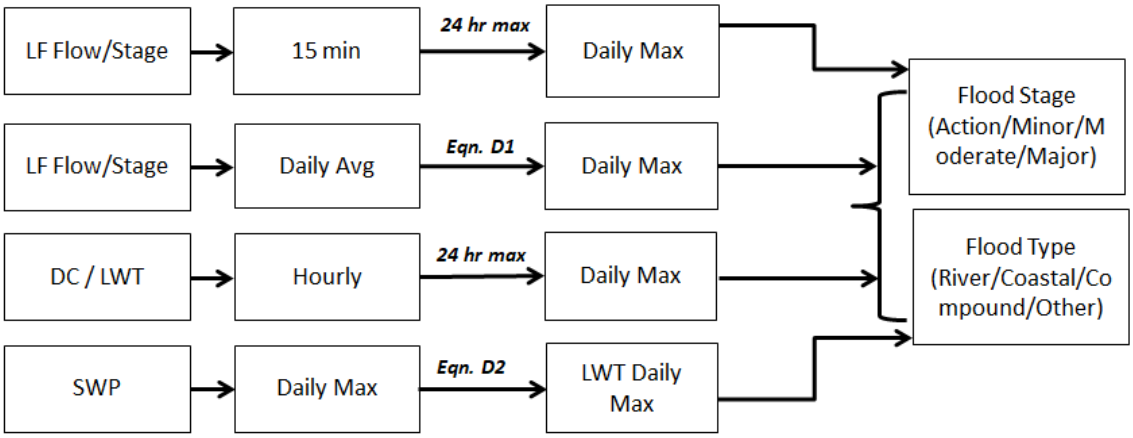

Figure D4 Data pre-processing flow chart

NWS provides flood stages for estimating the flood categories. However, LF does not have water level or stage data available for the whole study period. Therefore, we used rating curve data of LF station from USGS (https://waterwatch.usgs.gov/?id=mkrc) and converted the streamflow into water level (Figure D5). Although flow is the

dominant flood river in DC, converting it into the stage helped to understand the flooding condition clearly based on NWS stages. The equation for the rating curve at LF is a polynomial 2nd order equation:

Equation D3

$$Y = -4x10^{-9}X^2 + 0.0005X + 1.2132$$

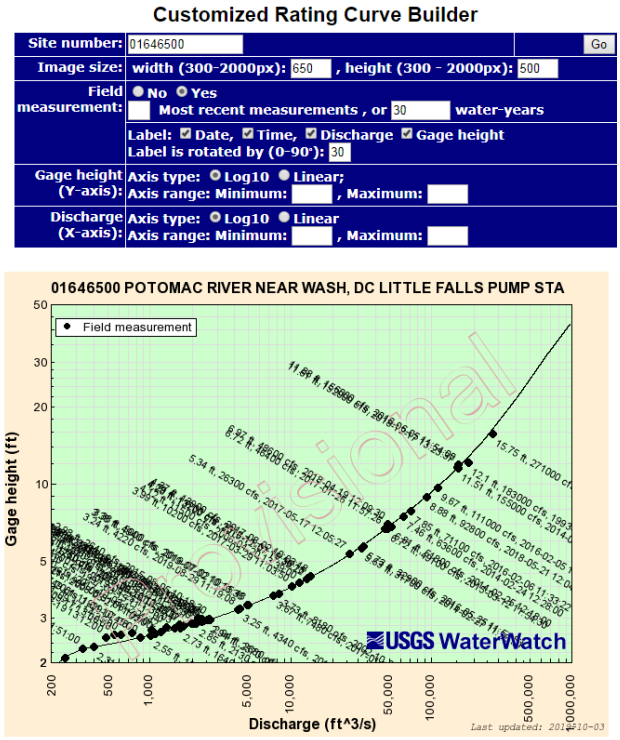

Figure D5 USGS rating curve values for LF

When all the interpolated datasets were processed, we tested the dataset against the daily maximum data from Washington DC as this station has available data for the full study period (Figure D6). The events peaks were captured significantly by those dataset as they could capture the flood stages of the historical storms. Figure D7 shows the data availability summary in the study area.

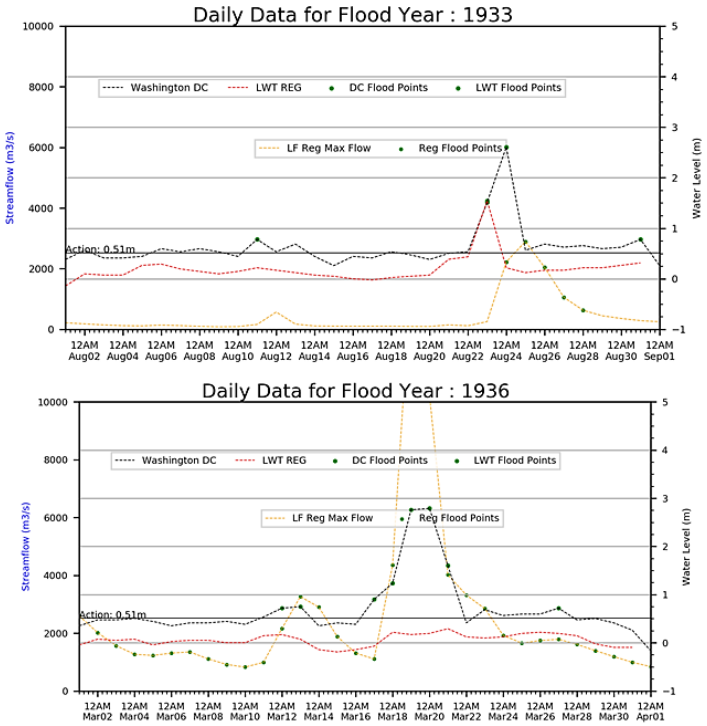

Figure D6 Interpolated dataset for historical storms

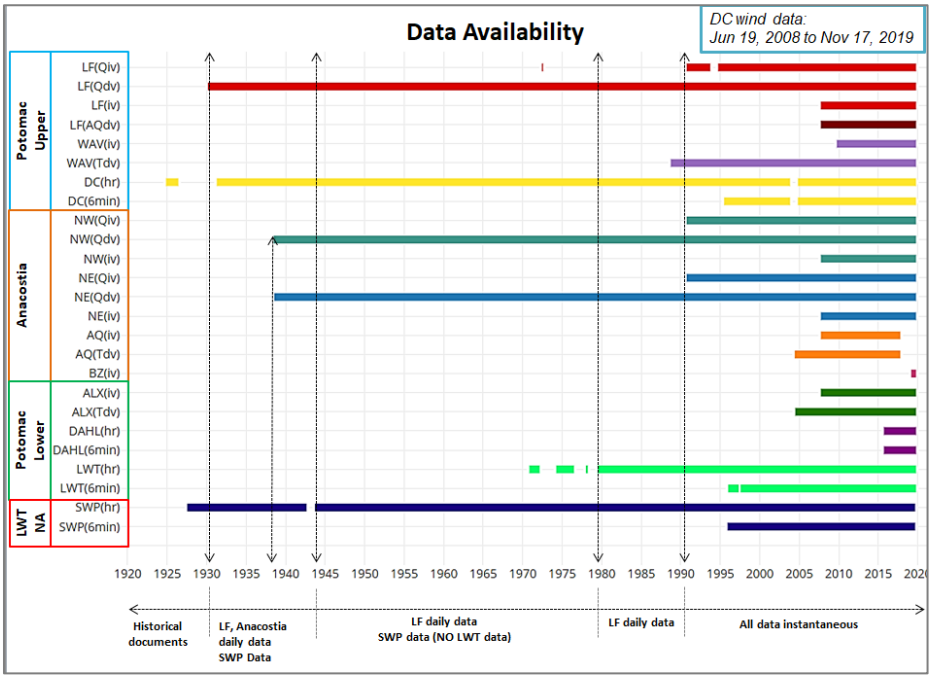

Figure D7 Summary of data availability

Appendix E - Impact of the Flood Drivers in DC station and the Urban Areas

The flood drivers considered in this study are riverine flow from Little Falls, coastal storm surges from Lewisetta, local wind at Washington, DC, and urban runoff from Rock Creek. Anacostia River is connected to the Potomac River and was used as a boundary for the model simulation. However, we did not consider the flow from Anacostia as an independent driver for flooding in Washington, DC. Anacostia river flow is high during the events when Potomac River flow is also high. For example, the Northwest and Northeast Anacostia rivers had the maximum streamflow of $509m^3/s$ and $340m^3/s$ on Jun 22, 1972, the same event when the Potomac River flow was high due to flooding from hurricane Agnes. The figure (Figure E1) shows different events during which both Potomac and Anacostia River flow was high. Therefore, the Anacostia River flooding had no independent impact as a flood driver in Washington, DC.

Flood events from 1980-2019 were plotted to study the impact of all the four flood drivers on those events. The events were initially plotted with LF and LWT to check the impact of flow and surges and presented in the manuscript. Therefore, runoff, wind direction, and wind speed along with LF flow and LWT water level were included in Figure E2. This figure provided significant information on the contribution of wind and runoff to generate floods in DC. When neither LF nor LWT showed high flow or surge, the floods were generated by the wind in upward arrow or the high urban runoff with yellow and orange colors. All these drivers will change the water level in DC and generate the total water level. A combined plot with all the relevant information were plotted to provide the comprehensive estimation of such impact or interaction. Without

the wind speed, direction, and rainfall impact it was not possible to compare the changes in flood peaks during different types of floods. Table E1 shows how NWS defines point measurement or flood water level at DC station in terms of flooding around the area:

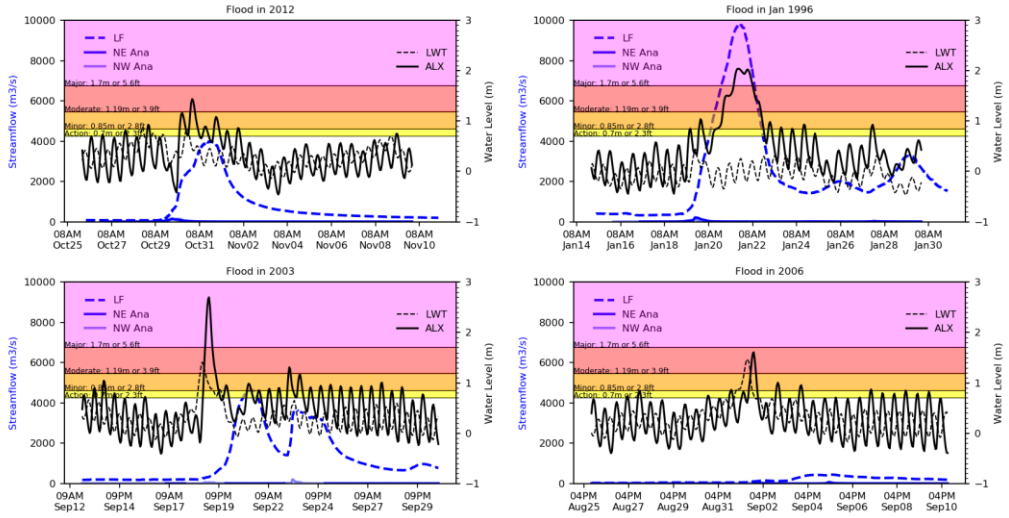

Figure E1 Flooding in Potomac and Anacostia Rivers

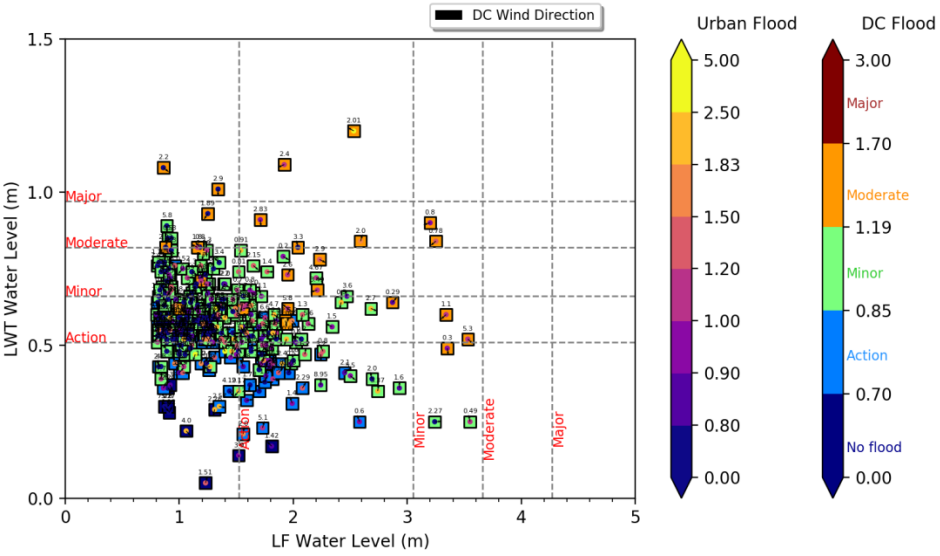

Figure E2 Compound flood drivers and their impact on DC flooding

Table E1 NWS information for flood stage at DC and inundation locations around DC from image (NWS, 2020)

Flood Locations (Source: NWS)		
Stage	WL	
Action	0.70	Lowest spots along the seawall adjacent to Ohio Drive and the Hains Point Loop Road
Minor	0.85	Sporadic portions of the seawall adjacent to Ohio Drive and the Hains Point Loop Road.
Moderate	1.19	Unprotected area on Southwest Waterfront at DC seafood market and parts of Hains Point Loop Road
Moderate	1.55	Part of East Potomac Park and Hains Point Loop Road. Western end of the DC seafood market on the Southwest Waterfront. Navy Yard begins to flood as minor inundation begins along the Anacostia River.

Major	Main Flood Locations	Other Locations	
1.71	East Potomac Golf Course parking. Independence and 17th, and East Basin Drive near the Jefferson Memorial	Freshwater flood: tidal basin overflows at Independence and 17th and on East Basin Drive near Jefferson Memorial	
1.86	Portions of the George Washington Memorial Parkway near the 14th Street bridge.		
2.13	Floodwaters cover Ohio Drive on the Potomac side at the railroad bridge.		
2.32	Most of East Potomac Park including some buildings. World War II Memorial on 17th Street NW.	Moderate flooding on Anacostia River and roads and buildings nearby	FDR Memorial, portion of the Navy Yard and taxiways at Reagan National Airport. Maine Avenue near the 14th Street bridge
2.62	Southern end of the runways at Reagan National Airport (likely to occur in tidal flood).	Almost all of East Potomac Park, western half of the Navy Yard. 5th Avenue SW up to C Street on Fort McNair. Threatens the basement of the Jefferson Memorial.	
2.93	North-south runway at Reagan National Airport and some taxiways. George Washington Parkway between Arlington National Cemetery and the Airport.	Back side of a business on north side of Maine Avenue near I-395. Widespread flooding on Anacostia, Navy Yard up to M Street SE.	
3.23	Widespread flooding: Very few high spots remain dry in East Potomac Park and around the tidal basin.	Fort McNair all the way up 5th Avenue. Cover M Street SE near the Navy Yard. Some runways and taxiways at Reagan National Airport partially flooded.	
4.15	Pentagon East parking area (mostly during freshwater flood). Most of the Reagan National Airport runways are flooded.	Tidal flood: portions of the economy parking at Reagan National Airport and nearby structures.	Arnold Avenue at Joint Base Anacostia Bolling and Most of Fort McNair. Tidal flood cause widespread flooding of the Base.

A simulation from the model is presented to show how water level in DC station is considered as a representation of flooding inundation in DC. In this figure, a major flood with 5.77m means the flood stage at DC is 5.77m and the areas that will be inundated with such flood are colored in blue. The inundation map based on the flood stage in DC is shown in Figure E3 (NWS map area).

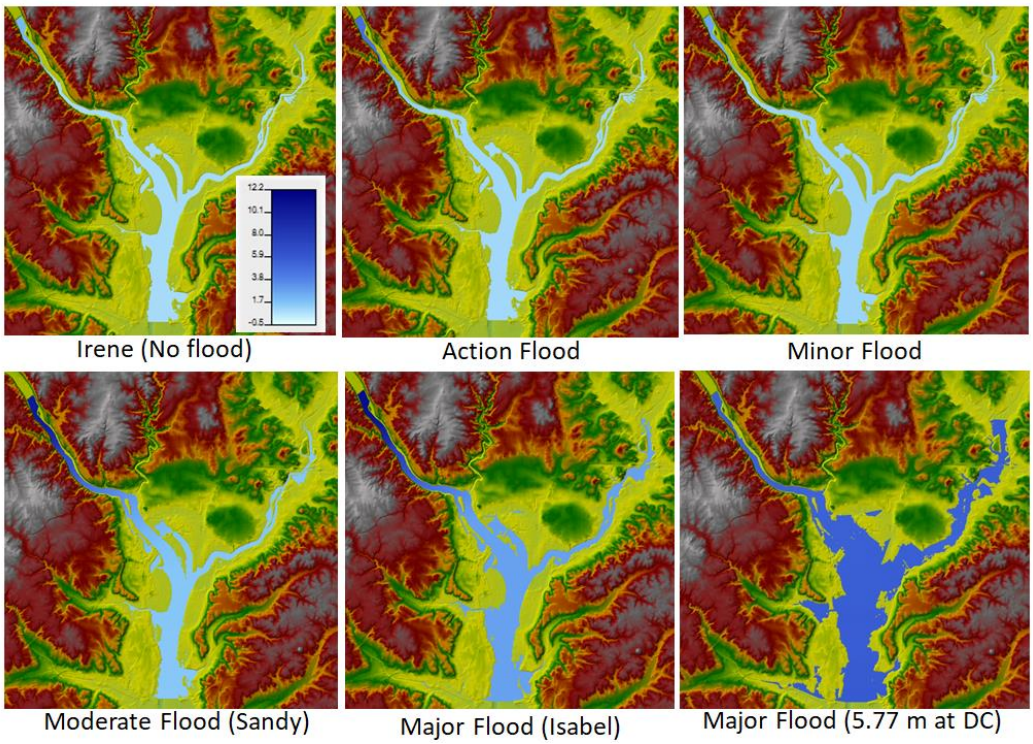

Figure E3 Flooding in Washington DC station and the surrounding area

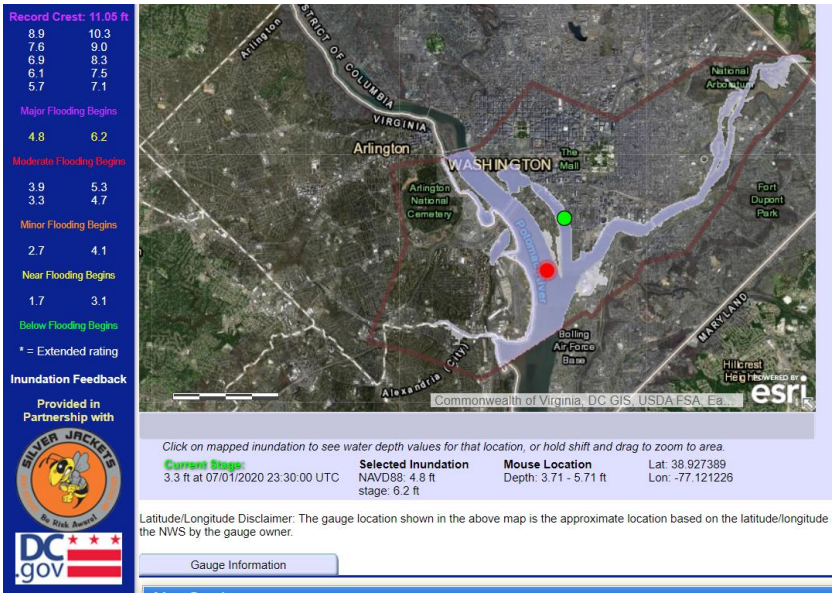

Figure E4 NWS flood inundation map (NWS, 2020)

REFERENCES

ACSM Bulletin, 2008. Understanding sea level change, Sea Level Change - Observations from Space.

Adams, T.E., Chen, ; Sherry, Dymond, R., 2018. Results from Operational Hydrologic Forecasts Using the NOAA/NWS OHRFC Ohio River Community HEC-RAS Model. J. Hydrol. Eng. 23. https://doi.org/10.1061/(ASCE)HE.1943-5584.0001663

Aerts, J.C.J.H., Lin, N., Botzen, W., Emanuel, K., de Moel, H., 2013. Low-Probability Flood Risk Modeling for New York City. Risk Anal. 33, 772–788. https://doi.org/10.1111/risa.12008

Afshari, S., Tavakoly, A.A., Rajib, M.A., Zheng, X., Follum, M.L., Omranian, E., Fekete, B.M., 2018. Comparison of new generation low-complexity flood inundation mapping tools with a hydrodynamic model. J. Hydrol. 556, 539–556. https://doi.org/10.1016/j.jhydrol.2017.11.036

Allaire, M.C., 2016. Disaster loss and social media: Can online information increase flood resilience? Water Resour. Res. 7408–7423. https://doi.org/10.1111/j.1752-1688.1969.tb04897.x

Ammar, M.E., Gharib, A., Islam, Z., Davies, E.G.R., Seneka, M., Faramarzi, M., 2020. Future floods using hydroclimatic simulations and peaks over threshold: An alternative to nonstationary analysis inferred from trend tests. Adv. Water Resour.

136, 103463. https://doi.org/10.1016/j.advwatres.2019.103463

Ayyub, B.M., Braileanu, H.G., Qureshi, N., 2012. Prediction and Impact of Sea Level Rise on Properties and Infrastructure of Washington, DC. Risk Anal. 32, 1901–1918. https://doi.org/10.1111/j.1539-6924.2011.01710.x

Barthélémy, S., Ricci, S., Morel, T., Goutal, N., Le Pape, E., Zaoui, F., 2018. On operational flood forecasting system involving 1D/2D coupled hydraulic model and data assimilation. J. Hydrol. 562, 623–634. https://doi.org/10.1016/j.jhydrol.2018.05.007

Ben Daoued, A., Hamdi, Y., Mouhous-Voyneau, N., Sergent, P., 2020. Modelling dependence and coincidence of storm surges and high tide: Methodology and simplified case study in Le Havre (France). Nat. Hazards Earth Syst. Sci. 1–17. https://doi.org/10.5194/nhess-2019-407

Bevacqua, E., Maraun, D., Hobæk Haff, I., Widmann, M., Vrac, M., 2017. Multivariate statistical modelling of compound events via pair-copula constructions: Analysis of floods in Ravenna (Italy). Hydrol. Earth Syst. Sci. 21, 2701–2723. https://doi.org/10.5194/hess-21-2701-2017

Bevacqua, E., Maraun, D., Vousdoukas, M.I., Voukouvalas, E., Vrac, M., Mentaschi, L., Widmann, M., 2019. Higher probability of compound flooding from precipitation and storm surge in Europe under anthropogenic climate change. Sci. Adv. 5, 1–8. https://doi.org/10.1126/sciadv.aaw5531

Bevacqua, E., Vousdoukas, M., Shepherd, T., Vrac, M., 2020. Brief communication: The role of using precipitation or river discharge data when assessing global coastal

compound flooding. Nat. Hazards Earth Syst. Sci. 1–20. https://doi.org/10.5194/nhess-2019-415

Bhandari, M., Nyaupane, N., Mote, S.R., Kalra, A., Ahmad, S., 2017. 2D Unsteady Flow Routing and Flood Inundation Mapping for Lower Region of Brazos River Watershed. World Environ. Water Resour. Congr. 2017 292–303. https://doi.org/10.1061/9780784480625.027

Bilskie, M. V., Hagen, S.C., Medeiros, S.C., Passeri, D.L., 2014. Dynamics of sea level rise and coastal flooding. Geophys. Res. Lett 41, 927–934. https://doi.org/10.1002/2013GL058759.Standard

Blumenthal, B., Haas, J., Andersson, J.-O., 2018. A GIS-based multivariate approach to identify flood damage affecting factors. Nat. Hazards Earth Syst. Sci. Discuss. 1–27. https://doi.org/10.5194/nhess-2018-286

Brunner, G.W., 2016. HEC-RAS River Analysis System, 2D Modeling User's Manual Version 5.0.

Brunner, G.W., Piper, S.S., Jensen, M.R., Chacon, B., 2015. Combined 1D and 2D Hydraulic Modeling within HEC-RAS 1432–1443. https://doi.org/10.1061/9780784479162.141

Cadavid, L., Wilsnack, M., Qi, C., Han, J., Arteaga, R., Konyha, K., Hydrology, 2016. Simulation of Coastal Water Control Structure Operations in South Florida Using HEC-RAS, in: World Environmental and Water Resources Congress 2016. pp. 160–169.

Cho, K.-H., Wang, H. V, Shen, J., Valle-Levinson, A., Teng, Y.-C., 2012. A modeling

study on the response of Chesapeake Bay to hurricane events of Floyd and Isabel. Ocean Model. 49, 22–46. https://doi.org/10.1016/j.ocemod.2012.02.005

Contreras, M.T., Gironás, J., Escauriaza, C., 2020. Forecasting flood hazards in real-time: A surrogate model for hydrometeorological events in an Andean watershed. Nat. Hazards Earth Syst. Sci. 1–24. https://doi.org/10.5194/nhess-2019-384

Cortès, M., Turco, M., Ward, P., Sánchez-Espigares, J., Alfieri, L., Llasat, M.C., 2019. Changes in flood damage with global warming in the east coast of Spain. Nat. Hazards Earth Syst. Sci. Discuss. 1–40. https://doi.org/10.5194/nhess-2019-253

Couasnon, A., Eilander, D., Muis, S., Veldkamp, T.I.E., Haigh, I.D., Wahl, T., Winsemius, H., Ward, P.J., 2019. Measuring compound flood potential from river discharge and storm surge extremes at the global scale and its implications for flood hazard. Nat. Hazards Earth Syst. Sci. 1–24. https://doi.org/10.5194/nhess-2019-205

Deltares, 2019. Delft3D Flexible Mesh Suite. Delft, Netherlands.

Depietri, Y., Dahal, K., McPhearson, T., 2018. Multi-hazard risks in New York City. Nat. Hazards Earth Syst. Sci. 18, 3363–3381. https://doi.org/10.5194/nhess-18-3363-2018

Dhote, P.R., Thakur, P.K., Aggarwal, S.P., Sharma, V.C., Garg, V., Nikam, B.R., Chouksey, A., 2018. Experimental flood early warning system in parts of Beas Basin using integration of weather forecasting, hydrological and hydrodynamic models. Int. Arch. Photogramm. Remote Sens. Spat. Inf. Sci. - ISPRS Arch. 42, 221–225. https://doi.org/10.5194/isprs-archives-XLII-5-221-2018

Dickson, E., Baker, J.L., Hoornweg, D., Asmita, T., 2012. Urban Risk Assessments,

Urban Risk Assessments. https://doi.org/10.1596/978-0-8213-8962-1

Dimitriadis, P., Tegos, A., Oikonomou, A., Pagana, V., Koukouvinos, A., Mamassis, N., Koutsoyiannis, D., Efstratiadis, A., 2016. Comparative evaluation of 1D and quasi-2D hydraulic models based on benchmark and real-world applications for uncertainty assessment in flood mapping. J. Hydrol. 534, 478–492. https://doi.org/10.1016/j.jhydrol.2016.01.020

Eilander, D., Couasnon, A., Ikeuchi, H., Muis, S., Yamazaki, D., Winsemius, H., Ward, P.J., 2020. The effect of surge on riverine flood hazard and impact in deltas globally. Environ. Res. Lett. 1–19. https://doi.org/10.1088/1748-9326/ab8ca6

Ezer, T., Atkinson, L.P., 2014. Accelerated flooding along the U.S. East Coast: On the impact of sea-level rise, tides, storms, the Gulf Stream, and the North Atlantic Oscillations. Earth's Futur. 2, 362–382. https://doi.org/10.1002/2014ef000252

Ezer, T., Atkinson, L.P., Tuleya, R., 2017. Observations and operational model simulations reveal the impact of Hurricane Matthew (2016) on the Gulf Stream and coastal sea level. Dyn. Atmos. Ocean. 80, 124–138. https://doi.org/10.1016/j.dynatmoce.2017.10.006

Fang, Jiayi, Wahl, T., Fang, Jian, Sun, X., Kong, F., Liu, M., 2020. Compound flood potential from storm surge and heavy precipitation in coastal China 1–24.

Federal Emergency Management Agency, 2010. Flood Insurance Study. Washington, D.C.

Feng, Y., Brubaker, K.L., 2016. Sensitivity of Flood-Depth Frequency to Watershed-Runoff Change and Sea-Level Rise Using a One-Dimensional Hydraulic Model. J.

Hydrol. Eng. 21. https://doi.org/10.1061/

Feng, Y., Brubaker, K.L., McCuen, R.H., 2017. New View of Flood Frequency Incorporating Duration. J. Hydrol. Eng. 22, 04017051. https://doi.org/10.1061/(asce)he.1943-5584.0001573

Finaud-Guyot, P., Delenne, C., Guinot, V., Llovel, C., 2011. 1D-2D coupling for river flow modeling. Comptes Rendus - Mec. 339, 226–234. https://doi.org/10.1016/j.crme.2011.02.001

Gallien, T.W., Kalligeris, N., Delisle, M.P.C., Tang, B.X., Lucey, J.T.D., Winters, M.A., 2018. Coastal flood modeling challenges in defended urban backshores. Geosci. 8. https://doi.org/10.3390/geosciences8120450

Hao, Z., Singh, V.P., Hao, F., 2018. Compound extremes in hydroclimatology: A review. Water (Switzerland) 10, 16–21. https://doi.org/10.3390/w10060718

Hecht, J.S., Vogel, R.M., 2020. Updating urban design floods for changes in central tendency and variability using regression. Adv. Water Resour. 136. https://doi.org/10.1016/j.advwatres.2019.103484

Hendry, A., Haigh, I.D., Nicholls, R.J., Winter, H., Neal, R., Wahl, T., Joly-Lauge, A., Darby, S.E., 2019. Assessing the characteristics and drivers of compound flooding events around the UK coast. Hydrol. Earth Syst. Sci. 23, 3117–3139. https://doi.org/10.5194/hess-23-3117-2019

Hernández-Guzmán, R., Ruiz-Luna, A., 2013. SARA – An enhanced curve number-based tool for estimating direct runoff. J. Hydroinformatics 15, 881–887. https://doi.org/10.2166/hydro.2013.145

Hicks, F.E., Peacock, T., 2005. Suitability of HEC-RAS for Flood Forecasting, Canadian Water Resources Journal.

Hu, R., Fang, F., Salinas, P., Pain, C.C., Sto.Domingo, N.D., Mark, O., 2019. Numerical simulation of floods from multiple sources using an adaptive anisotropic unstructured mesh method. Adv. Water Resour. 123, 173–188. https://doi.org/10.1016/j.advwatres.2018.11.011

Huanxin, W., Presley, B.J., Velinsky, D.J., 1997. Distribution and sources of phosphorus in tidal river sediments in the Washington, DC, area. Environ. Geol. 30, 224–230. https://doi.org/10.1007/s002540050150

Huong, H.T.L., Pathirana, A., 2013. Urbanization and climate change impacts on future urban flooding in Can Tho city, Vietnam. Hydrol. Earth Syst. Sci. 17, 379–394. https://doi.org/10.5194/hess-17-379-2013

Ikeuchi, H., Hirabayashi, Y., Yamazaki, D., Muis, S., Ward, P.J., Winsemius, H.C., Verlaan, M., Kanae, S., 2017. Compound simulation of fluvial floods and storm surges in a global coupled river-coast flood model: Model development and its application to 2007 Cyclone Sidr in Bangladesh. J. Adv. Model. Earth Syst. 9, 1847–1862. https://doi.org/10.1002/2017MS000943

IPCC, 2014. Climate Change 2014 Synthesis Report, Managing the Risks of Extreme Events and Disasters to Advance Climate Change Adaptation: Special Report of the Intergovernmental Panel on Climate Change. Geneva. https://doi.org/10.1017/CBO9781139177245.003

IPCC, 2012. Managing the Risks of Extreme Events and Disasters to Advance Climate

Change Adaptation: Special Report of the Intergovernmental Panel on Climate Change. https://doi.org/10.1017/CBO9781139177245.009

Jha, A., Lamond, J., Bloch, R., Bhattacharya, N., Lopez, A., Papachristodoulou, N., Bird, A., Proverbs, D., Davies, J., Barker, R., 2011. Five Feet High and Rising: Cities and Flooding in the 21st Century. https://doi.org/10.1596/1813-9450-5648

Johnson, W.F., 1889. History of the Johnstown Flood .

Kew, S.F., Selten, F.M., Lenderink, G., Hazeleger, W., 2013. The simultaneous occurrence of surge and discharge extremes for the Rhine delta. Nat. Hazards Earth Syst. Sci. 13, 2017–2029. https://doi.org/10.5194/nhess-13-2017-2013

Khalid, A., Ferreira, C.M., 2020. Advancing real-time flood prediction in large estuaries: iFLOOD a fully coupled surge-wave automated web-based guidance system. Environ. Model. Softw. 131, 104748. https://doi.org/10.1016/j.envsoft.2020.104748

Kim, Y., Engel, B.A., Lim, K.J., Larson, V., Duncan, B., 2002. Runoff Impacts of Land-Use Change in Indian River Lagoon Watershed. J. Hydrol. Eng. 7, 245–251. https://doi.org/10.1061/(asce)1084-0699(2002)7:3(245)

Klerk, W.J., Winsemius, H.C., Van Verseveld, W.J., Bakker, A.M.R., Diermanse, F.L.M., 2015. The co-incidence of storm surges and extreme discharges within the Rhine-Meuse Delta. Environ. Res. Lett. 10. https://doi.org/10.1088/1748-9326/10/3/035005

Kumbier, K., Carvalho, R.C., Vafeidis, A.T., Woodroffe, C.D., 2018. Investigating compound flooding in an estuary using hydrodynamic modelling: A case study from the Shoalhaven River, Australia. Nat. Hazards Earth Syst. Sci. 18, 463–477.

https://doi.org/10.5194/nhess-2017-360

Kundzewicz, Z.W., Su, B., Wang, Y., Wang, Guojie, Wang, Guofu, Huang, J., Jiang, T., 2019. Flood risk in a range of spatial perspectives - From global to local scales. Nat. Hazards Earth Syst. Sci. 19, 1319–1328. https://doi.org/10.5194/nhess-19-1319-2019

Kundzewicz, Z.W., Su, B., Wang, Y., Wang, Guojie, Wang, Guofu, Jiang, T., 2018. Flood Risk in a Range of Spatial Perspectives–from Global to Local. Nat. Hazards Earth Syst. Sci. 1–17.

Kunz, M., Mühr, B., Kunz-Plapp, T., Daniell, J.E., Khazai, B., Wenzel, F., Vannieuwenhuyse, M., Comes, T., Elmer, F., Schröter, K., Fohringer, J., Münzberg, T., Lucas, C., Zschau, J., 2013. Investigation of superstorm Sandy 2012 in a multi-disciplinary approach. Nat. Hazards Earth Syst. Sci. 13, 2579–2598. https://doi.org/10.5194/nhess-13-2579-2013

Laska, S., 2020. Louisiana ’s Response to Extreme Weather.

Laudan, J., Zöller, G., Thieken, A.H., 2020. Flash floods versus river floods-a comparison of psychological impacts and implications for precautionary behaviour. Nat. Hazards Earth Syst. Sci. 20, 999–1023. https://doi.org/10.5194/nhess-20-999-2020

Le Coz, J., Patalano, A., Collins, D., Guillén, N.F., García, C.M., Smart, G.M., Bind, J., Chiaverini, A., Le Boursicaud, R., Dramais, G., Braud, I., 2016. Crowdsourced data for flood hydrology: Feedback from recent citizen science projects in Argentina, France and New Zealand. J. Hydrol. 541, 766–777.

https://doi.org/10.1016/j.jhydrol.2016.07.036

Leonard, M., Westra, S., Phatak, A., Lambert, M., van den Hurk, B., Mcinnes, K., Risbey, J., Schuster, S., Jakob, D., Stafford-Smith, M., 2014. A compound event framework for understanding extreme impacts. Wiley Interdiscip. Rev. Clim. Chang. 5, 113–128. https://doi.org/10.1002/wcc.252

Liu, M., Smith, J.A., 2016. Extreme Rainfall from Landfalling Tropical Cyclones in the Eastern United States: Hurricane Irene (2011). J. Hydrometeorol. 17, 2883–2904. https://doi.org/10.1175/jhm-d-16-0072.1

Lombardo, F.T., Ayyub, B.M., 2015. Analysis of Washington, DC, Wind and Temperature Extremes with Examination of Climate Change for Engineering Applications. ASCE-ASME J. Risk Uncertain. Eng. Syst. Part A Civ. Eng. 1, 1–11. https://doi.org/10.1061/AJRUA6.0000812

Mark, O., Weesakul, S., Apirumanekul, C., Aroonnet, S.B., Djordjević, S., 2004. Potential and limitations of 1D modelling of urban flooding. J. Hydrol. 299, 284–299. https://doi.org/10.1016/S0022-1694(04)00373-7

Masek, J.G., Lindsay, F.E., Goward, S.N., 2000. Dynamics of urban growth in the Washington DC metropolitan area, 1973-1996, from Landsat observations. Int. J. Remote Sens. 21, 3473–3486. https://doi.org/10.1080/014311600750037507

Mashriqui, H.S., Halgren, J.S., Reed, S.M., 2014a. 1D River Hydraulic Model for Operational Flood Forecasting in the Tidal Potomac: Evaluation for Freshwater, Tidal, and Wind-Driven Events. J. Hydraul. Eng. 140. https://doi.org/10.1061/(ASCE)HY.1943-7900.0000862

Mashriqui, H.S., Halgren, J.S., Reed, S.M., 2014b. 1D river hydraulic model for operational flood forecasting in the tidal potomac: Evaluation for freshwater, tidal, and wind-driven events. J. Hydraul. Eng. 140, 1–14. https://doi.org/10.1061/(ASCE)HY.1943-7900.0000862

Mcenery, J., Ingram, J., Duan, Q., Adams, T., Anderson, L., 2005. NOAA's Advanced Hydrologic Prediction Service, American Meteorological Society.

Moftakhari, H., Schubert, J.E., AghaKouchak, A., Matthew, R.A., Sanders, B.F., 2019. Linking statistical and hydrodynamic modeling for compound flood hazard assessment in tidal channels and estuaries. Adv. Water Resour. 128, 28–38. https://doi.org/10.1016/j.advwatres.2019.04.009

Moftakhari, H.R., AghaKouchak, A., Sanders, B.F., Feldman, D.L., Sweet, W., Matthew, R.A., Luke, A., 2015. Increased nuisance flooding due to sea-level rise: past and future. Geophys. Res. Lett. 42, 9846–9852. https://doi.org/10.1002/2015GL066072

Moftakhari, H.R., Salvadori, G., AghaKouchak, A., Sanders, B.F., Matthew, R.A., 2017. Compounding effects of sea level rise and fluvial flooding. Proc. Natl. Acad. Sci. 114, 9785–9790. https://doi.org/10.1073/pnas.1620325114

Moriasi, D.N., Arnold, J.G., Liew, M.W. Van, Bingner, R.L., Harmel, R.D., Veith, T.L., 2007. MODEL EVALUATION GUIDELINES FOR SYSTEMATIC QUANTIFICATION OF ACCURACY IN WATERSHED SIMULATIONS. Am. Soc. Agric. Biol. Eng. 50, 885–900. https://doi.org/10.1234/590

Mortlock, T.R., Metters, D., Soderholm, J., Maher, J., Lee, S.B., Boughton, G., Stewart, N., Zavadil, E., Goodwin, I.D., 2018. Extreme water levels, waves and coastal

impacts during a severe tropical cyclone in northeastern Australia: A case study for cross-sector data sharing. Nat. Hazards Earth Syst. Sci. 18, 2603–2623. https://doi.org/10.5194/nhess-18-2603-2018

MRLC, 2020. Data | Multi-Resolution Land Characteristics (MRLC) Consortium [WWW Document]. URL https://www.mrlc.gov/data?f%5B0%5D=category%3ALand Cover (accessed 7.7.20).

National Academies of Sciences, 2019. Framing the Challenge of Urban Flooding in the United States. National Academies Press, Washington, DC. https://doi.org/10.17226/25381

National Capital Planning Commission, 2008. Report on Stormwater in Flooding and Washington, DC.

National Hurricane Center, 2020. Hurricane ISAIAS Advisory Archive [WWW Document]. URL https://www.nhc.noaa.gov/archive/2020/ISAIAS.shtml? (accessed 8.7.20).

National Weather Service, 2020a. 1936 Flood Retrospective [WWW Document].

National Weather Service, 2020b. Flooding in Washington, D.C. [WWW Document].

National Weather Service, 2020c. Advanced Hydrologic Prediction Service [WWW Document]. URL https://water.weather.gov/ahps2/index.php?wfo=lwx (accessed 3.12.19).

NBC4 Washington, 2020. Tropical Storm Isaias Floods Old Town Alexandria [WWW Document]. URL https://www.nbcwashington.com/weather/tropical-storm-isaias-floods-old-town-alexandria/2381089/ (accessed 8.7.20).

NOAA, 2020a. NOAA Tides and Currents [WWW Document]. URL https://tidesandcurrents.noaa.gov/ (accessed 1.21.20).

NOAA, 2020b. National Centers for Environmental Information [WWW Document]. URL https://www.ncdc.noaa.gov/ (accessed 1.30.20).

NOAA, 2020c. High Water Level Terminology [WWW Document].

NOAA, 2020d. High-Resolution Rapid Refresh (HRRR) [WWW Document]. URL https://rapidrefresh.noaa.gov/hrrr/ (accessed 8.10.20).

NOAA, 2018a. 2017 U.S. billion-dollar weather and climate disasters: a historic year in context | NOAA Climate.gov [WWW Document]. URL https://www.climate.gov/news-features/blogs/beyond-data/2017-us-billion-dollar-weather-and-climate-disasters-historic-year (accessed 7.4.20).

NOAA, 2018b. NOAA ENC®- Electronic Navigational Charts [WWW Document]. URL https://nauticalcharts.noaa.gov/charts/noaa-enc.html (accessed 3.12.19).

NOAA NWS, 2018. About AHPS [WWW Document].

Noh, S.J., Lee, S., An, H., Kawaike, K., Nakagawa, H., 2016. Ensemble urban flood simulation in comparison with laboratory-scale experiments: Impact of interaction models for manhole, sewer pipe, and surface flow. Adv. Water Resour. 97, 25–37. https://doi.org/10.1016/j.advwatres.2016.08.015

NRCS, 2020. Web Soil Survey [WWW Document]. URL https://websoilsurvey.sc.egov.usda.gov/App/WebSoilSurvey.aspx (accessed 7.7.20).

NYC Emergency Management, 2015. New York City's Risk Landscape: A Guide to Hazard Mitigation. https://doi.org/10.1017/CBO9781107415324.004

Office of Water Prediction, 2018. The National Water Model [WWW Document]. URL http://water.noaa.gov/about/nwm (accessed 10.12.18).

Ogie, R.I., Clarke, R.J., Forehead, H., Perez, P., 2019. Crowdsourced social media data for disaster management: Lessons from the PetaJakarta.org project. Comput. Environ. Urban Syst. 73, 108–117. https://doi.org/10.1016/j.compenvurbsys.2018.09.002

Orton, P.M., Conticello, F.R., Cioffi, F., Hall, T.M., Georgas, N., Lall, U., Blumberg, A.F., MacManus, K., 2018. Flood hazard assessment from storm tides, rain and sea level rise for a tidal river estuary. Nat. Hazards 1–29. https://doi.org/10.1007/s11069-018-3251-x

Oubennaceur, K., Chokmani, K., Nastev, M., Tanguy, M., Raymond, S., 2018. Uncertainty analysis of a two-dimensional hydraulic model. Water (Switzerland) 10, 1–19. https://doi.org/10.3390/w10030272

Paprotny, D., Vousdoukas, M.I., Morales-Nápoles, O., Jonkman, S.N., Feyen, L., 2018. Compound flood potential in Europe. Hydrol. Easth Syst. Sci.

Pasquier, U., He, Y., Hooton, S., Goulden, M., Hiscock, K.M., 2018. An integrated 1D–2D hydraulic modelling approach to assess the sensitivity of a coastal region to compound flooding hazard under climate change. Nat. Hazards 0123456789. https://doi.org/10.1007/s11069-018-3462-1

Patch, 2020. Isaias Soaks VA: 120K Without Power; Street Flooding Subsides | Across Virginia, VA Patch [WWW Document]. URL https://patch.com/virginia/across-va/isaias-crossing-va-330k-without-power-flash-flooding-likely (accessed 8.7.20).

Patel, D.P., Ramirez, J.A., Srivastava, P.K., Bray, M., Han, D., 2017. Assessment of flood inundation mapping of Surat city by coupled 1D/2D hydrodynamic modeling: a case application of the new HEC-RAS 5. Nat. Hazards 89, 93–130. https://doi.org/10.1007/s11069-017-2956-6

Poblet, M., García-Cuesta, E., Casanovas, P., 2018. Crowdsourcing roles, methods and tools for data-intensive disaster management. Inf. Syst. Front. 20, 1363–1379. https://doi.org/10.1007/s10796-017-9734-6

Quirogaa, V.M., Kurea, S., Udoa, K., Manoa, A., 2016. Application of 2D numerical simulation for the analysis of the February 2014 Bolivian Amazonia flood: Application of the new HEC-RAS version 5. Ribagua 3, 25–33. https://doi.org/10.1016/j.riba.2015.12.001

Ray, T., Stepinski, E., Sebastian, A., Bedient, P.B., 2011. Dynamic Modeling of Storm Surge and Inland Flooding in a Texas Coastal Floodplain. J. Hydraul. Eng. 137, 1103–1110. https://doi.org/10.1061/(asce)hy.1943-7900.0000398

Reistetter, J.A., Russell, M., 2011. High-resolution land cover datasets, composite curve numbers, and storm water retention in the Tampa Bay, FL region. Appl. Geogr. 31, 740–747. https://doi.org/10.1016/j.apgeog.2010.12.005

Resio, D.T., Westerink, J.J., 2008. Modeling the physics of storm surges. Phys. Today 61, 33–38. https://doi.org/10.1063/1.2982120

Ridder, N., De Vries, H., Drijfhout, S., 2018. The role of atmospheric rivers in compound events consisting of heavy precipitation and high storm surges along the Dutch coast. Nat. Hazards Earth Syst. Sci. 18, 3311–3326. https://doi.org/10.5194/nhess-

18-3311-2018

Rosgen, D.L., 1994. A classification of natural rivers. Catena 22, 169–199.

Roth, D., Cobb, H., 2001. Virginia Hurricane History [WWW Document]. URL https://www.wpc.ncep.noaa.gov/research/roth/vahur.htm (accessed 1.7.20).

Sadegh, M., Moftakhari, H., Gupta, H. V., Ragno, E., Mazdiyasni, O., Sanders, B., Matthew, R., AghaKouchak, A., 2018. Multihazard Scenarios for Analysis of Compound Extreme Events. Geophys. Res. Lett. 45, 5470–5480. https://doi.org/10.1029/2018GL077317

Saleh, F., Ramaswamy, V., Wang, Y., Georgas, N., Blumberg, A., Pullen, J., 2017. A multi-scale ensemble-based framework for forecasting compound coastal-riverine flooding: The Hackensack-Passaic watershed and Newark Bay. Adv. Water Resour. 110, 371–386. https://doi.org/10.1016/j.advwatres.2017.10.026

Santiago-Collazo, F.L., Bilskie, M. V., Hagen, S.C., 2019. A comprehensive review of compound inundation models in low-gradient coastal watersheds. Environ. Model. Softw. 119, 166–181. https://doi.org/10.1016/j.envsoft.2019.06.002

Schaffranek, R.W., 1987. A Flow-Simulation Model of the Tidal Potomac River. United States Geol. Surv. Water-Supply Pap. 2234, 1–41.

Serafin, K.A., Ruggiero, P., Parker, K.A., Hill, D.F., 2019. What's streamflow got to do with it? A probabilistic simulation of the competing oceanographic and fluvial processes driving extreme along-river water levels. Nat. Hazards Earth Syst. Sci. Discuss. 1–30. https://doi.org/10.5194/nhess-2018-347

Shen, J., Gong, W., 2009. Influence of model domain size, wind directions and Ekman

transport on storm surge development inside the Chesapeake Bay: A case study of extratropical cyclone Ernesto, 2006. J. Mar. Syst. 75, 198–215. https://doi.org/10.1016/j.jmarsys.2008.09.001

Sheng, Y.P., Alymov, V., Paramygin, V.A., 2010. Simulation of storm surge, wave, currents, and inundation in the outer banks and Chesapeake bay during Hurricane Isabel in 2003: The importance of waves. J. Geophys. Res. Ocean. 115, C04008. https://doi.org/10.1029/2009JC005402

Svensson, C., Jones, D.A., 2004. Dependence between sea surge, river flow and precipitation in south and west Britain. Hydrol. Earth Syst. Sci. 8, 973–992. https://doi.org/10.5194/hess-8-973-2004

Svensson, C., Jones, D.A., 2002. Dependence between extreme sea surge, river flow and precipitation in eastern Britain. Int. J. Climatol. 22, 1149–1168. https://doi.org/10.1002/joc.794

Taylor, R., 1990. Interpretation of the Correlation Coefficient:A Basic. J. Diagnostic Med. Sonogr. 6.

The Great Chesapeake Bay Swim, 2019. Tide and Weather [WWW Document]. URL http://www.bayswim.com/tide-and-weather/ (accessed 1.8.20).

Thyng, K.M., Hetland, R.D., Socolofsky, S.A., Fernando, N., Turner, E.L., Schoenbaechler, C., 2020. Hurricane Harvey Caused Unprecedented Freshwater Inflow to Galveston Bay. Estuaries and Coasts. https://doi.org/10.1007/s12237-020-00800-6

University of Maryland, Texas A&M University, 2018. The growing threat of urban

flooding: A national challenge.

US National Weather Service Baltimore/Washington, 2020. The January 1996 Flood in the Mid-Atlantic [WWW Document]. URL https://www.arcgis.com/apps/MapJournal/index.html?appid=8ac21bbee3654115a28ba6d46fd8506e (accessed 1.7.20).

USACE Hydrologic Engineering Center, 2016. HEC-RAS River Analysis System, User's Manual, Version 5.0. https://doi.org/CPD-68

USDA, 1986. Urban Hydrology for Small Watersheds, Soil Conservation.

USGS, 2020. National Water Information System: Mapper [WWW Document]. URL https://maps.waterdata.usgs.gov/mapper/index.html (accessed 1.21.20).

USGS, 2017. National Water Information System (NWIS): Mapper [WWW Document]. URL https://maps.waterdata.usgs.gov/mapper/index.html (accessed 3.12.19).

USGS, 2016. TNM Download [WWW Document]. URL https://viewer.nationalmap.gov/basic/ (accessed 3.12.19).

Van Den Hurk, B., Van Meijgaard, E., De Valk, P., Van Heeringen, K.J., Gooijer, J., 2015. Analysis of a compounding surge and precipitation event in the Netherlands. Environ. Res. Lett. 10. https://doi.org/10.1088/1748-9326/10/3/035001

Van Oldenborgh, G.J., Van Der Wiel, K., Sebastian, A., Singh, R., Arrighi, J., Otto, F., Haustein, K., Li, S., Vecchi, G., Cullen, H., 2017. Attribution of extreme rainfall from Hurricane Harvey, August 2017. Environ. Res. Lett. 12. https://doi.org/10.1088/1748-9326/aa9ef2

Visser-Quinn, A., Beevers, L., Collet, L., Formetta, G., Smith, K., Wanders, N., Thober,

S., Pan, M., Kumar, R., 2019. Spatio-temporal analysis of compound hydro-hazard extremes across the UK. Adv. Water Resour. 130, 77–90. https://doi.org/10.1016/j.advwatres.2019.05.019

Viterbo, F., Mahoney, K., Read, L., Salas, F., Bates, B., Elliott, J., Cosgrove, B., Dugger, A., Gochis, D., Cifelli, R., 2020. A multiscale, hydrometeorological forecast evaluation of national water model forecasts of the may 2018 Ellicott City, Maryland, Flood. J. Hydrometeorol. 21, 475–499. https://doi.org/10.1175/JHM-D-19-0125.1

Wahl, T., Jain, S., Bender, J., Meyers, S.D., Luther, M.E., 2015. Increasing risk of compound flooding from storm surge and rainfall for major US cities. Nat. Clim. Chang. 5, 1093–1097. https://doi.org/10.1038/nclimate2736

Wang, D.P., Elliott, A.J., 1978. Non-tidal variability in the Chesapeake Bay and Potomac River: evidence for non-local forcing. J. Phys. Oceanogr. https://doi.org/10.1175/1520-0485(1978)008<0225:ntvitc>2.0.co;2

Wang, H., Loftis, J., Forrest, D., Smith, W., Stamey, B., 2015. Modeling Storm Surge and Inundation in Washington, DC, during Hurricane Isabel and the 1936 Potomac River Great Flood. J. Mar. Sci. Eng. 3, 607–629. https://doi.org/10.3390/jmse3030607

Wang, Y., Chen, A.S., Fu, G., Djordjević, S., Zhang, C., Savić, D.A., 2018. An integrated framework for high-resolution urban flood modelling considering multiple information sources and urban features. Environ. Model. Softw. 107, 85–95. https://doi.org/10.1016/j.envsoft.2018.06.010

Ward, P.J., Couasnon, A., Eilander, D., Haigh, I.D., Hendry, A., Muis, S., Veldkamp, T.I.E., Winsemius, H.C., Wahl, T., 2018. Dependence between high sea-level and high river discharge increases flood hazard in global deltas and estuaries. Environ. Res. Lett. 13. https://doi.org/10.1088/1748-9326/aad400

Webster, P.J., Holland, G.J., Curry, J.A., Chang, H.R., 2005. Atmospheric science: Changes in tropical cyclone number, duration, and intensity in a warming environment. Science (80-.). 309, 1844–1846. https://doi.org/10.1126/science.1116448

Wu, W., McInnes, K., O'Grady, J., Hoeke, R., Leonard, M., Westra, S., 2018. Mapping Dependence Between Extreme Rainfall and Storm Surge. J. Geophys. Res. Ocean. 123, 2461–2474. https://doi.org/10.1002/2017JC013472

Yagoub, M.M., Alsereidi, A.A., Mohamed, E.A., Periyasamy, P., Alameri, R., Aldarmaki, S., Alhashmi, Y., 2020. Newspapers as a validation proxy for GIS modeling in Fujairah, United Arab Emirates: identifying flood-prone areas, Natural Hazards. Springer Netherlands. https://doi.org/10.1007/s11069-020-04161-y

Yue, H., Gebremichael, M., 2020. Evaluation of high-resolution rapid refresh (HRRR) forecasts for extreme precipitation. Environ. Res. Commun. 2, 065004. https://doi.org/10.1088/2515-7620/ab9002

Zheng, F., Westra, S., Sisson, S.A., 2013. Quantifying the dependence between extreme rainfall and storm surge in the coastal zone. J. Hydrol. 505, 172–187. https://doi.org/10.1016/j.jhydrol.2013.09.054

Zscheischler, J., Westra, S., Van Den Hurk, B.J.J.M., Seneviratne, S.I., Ward, P.J.,

Pitman, A., Aghakouchak, A., Bresch, D.N., Leonard, M., Wahl, T., Zhang, X., 2018. Future climate risk from compound events. Nat. Clim. Chang. 8, 469–477. https://doi.org/10.1038/s41558-018-0156-3

BIOGRAPHY

Selina Jahan Sumi was born in Rangpur, Bangladesh. She received a Bachelor of Science in Water Resources Engineering from Bangladesh University of Engineering Technology (BUET) in 2012. She joined the World University of Bangladesh as a lecturer in 2013 and worked there for six months. Selina completed her M.S. in Civil Engineering from the University of Louisiana at Lafayette on August 2015. Her M.S. research was funded by the Louisiana Sea Grant through the Coastal Science Assistantship Program (CSAP). As a part of this program, she joined an internship position in the regional office of the Louisiana Coastal Protection and Restoration Authority (CPRA) which is located in Lafayette, LA. She joined the Ph.D. program of the Civil, Environmental, and Infrastructure Engineering Department at George Mason University (GMU) in Fall-2016. She was awarded the 4-year Presidential Fellowship by GMU to complete her Ph.D. study.